

AD-A115 600

OHIO STATE UNIV RESEARCH FOUNDATION COLUMBUS

F/G 13/6

DESIGN STUDY FOR AN ACTIVELY TERRAIN-ADAPTIVE OFF-ROAD VEHICLE.(U)

JUN 82 R B MCGHEE, K J WALDRON

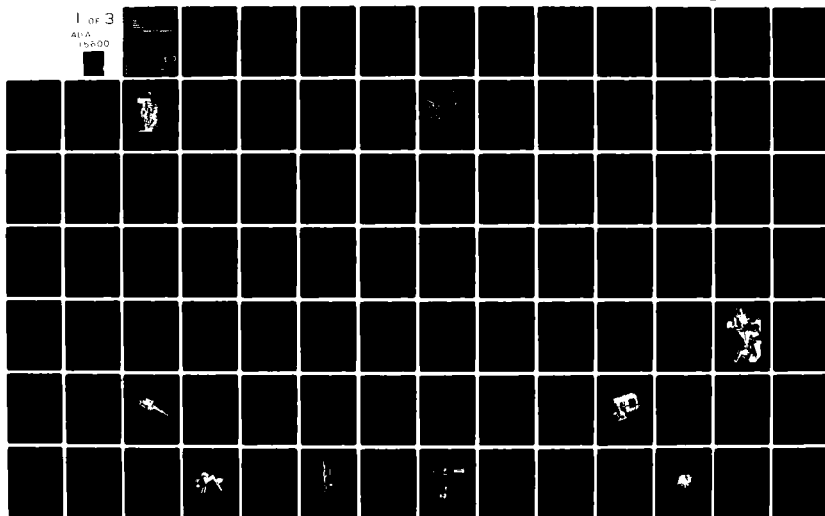
MDA903-81-C-0138

NL

UNCLASSIFIED

1 OF 3

ALIA
15800



12

RF Project 762565/713786
Final Report

the
ohio
state
university

research foundation

1314 kinnear road
columbus, ohio
43212

DESIGN STUDY FOR AN ACTIVELY TERRAIN-ADAPTIVE
OFF-ROAD VEHICLE

Robert B. McGhee
Department of Electrical Engineering

Kenneth J. Waldron
Department of Mechanical Engineering

For the Period
January 29, 1981 - January 28, 1982

DEFENSE SUPPLY SERVICE
Washington, D.C. 20310

Contract No. MDA903-81-C-0138

Copy available to DTIC does not
guarantee fully legible reproduction

June 3, 1982

This document has been approved
for public release and sale; its
distribution is unlimited.

82 06 15 009

AD A115600

DTIC FILE COPY

DISCLAIMER NOTICE

**THIS DOCUMENT IS BEST QUALITY
PRACTICABLE. THE COPY FURNISHED
TO DTIC CONTAINED A SIGNIFICANT
NUMBER OF PAGES WHICH DO NOT
REPRODUCE LEGIBLY.**

Unclassified

SECURITY CLASSIFICATION OF THIS PAGE (When Data Entered)

REPORT DOCUMENTATION PAGE		READ INSTRUCTIONS BEFORE COMPLETING FORM
1. REPORT NUMBER	2. GOVT ACCESSION NO.	3. RECIPIENT'S CATALOG NUMBER
4. TITLE (and Subtitle) DESIGN STUDY FOR AN ACTIVELY TERRAIN-ADAPTIVE OFF-ROAD VEHICLE		5. TYPE OF REPORT & PERIOD COVERED Final 1/29/81-1/28/82
		6. PERFORMING ORG. REPORT NUMBER 762565/713786
7. AUTHOR(s) Robert B. McGhee and Kenneth J. Waldron		8. CONTRACT OR GRANT NUMBER(s) Contract No. MDA903-81-C-0138
9. PERFORMING ORGANIZATION NAME AND ADDRESS The Ohio State University Research Foundation, 1314 Kinnear Road Columbus, Ohio 43212		10. PROGRAM ELEMENT, PROJECT, TASK AREA & WORK UNIT NUMBERS 1001/1011
11. CONTROLLING OFFICE NAME AND ADDRESS		12. REPORT DATE June 3, 1982
		13. NUMBER OF PAGES 223
14. MONITORING AGENCY NAME & ADDRESS (if different from Controlling Office)		15. SECURITY CLASS. (of this report) Unclassified
		15a. DECLASSIFICATION/DOWNGRADING SCHEDULE
16. DISTRIBUTION STATEMENT (of this Report) Approved for public release; distribution unlimited.		
17. DISTRIBUTION STATEMENT (of the abstract entered in Block 20, if different from Report)		
18. SUPPLEMENTARY NOTES		
19. KEY WORDS (Continue on reverse side if necessary and identify by block number) Robotic mobility, legged locomotion, rough terrain mobility, hybrid locomotion, coordination algorithm, robotic sensors.		
20. ABSTRACT (Continue on reverse side if necessary and identify by block number) This project consisted of studies directed at establishing the feasibility of building a practical vehicle using fully adaptive legged locomotion. The objective of building such a vehicle is mobility in extreme rough terrain condi- tions. New technologies essential to feasibility include computer control of leg coordination, efficient power transmission for coordinated motion of large num- bers of mechanical degrees of freedom, development of terrain sensing systems and utilization of the information provided by those systems in control of the machine.		

DD FORM 1 JAN 73 1473

EDITION OF 1 NOV 68 IS OBSOLETE

Unclassified

SECURITY CLASSIFICATION OF THIS PAGE (When Data Entered)

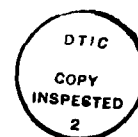
Contract No. MDA-903-81-C-0138

Design Study for an Actively Terrain-Adaptive Off-Road Vehicle

Final Report

to the

Defense Advanced Research Projects Agency



Robert B. McGhee
Department of Electrical Engineering
Ohio State University

Kenneth J. Waldron
Department of Mechanical Engineering
Ohio State University

Accession For	
NTIS GRA&I	<input checked="checked" type="checkbox"/>
DTIC TAB	<input type="checkbox"/>
Unannounced	<input type="checkbox"/>
Justification	
By _____	
Distribution/	
Availability Codes	
Dist	Avail and/or Special
A	

The views and conclusions contained in this document are those of the authors and should not be interpreted as representing the official policies, either expressed or implied, of the Defense Research Projects Agency or the U. S. Government.

1. INTRODUCTION

This report provides a summary of research accomplished under DARPA Contract MDA 903-81-C-0138 during the period January 29, 1981, through January 28, 1982. Additional information can be found in our three previous Quarterly Status Reports, in published papers referenced in the body of this report, and in the attached appendices.

2. RESEARCH ACCOMPLISHED

The work covered by this report is described in our proposal, Design Study for an Actively Terrain-Adaptive Off-Road Vehicle, dated September 19, 1980. In this proposal, the research to be done is organized into ten distinct tasks. For the convenience of the reader, research accomplished under the subject contract is reported in the following paragraphs relative to each of these tasks.

Task 1: Actuator Configuration Alternatives

The RECSYN II linkage synthesis program was used as a design tool for rapidly generating and evaluating leg geometries in conjunction with a specially written program to trace foot paths. Geometrically optimized versions of the original concept of a four-bar linkage with an adjustable length crank, and of a later concept, in which the four-bar linkage has fixed geometry but has a movable coupler-point, were developed. These are shown in Figures 1 and 2, respectively. The second concept which possesses, effectively, a variable-length shank, has a much superior operating height range. Therefore, it is the currently operative design for the breadboard hydraulic leg, in development under Contract MDA 903-82-K-0058, and for the

MENU
 1-NEW LINKAGE 2-ANIMATE 3-COUPLES POINT
 4-CHANGE LINK LENGTH 5-DATA 6-SPEED CHANGE
 7-VEL. ACCEL. PLOTS 8-LIMIT INPUT ROT
 9-ALTER C.P. CURVE 10-EXIT
 2
 1-NEW ANIMATION 2-RERUN
 3
 INPUT ANIMATION TYPE
 0-OVERLAY 2-WRITE THRU
 2
 INPUT DRIVE CRANK INDEXING ANGLE (DEG)
 3
 STOP ANIMATION BY INPUTTING C-INTEGER RETURN

DRAW PREVIOUS C.P. CURVE? (1=YES, 0=NO)
 1

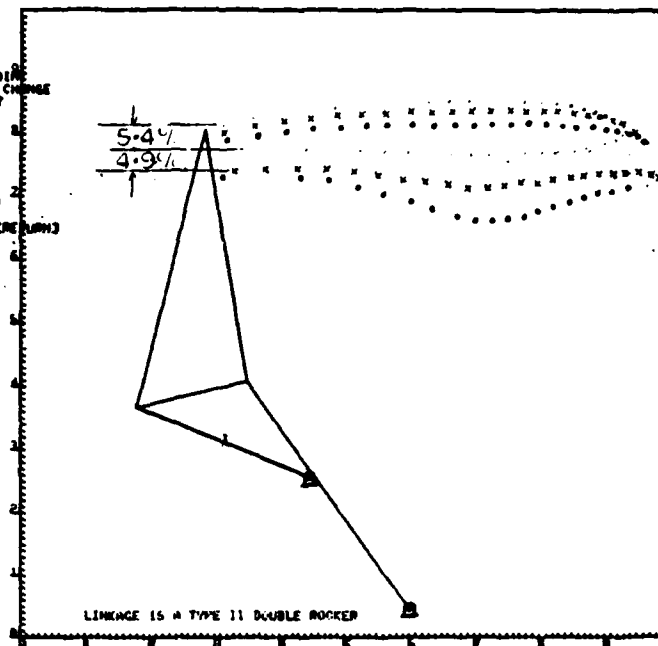
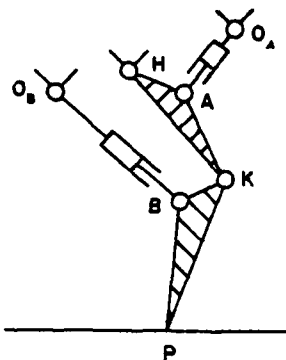


Figure 1. Leg concept with adjustable length crank. Schematic of leg mechanism is at left. Computer generated geometric model is at right.

MENU
 1-NEW LINKAGE 2-ANIMATE 3-CPLA PT. 4
 4-CHANGE LINK LENGTH 5-DATA 6-INPUT VEL.
 7-VEL. ACCEL. PLOTS 8-LIMIT INPUT ROT
 9-ALTER C.P. CURVE 10-EXIT
 2
 1-NEW ANIMATION 2-RERUN
 3
 INPUT ANIMATION TYPE
 0-OVERLAY 2-WRITE THRU
 2
 INPUT DRIVE CRANK INDEXING ANGLE (DEG)
 3
 STOP ANIMATION BY C-INTEGER RETURN
 INPUT C.P. CO-SAME 1-CURSOR 2-(X,Y) 30
 INPUT FORCE AT COUPLES POINT
 F(X)=, F(Y)= (LBF) 10.00
 LINEAR ACTUATOR? (0=NO 1=YES) 0
 C.P. FOOT? (0=NO, 1=ROUND, 2=OTHER) 0

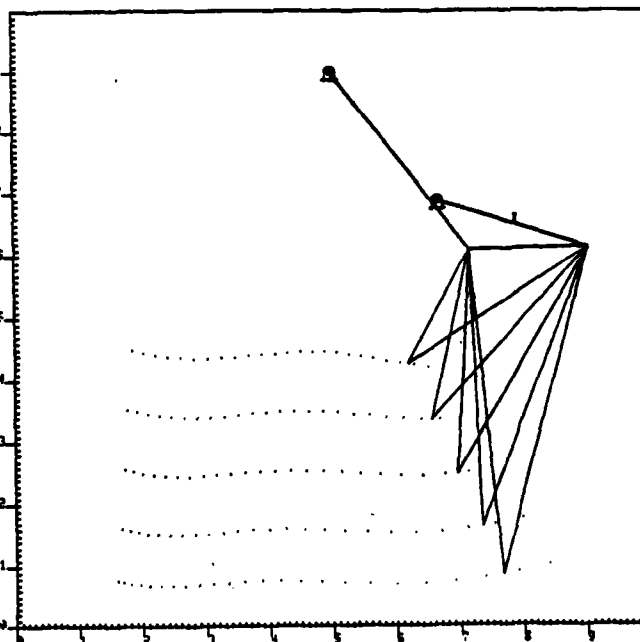
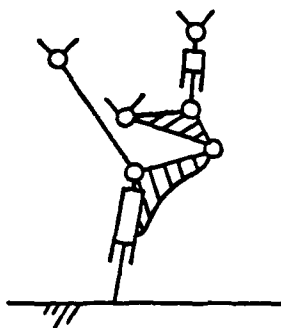


Figure 2. Leg concept with adjustable shank length. Schematic of leg mechanism is at left. Computer generated geometric model is at right.

adaptive suspension vehicle (ASV-84) to be designed under that contract. The earlier concept shown in Figure 1 was used for the electric monopod discussed below.

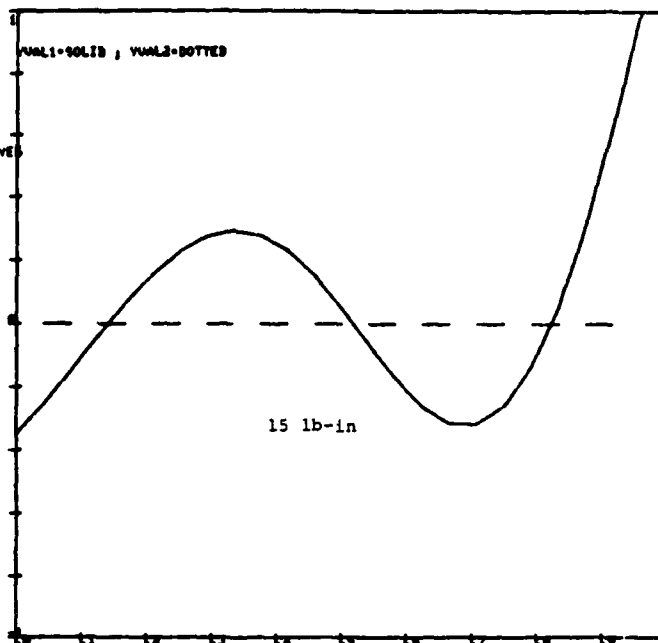
In addition, a partial pantograph leg configuration is being evaluated as an alternative. The absolutely linear relationship between drive actuator displacement and foot displacement achievable with this geometry is attractive from the point of view of the control and actuation system dynamics. However, this type of linkage has mounting length and geometric singularity problems. These difficulties, together with progress in optimizing the drive actuator mounting to minimize non-linearity have led to retention of the four-bar leg as the operative design.

The operation of the interactive design software developed from the RECSYN II program is shown on the videotape submitted in conjunction with this report. This portion of the work was also the subject of the paper, "Computer Aided Design of a Leg for an Energy Efficient Walking Machine," presented at the 7th Applied Mechanisms Conference and appended to the third-quarter report on the present contract.

Task 2: Actuator Geometrical and Structural Optimization

A computer program was written to compute drive actuator load as a function of actuator displacement throughout the support phase of the cycle. Figure 3 is a display generated by this program. The program was used in sizing the actuators of the monopod and for the breadboard hydraulic leg presently under construction. It has been incorporated into a macroscopic simulation of the ASV which is being used to generate load-displacement-time histories of the actuators for use in hydraulic control system simulation studies.

LINKAGE DESIGN NO. 3
 LOAD AT COUPLER POINT
 P(1) = 0.000 P(2) = -110.000
 VVAL1=REQUIRED TORQUE AT DRIVER
 DO YOU WANT TABULAR RESULTS ? 0=NO, 1=YES



DIMENSIONLESS PLOT, V-VALUE VS % TOTAL DRIVE CRANK ROTATION
 VVAL1= 46.7838 ROTATION= 60.000 TO 180.001 DEG

Figure 3. Drive actuator load displacement curve. The zero crossings correspond to the extrema of the foot path.

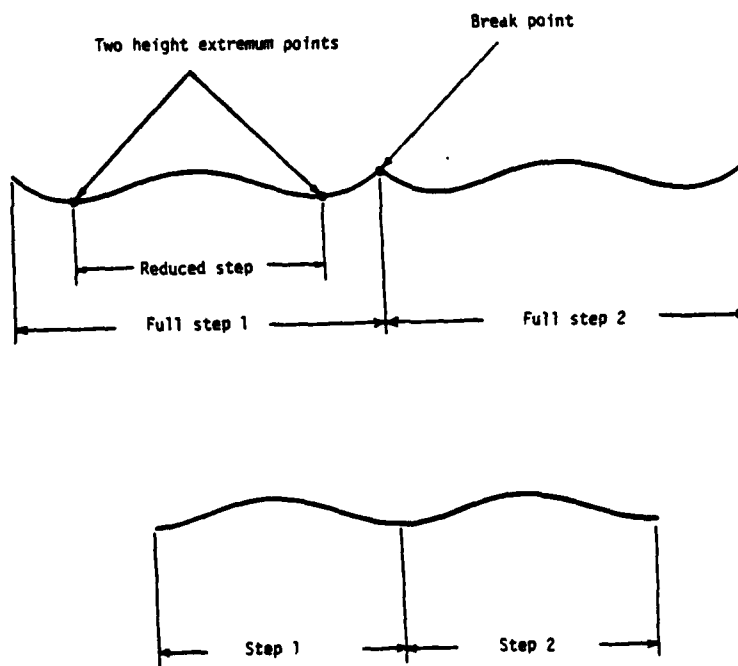


Figure 4. Matching of foot path curves. Top curve shows composite foot path for stride longer than optimum. Bottom curve is optimum curve obtained by interchanging legs at minima of foot path.

Further work under this heading has been focused on understanding the mechanisms of passive energy transfer within the machine. It is vital that leg kinetic energy not be wasted at the end of the support stroke, but rather be converted to potential energy and re-used to drive the return stroke of the leg. These studies have led to definition of an optimum mode of operation of the machine when cruising. The concept is that the tripod gait would be used permitting the shank actuator to be locked during load-bearing. The resulting small vertical oscillation of the machine is acceptable and involves, in principle, no energy loss provided leg interchange takes place at the lowest points of the foot path relative to the body as shown in Figure 4. At the end of the contact phase, the leg is braked by gravity converting kinetic energy into gravitational potential energy. This energy is then available to drive the leg forward through the return stroke. Additional energy to ensure a complete return stroke is provided by extra lift using the shank actuator at the beginning of the return stroke.

In order to further understand the relationships between leg and body weight distribution and the mechanics of this process, a machine called the DUWE (Dynamic Unpowered Walking Experiment) has been designed and is presently being assembled. This is an unpowered, 6-legged walking machine. Its only active elements are solenoids on each of the 6 legs which lift the legs by shortening an adjustable length crank and two additional solenoids which operate latches to hold the legs in the ready position at the beginning of the contact phase. The solenoids are controlled by an Apple II microcomputer which monitors foot position and ground velocity. The machine is designed to permit adjustment of the weight distributions of individual leg members. A computer simulation of the operation of this machine has also been developed.

It is planned that data from tests of the DUWE will be used to validate the simulation which will then be used as a design tool when setting up the ASV structure and weight distribution.

Preliminary data from this experiment should be available in April, 1982. The DUWE structure and the display generated by the simulation are shown on the videotape portion of this report. Some of the ideas described above were presented in the paper, "The Relationship Between Actuator Geometry and Mechanical Efficiency in Robots," presented at the 4th CISM-IFTOMM Symposium on Theory and Practice of Robots and Manipulators and appended to the first-quarter report on the present contract.

Task 3: Power Transmission System Simulation

It was concluded quite early in the project that the force-to-weight characteristics required to actuate a system of the size and complexity needed by the ASV would necessitate use of a hydraulic power transmission system. After considerable analysis of the operating characteristics of various actuators, and of the power loss mechanisms inherent in different types of hydraulic circuits, a configuration was devised in which three separate hydraulic circuits are used: One for all the drive actuators,* one for all the shank actuators, and one for all the abduction-adduction actuators. Each circuit is to be served by its own variable displacement pump with pump displacement controlled by the coordination computer. In order to provide a high peak power capacity to overcome obstacles and to provide a regenerative energy storage capability, a flywheel storage package

* The drive circuit may be further subdivided into two separate circuits; one serving each side of the machine.

will be used. The flywheel and prime mover package is being developed by the University of Wisconsin under separate contract.

A simulation of the hydraulic power transmission and control system is being developed using the ACSL dynamic simulation language. In order to provide the actuator load-displacement time histories required as input to this simulation, a macroscopic simulation of the ASV is also being developed. Both simulations are operational for base-line system configurations and operating conditions.

Task 4: Mechanical Component Evaluation

Extensive evaluation studies have been performed on electric and hydraulic actuation and control system components. As a result of the monopod study, we believe we have good information on the performance to be expected of high quality electrical components. We have also evaluated a number of different speed reducer and brake configurations. It was, however, concluded that electric actuation was not viable for the 1984 ASV.

Studies have been conducted of hydraulic system configurations and of available components. Decisions on the extent of valve control versus displacement control to be used are crucial both with respect to minimizing power wastage and with respect to maximizing dynamic response. Considerations of actuator type, weight, and mounting geometry, have also received study in depth. In order to further these studies and to test control concepts, a set of pumps, control valves and actuators have been ordered for the construction of a full-sized leg referred to elsewhere in this report as the "breadboard leg." This is scheduled to be operational in fall 1982 and will be used to provide data for final selection of hydraulic system configuration and hardware and of controller hardware and software structure.

A new generation 16 bit microprocessor (Motorola 68000 or Intel 8086/8087) will be used as a controller for the breadboard leg. Again, the objective is evaluation of hardware and software. Extensive comparative studies of these two types of microprocessors and their support software and hardware are in progress.

Task 5: Energy-Efficient Leg Demonstration

A single leg has been designed, constructed and is under test. This unit is referred to as the Monopod elsewhere in this report. It was designed to match the size and performance characteristics of the OSU Hexapod Vehicle legs although, in fact, it is capable of about twice the maximum speed and is designed for a maximum 50 percent gradient. The primary objective is to demonstrate the improvement in power demand realizeable by use of careful geometric and dynamic design of a leg and selection of electrical and mechanical components properly matched to their functional requirements. Test data indicate a reduction in power demand by a factor of between 10 and 30 as compared to the Hexapod legs. In particular, when differences in the power supply electronics are corrected for, the ratio of lift to effective drag is about 25 times that of the Hexapod.

The Monopod is mounted in a three-wheeled test cart on a vertical slide enabling it to be weighted and to move in a manner closely simulating its function if used on a walking machine. In one present mode of operation, the leg speed may be synchronized to cart speed enabling the cart to be towed to simulate motion of the walking machine body. Another mode of operation is, essentially, open loop with the leg driving the cart. Testing will include motion on straight and curved paths and on gradients. In addition to providing power demand data, this system will provide a test bed for software development

for control of linkage legs. At present the system is being controlled by the PDP-11/70 computer. However, it is planned to mount a 16-bit microprocessor controller on the test cart and to operate in a stand-alone mode. This will be done after initial tests of the system are complete.

The Monopod construction and its operation in the test cart are shown on the videotape. Mr. V. Vohnout's Master of Science thesis, which is attached to this report, as Appendix 1, describes the design and testing of this system in detail.

Task 6: Overall Structural Simulation

A model of the ASV structure has been constructed using the SUPERTAB geometric modelling program. This model has been used to study the weight distribution and spatial location of major components of the vehicle. It has also been used as the basis of finite element stress and deflection analyses. The results of these analyses are being used in the selection of the structural configuration and of member cross-sections and materials.

Displays generated by the SUPERTAB program and by the SUPERB finite element analysis program are shown on the videotape.

Task 7: Fully Terrain-Adaptive Locomotion by OSU Hexapod

The OSU Hexapod Vehicle has been modified to include vector force sensing on all legs. In addition, a two-axis vertical gyroscope has been mounted on its body. These two features have permitted the writing of software to provide for regulation of body attitude to a desired set-point in pitch and roll, while automatically accommodating terrain irregularities through adjustment of limb cycles. All of this action takes place automatically without intervention by the operator, who nevertheless retains full control of forward velocity,

lateral velocity, and steering through either a keyboard controller or a three-axis joystick. Figure 5 is a photograph of the OSU Hexapod showing the force sensors and the vertical gyro in place. A videotape entitled The Adaptive Suspension Vehicle Concept, dated March, 1982, and showing the combined action of the gyro and force sensors during locomotion of this vehicle over obstacles in a laboratory environment, has been previously provided to DARPA.

Task 8: Dynamic Simulation of Complete Vehicle System

This is a complicated task involving three major subtasks. The first of these relates to realization of an articulated rigid body computer model of the ASV-84 vehicle for both design and simulation purposes. This task has been completed to the extent that a detailed kinematic model is available and can be used to drive a computer display for limb motion coordination studies. Typical results obtained from this simulation are included in the videotape portion of this report and in the earlier videotape dated March, 1982. In addition to this kinematic model, a full dynamic simulation of the adjustable link leg configuration has been completed and used for control and energy consumption studies prior to completion of the electric Monopod described in Appendix 1 of this report. A summary of this work can be found in the paper, "Dynamic Computer Simulation of Robotic Mechanisms," presented at the 4th CISM-IFTOMM Symposium on Theory and Practice of Robots and Manipulators and appended to the first-quarter progress report for this contract. Details are provided in the M.S. thesis of Mr. Fan-Tien Cheng, Computer Simulation of the Dynamics and Control of an Energy-Efficient Robot Leg, dated January, 1982.

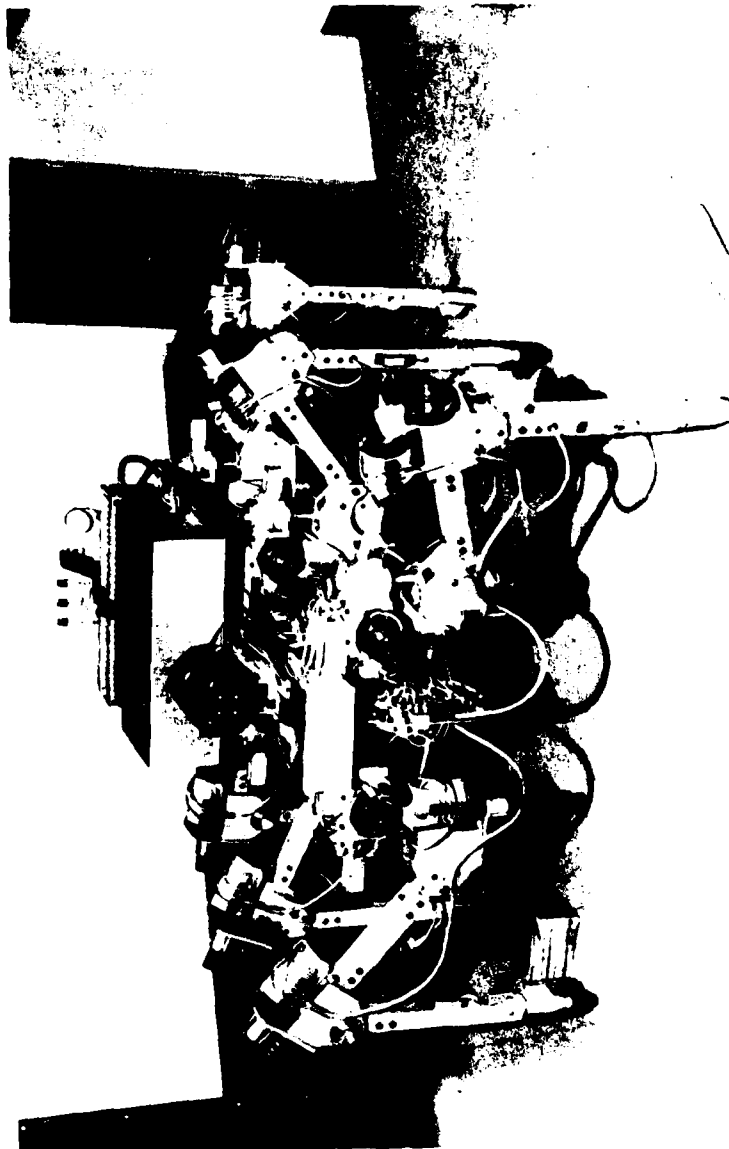


Figure 5. O.S.U. Hexapod showing modifications made during this project. The cylindrical "feet" contain axial force sensors. The black cylinder mounted on the spine is a vertical gyroscope.

The second part of this task involved the use of vehicle simulation models for the development of improved foothold selection algorithms and foot-force setpoint calculations. With respect to the first issue, three-axis joystick control including a cruise mode, a turn-in-place mode, and a side-step mode has been realized and demonstrated with the OSU Hexapod as described in the above discussion of Task 7. The algorithms used for this purpose are detailed in the paper "Three-Axis Joystick Control of a Hexapod Vehicle over Constant-Slope Terrain," to appear in the March, 1982, issue of Robotics Research and appended to our Second Quarterly Status Report. Modification of these algorithms for ASV-84 control is proceeding by means of computer simulation. Typical results are included in the videotape. So far as force optimization is concerned, a pseudo-inverse approach has yielded an analytic solution to this problem. This result eliminates the need to solve the large linear programming problem incorporated in earlier simulation studies, and significantly reduces the projected computational load on the on-board computer for the ASV-84 vehicle. Details of this improved algorithm will be presented in the thesis of Mr. Dennis Pugh, to be completed during the present academic year.

The third subtask of Task 8 is entitled "Evaluate hybrid vehicle propulsion concepts originated at OSU and by other DARPA contractors." The major activity under this heading has been a study of locomotion systems which utilize both wheels and legs. The rationale here is that wheeled locomotion would be used for relatively high speed movement on good terrain. Walking would be used to provide mobility in difficult terrain. Concepts such as legs with wheels at their ends, separate body mounted wheels, and combinations of wheels and legs have been investigated. An existing vehicle which falls

in the last class, the Kaiser Spyder, was studied at a demonstration held in Palm Bay, Florida, on December 17, 1981. A summary of observations made on that occasion is attached as Appendix 2.

At present, a concept has crystallized which seems attractive for application to an operational prototype vehicle to follow the ASV-84. This concept is one of a legged vehicle, viewed as a refinement of the ASV concept, capable of operating in a fully coordinated walking mode but with the addition of dismountable wheels. The wheels would be mounted on the ends of the legs which would act as variable characteristic suspensions under computer control when in the wheeled mode. The wheels would include hub mounted hydraulic motors with epicyclic speed reducers to provide traction. These would be linked to the vehicle hydraulic power transmission system via quick release couplings. The current concept of the shank actuator circuit is quite compatible, in terms of the hardware to be used, with use as a variable rate suspension system, although additional valving would be necessary. Correspondingly, the current concept of the main drive circuit seems well adapted to providing power to the wheel motors. Actuators would need to be provided on the front and/or back legs to turn the wheels in order to provide steering. These might be adapted from ankle actuators which are likely to be used in the walking mode. Note that, in this system, it would be possible to use wheels on all legs, wheels on no legs, or any intermediate combination. Thus, Kaiser Spyder-type hybrid locomotion would be entirely feasible.

Task 9: On-Board Computer Design

As anticipated in our proposal, under the subject contract, this task was initiated, but not completed. However, we have proceeded far enough to believe that a loosely-coupled network of micro-computers probably constitutes

the most effective computer architecture for the ASV-84 on-board computer. We currently favor the Intel family of micro-computers for this purpose and have purchased one 8086/8087/8088 system in order to evaluate its suitability.

Task 10: Prototype Vehicle Development Plan

Specifications have been developed for a prototype proof-of-concept vehicle, referred to as the "Adaptive Suspension Vehicle" (ASV-84) above. This vehicle is to be operational in 1984. A concept drawing for this machine is shown in Figure 6. Anticipated vehicle characteristics are provided in Table 1. All of the work described above is either preparatory to, or directly applicable to, the design of this vehicle. In particular, design studies of the vehicle structure, the power supply and transmission system, and of the leg geometry and actuation system are well advanced. An animated graphic simulation of the ASV has been developed and is included in the videotape.

As part of our work under the subject contract, a proposal was prepared setting forth a plan for realization of an operational ASV-84 vehicle by September, 1984. This proposal, entitled An Experimental Study of an Ultra-Mobile Vehicle for Off-Road Transportation, dated May 13, 1981, provides a detailed plan for this undertaking. This proposal was subsequently funded as Contract MDA 903-82-K-0058 for the period October 1, 1981, to September 30, 1984. Work under this contract began on the scheduled starting date and, together with the research accomplishments cited above, constitutes successful realization of all of the major goals of Contract MDA 903-81-C-0138, the subject of this final report.

TABLE 1

DESIGN GOALS FOR 1984 ADAPTIVE SUSPENSION VEHICLE (ASV)

- . SUPPORT AND PROPULSION BY POWERED ARTICULATED SYSTEMS OF LEVERS (LEGS) RATHER THAN WHEELS OR TRACKS, SIX-LEGGED CONFIGURATION MOST PROBABLE.
 - . AUTOMATIC COMPUTER COORDINATION OF LEG AND BODY MOTIONS UTILIZING JOYSTICK AND PUSH-BUTTON COMMANDS FROM AN ONBOARD HUMAN OPERATOR. FULLY AUTOMATED FOOTHOLD SELECTION IN EASY TO MODERATELY SEVERE TERRAIN CONDITIONS. OPTICAL (LASER) DESIGNATION OF FOOTHOLDS BY OPERATOR FOR LOCOMOTION IN EXTREME TERRAIN CONDITIONS.
 - . LEVEL WALKING CRUISE SPEED OF APPROXIMATELY 5 MPH.
 - . SPRINT CAPABILITY OF 8 MPH.
 - . ABILITY TO NEGOTIATE ROUGH TERRAIN AT SLOPES OF UP TO 50 PERCENT AT ARBITRARY TRACK ANGLE RELATIVE TO SLOPE.
 - . MINIMUM RANGE OF 50 MILES WITHOUT REFUELING WHILE WALKING ON SUBSTANTIALLY LEVEL GROUND AT CRUISE SPEED.
 - . PAYLOAD CAPACITY OF 500 LBS.
 - . TOTAL VEHICLE WEIGHT IN THE RANGE OF 3000 LBS. TO 4000 LBS.
 - . TRACK WIDTH ADJUSTABLE, DESIGN VALUE 4 FT. PROBABLE HEIGHT AROUND 9 FT., LENGTH AROUND 14 FT.
-

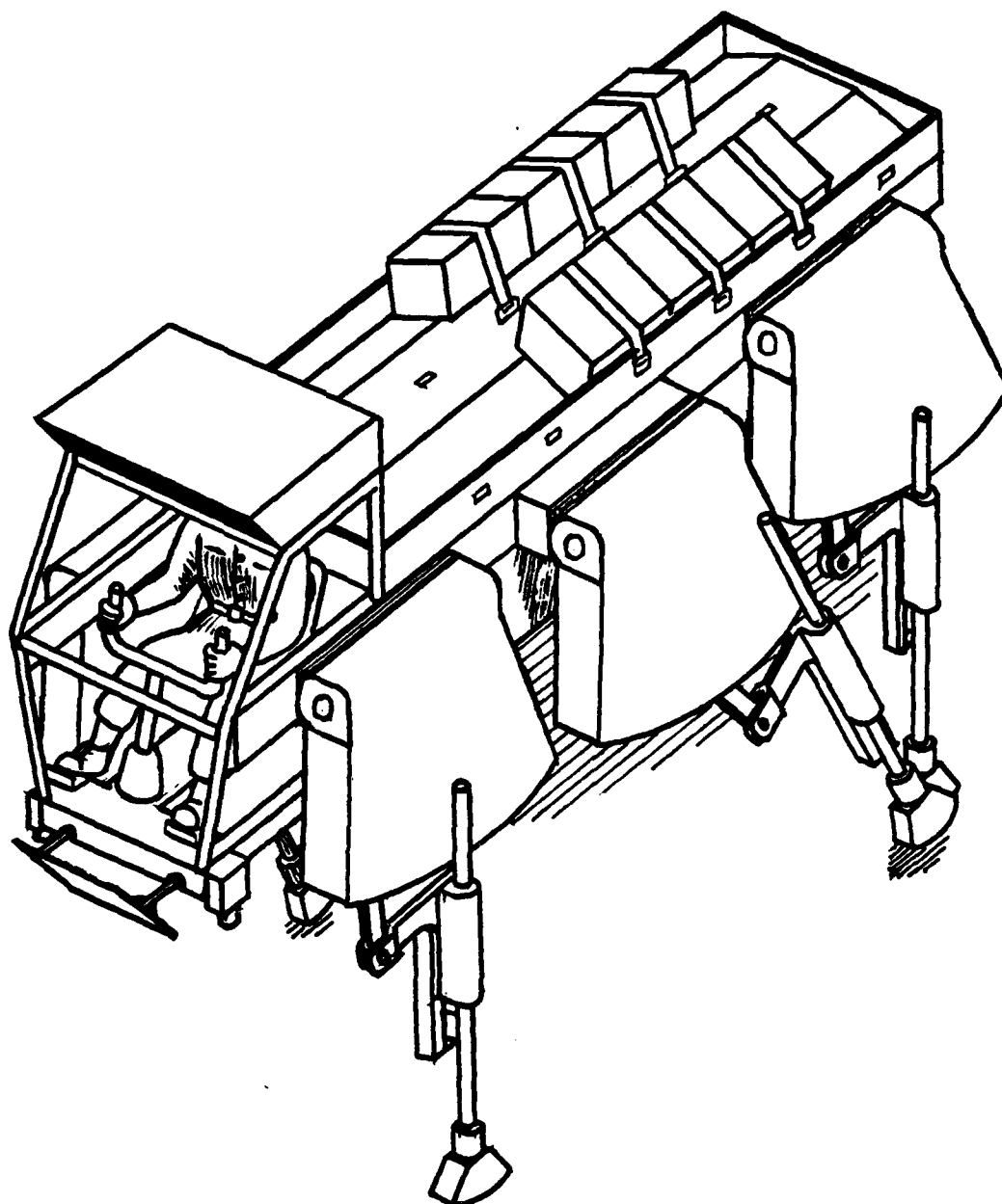


Figure 6. Artists conception of the Adaptive Suspension Vehicle.

3. FUNDS EXPENDED

As of the date of this report, all funds provided under this contract have been expended. A detailed financial report will be separately provided by the Ohio State University Research Foundation in accordance with contract requirements.

THESIS ABSTRACT

THE OHIO STATE UNIVERSITY
GRADUATE SCHOOL
(Please type.)

NAME: Vincent J. Vohnout

QUARTER/YEAR: Spring 1982

DEPARTMENT: Mechanical Engineering

DEGREE: M.S.

TITLE OF THESIS:

Mecanical Design of an Energy Efficient Robotic Leg
for use on a Multi-Legged Walking Vehicle

Summarize in the space below the purpose
and principal conclusions of your thesis.

The failure to produce a usable walking vehicle from past efforts is identified as much a problem in machine design as controls. The planar, mammalian type leg is chosen as the general configuration best suited for an efficient walking vehicle. A four bar linkage solution to the kinematics of the problem is found and refined using interactive synthesis and analysis computer programs. A D.C. electric powered leg mechanism design, based on the kinetic study and scaled to the OSU Hexapod Vehicle is presented. Simplified, discrete mode, velocity feedback control is used to run the leg installed in a three wheeled test cart. Instantaneous power and velocity data from the "Monopod" system is time averaged and a complete electrical energy audit of the system is presented. Two methods are used to compare the relative energy consumption between the Monopod and Hexapod. Both methods indicate greater than an order of magnitude reduction in energy and power requirements for a vehicle using the planar linkage leg of the Monopod type rather than the joint powered "arthropod" leg of the Hexapod type.


Advisor's Signature

Acknowledgments

I would like to thank Dr. Kenneth J. Waldron and Dr. Gary Kinzel for their patience and guidance during the writing of this thesis. I thank the secretaries, technicians, and craftsmen whose conscientious work played a major part in the success of the Monopod project and the completion of this thesis. I thank my friends and fellow graduate students for their many helpful suggestions and diversions over the past two years. And I gratefully acknowledge the unshakeable faith and understanding of my family during the prolong term of my tenure as a student.

Table of Contents

	Page
List of Tables	iv
List of Figures	v
Chapter 1: Overview of "Efficient Leg" Problem	1
1.1 Introduction	1
1.2 Requirements for Efficient Walking	4
1.3 General Leg Configurations	5
1.4 Project Goals	14
Chapter 2: Kinematic Design of Leg Mechanism	16
2.1 Introduction	16
2.2 Choosing the Third Degree of Freedom	16
2.3 Synthesis of the Four Bar Leg Mechanism	20
2.4 Kinematic and Force Analysis of Leg Mechanism	23
Chapter 3: Mechanical Design of Leg Mechanism	34
3.1 Introduction	34
3.2 Linear Actuator	38
3.3 Main Drive Actuator	47
3.4 Coupler (Knee Joint and Shank)	55
3.5 Drive Crank and Shaft	59
3.6 Base Link Plate	63
3.7 Leg Instrumentation	65

	Page
Chapter 4: Planar Leg Test Support System	67
4.1 Introduction	68
4.2 Test Cart Frame	69
4.3 Cart Instrumentation	74
Chapter 5: Actuator Power Control	77
5.1 Introduction	77
5.2 The Resistor Versus the Switch	77
5.3 Motor Power Bridge Circuits	82
5.4 Digital Word-to-Pulse Width Conversion	84
Chapter 6: Control Program for Leg Mechanism	87
6.1 Introduction	87
6.2 Simplified Control Scheme; Mode Control	90
6.3 Actual Control Program	94
6.4 Control Hardware	97
Chapter 7: Energy/Power Tests of the Monopod System	101
7.1 Introduction	102
7.2 Method for comparing Monopod Data to Hexapod Data	102
7.3 Comparison of Monopod and Hexapod in Terms of Power and Energy Usage	103
Chapter 8: Discussion, Conclusions, and Extentions	126
References	130
Appendix A: Calculation Results	135
Appendix B: Component Specifications and Calibration Data	150
Appendix C: Additional Figures	164

List of Tables

<u>Table</u>	<u>Page</u>
6.1 Actuator states versus leg mode	92
7.1 Monopod power/energy use for one cycle forward stride ..	107
7.2 Monopod power/energy use for one cycle reverse stride ..	108
7.3 Power/energy cost for Monopod one leg cycle, no load ...	109
7.4 Monopod energy audit, one cycle, forward stride	114
7.5 Monopod energy audit, one cycle, reverse stride	115
7.6 Comparison of Monopod to Hexapod power/energy requirements for one foot of level locomotion	116
7.7 Estimated Monopod power/energy usage with SCR motor drivers one foot of level locomotion.....	117
7.8 Comparison of mean power ratio and specific resistance ratio for power transistor and SCR type motor controllers.....	124

List of Figures

Figure	Page
1.1 Insect leg dyad model	6
1.2 Mammalian leg dyad model	16
1.3 Simplified loading of mammalian leg	10
2.1 Anatomy of a four bar linkage leg mechanism	17
2.2 Conventions for kinematic synthesis	19
2.3 A full step of the walking machine leg	19
2.4a Schematic of planar leg from FPRBAR program	24
2.4b Rotated schematics of planar leg from FORBAR program ...	25
2.5 Coupler and Driven crank angular velocity versus drive crank positions	26
2.6 Coupler and driven crank angular acceleration versus drive crank position	27
2.7 Driven and drive crank bearing loads versus drive crank position	28
2.8 Required drive crank shaft torque versus drive crank position	29
2.9 Schematic of planar leg attached to vehicle frame	31
3.1a General assembly of planar leg mechanism	35
3.1b General assembly of planar leg mechanism	36
3.2 Photograph of planar leg mechanism	37
3.3 Linear actuator general assembly	39

Figure	Page
3.4 Photograph of linear actuators	41
3.5 Ball bearing duplex arrangement	44
3.6 Photograph of rotory actuator	49
3.7 General assembly of rotory actuator speed reduced	52
3.8 Photograph of coupler bar with force transducer shank ..	56
3.9 Photograph of solid and force transducer shanks	58
3.10 Photograph of drive crank and shaft	60
3.11 Photograph of typical joint potentiometer mounting	64
4.1 Monopod general assembly	68
4.2 Photograph of test cart with leg installed	70
4.3 Photograph of test cart with leg and electronics	73
4.4 Photograph of tachometer/generator cart speed transducer	75
5.1a Schematic of variable resistor D.C. motor power control circuit	78
5.1b Pulse width motor power control	78
5.2a Pulse train from an ideal switch	80
5.2b Pulse train after smoothing inductors	80
5.3 Schematic of motor power bridge circuit	83
5.4 Block diagram of digital word to pulse width converter	85
6.1a Foot trajectory with reference to vehicle frame	89
6.1b Foot trajectory with reference to ground	89
6.2 Block diagram of total leg system	91
6.3 Flow chart of simplified control program	96
6.4 Block diagram of Monopod control system hardware configuration	99

Figure		Page
7.1	Relationship between Monopod average power and speed ...	110
7.2	Actuator average power vs. cart speed	111
7.3	Plot of specific resistances and resistance ratios between Monopod and Hexapod	118
7.4	Actuator power versus real time for 95 lb leg load	119
7.5	Actuator power versus real time for 0.0 lb leg load	120
7.6	Specific resistance versus maximum vehicle speed	121

ABSTRACT

Mechanical Design of an Energy Efficient Robotic Leg for Use on a Multi-Legged Walking Vehicle

The failure to produce a usable walking vehicle from past efforts is identified as much a problem in machine design as controls. The planar, mammalian type leg is chosen as the general configuration best suited for an efficient walking vehicle. A four bar linkage solution to the kinematics of the problem is found and refined using interactive synthesis and analysis computer programs. A D.C. electric powered leg mechanism design, based on the kinetic study and scaled to the OSU Hexapod Vehicle is presented. Simplified, discrete mode, velocity feedback control is used to run the leg installed in a three wheeled test cart. Instantaneous power and velocity data from the "Monopod" system is time averaged and a complete electrical energy audit of the system is presented. Two methods are used to compare the relative energy consumption between the Monopod and Hexapod. Both methods indicate greater than an order of magnitude reduction in energy and power requirements for a vehicle using the planar linkage leg of the Monopod type rather than the joint powered "arthropod" leg of the Hexapod type.

Chapter I

OVERVIEW OF "EFFICIENT LEG" PROBLEM

1.1 Introduction

About the time that motorized wheeled locomotion was becoming the predominant means of transportation, there were already some people interested in reverting back to walking, that is, vehicles which ambulated instead of rolled.* By the mid-1950's walking vehicles were under serious study at such places as the U.S. Army Land Locomotion Lab. The theoretical advantages of traversing soft unprepared surfaces by walking rather than rolling were discussed in the text books on vehicle systems by 1960 [14]. In 1961 the first international conference on Soil-Vehicle System was held. At this conference two papers were presented which dealt with ideas for practical practical walking vehicles [4, 16]. In this same year, the American Rocket Society published a paper investigating the possibility of a walking Moon Rover [23]. Also during this same time interest in walking systems from a control and theoretical gait optimization view began to surface [21,22,39]. From the early sixties to the present a significant number of papers have been published on motion planning, motion control, body stability dynamic simulation, dynamic gait control, and various other "software" topics , selected references [27, 28,29,31,32,36].

* In 1913 a German patent was issued to Dr. Von Bechtolsheim for a walking vehicle "Der Schreitwagen" [16]. (See diagram, Appendix C.)

There have also been various machines built over the past twenty years with one, two, four, six, and eight legs. With the exception of the eight legged Space General machine [5], these machines were essentially test beds for control algorithms. For this reason the mechanical efficiency of these machines was of little or no concern to their designers. Consequently the theoretical energy cost advantage of walking over rolling was completely overwhelmed by poor mechanical efficiency. Before advantage can be taken of recent successes in computer coordination and supervisory control, the mechanical efficiency of a walking machine must be high enough to allow realization of the inherent energy cost savings of walking.

Conceptually the advantage of walking over soft ground instead of rolling is quite simple. The central idea is that, for any land locomotion system to proceed from point A to point B, some work must be done on the environment. For travel across soft ground, this environmental work is minimally the energy expended in compacting the soil.* The physical evidence of this energy expenditure is the visible depressed track generated from A to B. Clearly, for physically similar systems, rolling from A to B requires more environmental work than walking simply due to the fact that rolling generates a continuous compacted track, while walking generates discrete compressed patches of the soil. Equating two legs to a single wheel, only in the limit as stride length approaches foot length, does this idealized compaction energy of walking approach that of rolling. In reference [15] M. Bekker presents an analytical, quantita-

* Although no noticeable soil compaction results in traversing a hard surface road bed, the environmental energy cost has been "prepaid" during the construction of the road.

tive comparison of walking to rolling in terms of a soil compaction resistance ratio between two legs with flat plate feet and a wheel twice the width of a foot. The comparison shows that the ratio of walking resistance to rolling resistance becomes smaller as the "looseness" of the soil increases and, as might be expected, is reduced with increasing stride length.

Additional theoretical advantages of walking are in the areas of maximum drawbar pull and the bump height effect. Drawbar pull is a quantity often used in comparing tractors. Regardless of the engine power of a tractor, the maximum net force (pull) it can exert is limited by the amount of shear stress it can produce at the soil-vehicle interface. It was shown by Von Sybel et.al. [16] that a wheel which is locked from rotation and pulled in a step-like manner can generate a much more uniform shear stress distribution over the contact patch than an identical rotating wheel can. Since the maximum shear stress occurring in both cases is the same, the net force generated by the pulled wheel will be greater. This indicates that walking vehicles are theoretically able to transfer more of their available power to the ground allowing them to climb steeper grades or drag heavier loads than a dimensionally similar wheeled vehicle with the same output power.

Rough terrain implies not only soft soils but high surface irregularity. a reduction in speed and increase in energy is required to climb over or traverse around surface irregularities such as large rocks, crevices, fallen trees etc. Obviously, the option of stepping over obstacles is not available to conventional wheeled or tracked vehicles. Even if a walking vehicle must step on or in an obstacle, given adequate active gait control, it does not necessarily need to raise its body mass center as would a tracked or wheeled vehicle. The ability to traverse

obstacles while minimizing the vertical oscillation of the mass center represents another theoretical energy cost advantage of walking over rolling.

Corresponding, with the significant advantages of ambulatory systems in off-road locomotion are significant unsolved problems which have succeeded thus far in constraining the major commercial use of walking machines to clever toys. As previously mentioned most recent work in walking machine technology has been in the area of controls. The energy cost problem of walking vehicles must now be addressed in the same systematic way in which motion control has. Otherwise the theoretical advantages of legs in rough terrain locomotion will never be realized by man made systems.

1.2 Requirements for Efficient Walking.

An essential criterion for a low energy cost ambulatory system is the ability to effectively exchange kinetic and potential energy within itself and the environment. Evidence of this is present in many biological systems including Man [20]. Consequently, if the mass center of the system rises during some phase of a stride then the system must be able to reconvert this potential energy into kinetic during the subsequent drop in the mass center elevation. or at least, the fluctuations in the mass center elevation must be kept to a tolerable minimum. It has been observed in human locomotion that the variation in body center of mass elevation decreases as forward velocity increases and that a significant portion of the energy required to raise the body center of mass is transferred to forward propulsion work [26].

If a leg is viewed as a completely separate system, the need for some conservative energy transfer mechanism becomes even more apparent.

All legs, robotic or animal show a common, fundamental trait. They all oscillate. A direct consequence of this is that the kinetic energy of the leg fluctuates greatly during a stride cycle. Regardless of the internal efficiency of the mechanism, energy is still required to accelerate the leg. An efficient leg will need to store a significant portion of the energy available when decelerating the leg and to make use of it for reacceleration or for some other positive work.

All present walking machines throw away the kinetic energy stored in the leg during the transfer phase. In the case of the OSU Hexapod this energy is stored principally in the high speed rotation of the azimuth joint actuator motor armature and amounts to approximately 22% of the total energy required for level, constant speed walking [42]. This is clearly an intolerable loss.

The overall effect of a legged vehicle system with good energy transfer ability will be a system that, like most biological systems, has a definite preferred walking speed or set of speeds. Each speed will correspond to a natural frequency of gait established by the exchange of energy between the legs, the legs and the body and between the system and the gravitational field. The control of the actuators of such a system should be of a pulsed nature so as to not interfere with the natural (designed) dynamics of the system but allow it to "free wheel" as much as possible [18].

1.3 General Leg Configurations.

There is an infinite number of conceivable mechanical leg configurations. Some types of legs will be better suited to the energy exchange concept than others. It may not be surprising that most of the walking

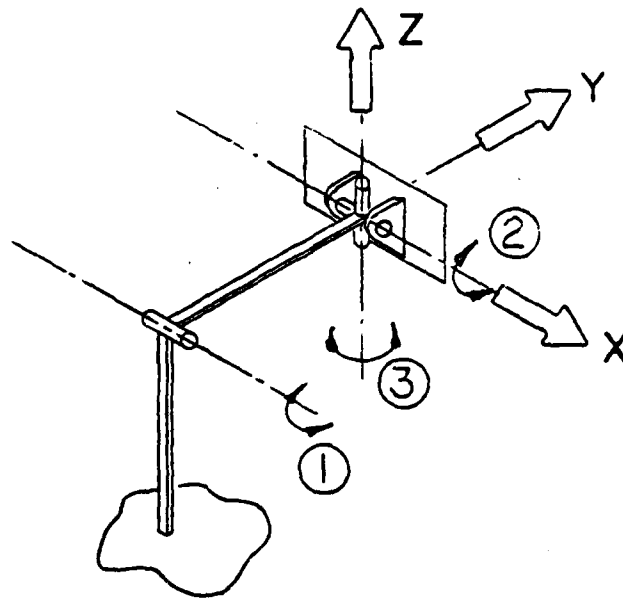


FIGURE 1.1 INSECT LEG DYAD MODEL

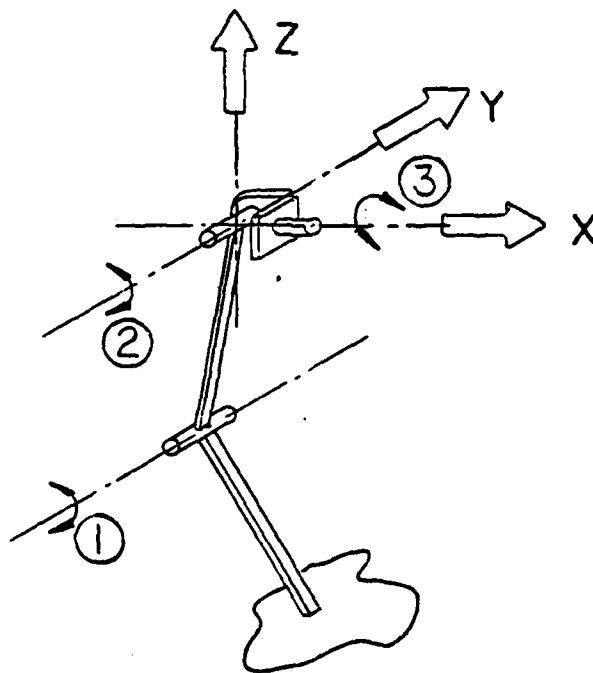


FIGURE 1.2 MAMMALIAN LEG DYAD MODEL

machines designed thus far have had legs which are morphologically similar to one of the two types used by biological systems.

All biological legs can be classified loosely as either insect type or mammalian type. Both can be simply modeled with three major degrees of freedom (see Figure 1.1 and 1.2). One distinguishing feature between these two basic leg types is the orientation of the principal plane of the leg with respect to the sagittal plane (long axis plane) of body symmetry. The plane of the insect (Arthropod) type leg is nominally perpendicular to the major plane of body symmetry. The plane of the mammalian (planar) leg is oriented parallel to the major plane of symmetry. Another essential difference between these leg types is that the insect leg motion is generally more three dimensional, whereas the mammalian leg essentially moves in a plane and therefore has generally two dimensional motion. The insect leg has been most often used on recent experimental walking machines [29, 29, 32]. The OSU Hexapod (see Figure Appendix C) is an example of a walking machine based on the insect leg dyad. The major motions of these legs is a rotation about the vertical "hip" or azimuth axis (axis 3 in Figure 1.1). For the foot tip of these legs to trace a path parallel to the body center line, the knee joint (joint 1 in Figure 1.1) must be flexed. This in turn necessitates corrective rotation about joint 2 if the body center of mass is to remain at a constant elevation.

The insect configuration has certain advantages. Principal among them is the high degree of stability afforded by the wide stance. Another major attribute is that the drive (azimuth) actuator does not carry the support load which is taken by the elevation actuator. Also, the nominal elevation of the body center of mass can be changed easily from a kinematic view point.

There are also major draw backs inherent in insect type legs. The large torque required at joint 2 (Figure 1.1) simply for support is possibly the worst. Particularly when an electric drive is used since electric motors perform poorly in low-speed, heavy-load situations. Another draw back from the energy view is that the major leg motion is nominally perpendicular to the gravitational field and therefore eliminates any possibility of establishing an energy exchange between the leg and the field. In addition, the advantage in stability gain by the wide stance of an insect configuration may well turn into an operational disadvantage. A wide machine requires an equally wide path, which is a serious consideration if a walking machine is ever to become practical.

The G.E. Quadruped [24] is one example of a machine built which employed a mammalian type leg. It is very similar, in fact, to the mammalian dyad model. A few other machines have been built with strictly planar type legs [4,5,30] which cannot be exactly classified as mammalian type since they lack a third degree of freedom.

There are several advantages to a mammalian leg, not least of which is its static load capability. The legs of most mammals, especially those of large quadrupeds, are positioned more or less to accept the standing weight of the animal in a columnar fashion. The resulting essentially compressive stress in the material of the leg can be carried more efficiently than the bending stress predominant in the insect dyad configuration. This may be a principle reason that the insect leg configuration is found in few animals that weigh more than a pound.* The basic geometry of the mammalian type leg allow it to interact with the

* The exception being some large reptiles such as crocodiles. However, these animals spend a great deal of their time lying on their bellies or swimming.

gravitational field in a manner similar to a compound pendulum. It is therefore possible to set up a kinetic potential energy exchange if a mammalian dyad is used.

Before dismissing the insect type leg as unsuitable for a practical vehicle it should be noted that it is not without adherents. Specifically, S. Hirose has stated in reference [33] that the insect type leg is, in fact, superior to the mammalian. Besides the already mentioned advantages of the insect type leg he maintains that it is not less energy efficient than the mammalian type. Reference [34] is sighted where it is reported that the energy consumption of a lizard and cat of the same weight was approximately the same for controlled treadmill walking. A similar conclusion is reached in reference [35]. However, data also presented in reference [35] indicates that a land crab has a minimum specific energy consumption per kilometer at least twice as high as a ground squirrel of approximately the same weight.

The validity of these comparison can be questioned when applied to ascertaining the kinematic/kinetic advantage of a particular leg type outside the context of the entire system. To be a more valid selection criteria for the leg type alone, the metabolic system driving each leg should be the same, ie, compare a regular cat with one having arthropod legs. This is not to repute the possible usefulness of these studies in choosing the best leg type for a walking vehicle. Another, possibly more significant, valid, observation can be made from these physiology studies which concerns the relation between the leg type and the total system mass.

It is apparent that there exists a size factor involved in nature's use of the two leg types. There is no evidence fossil or other-

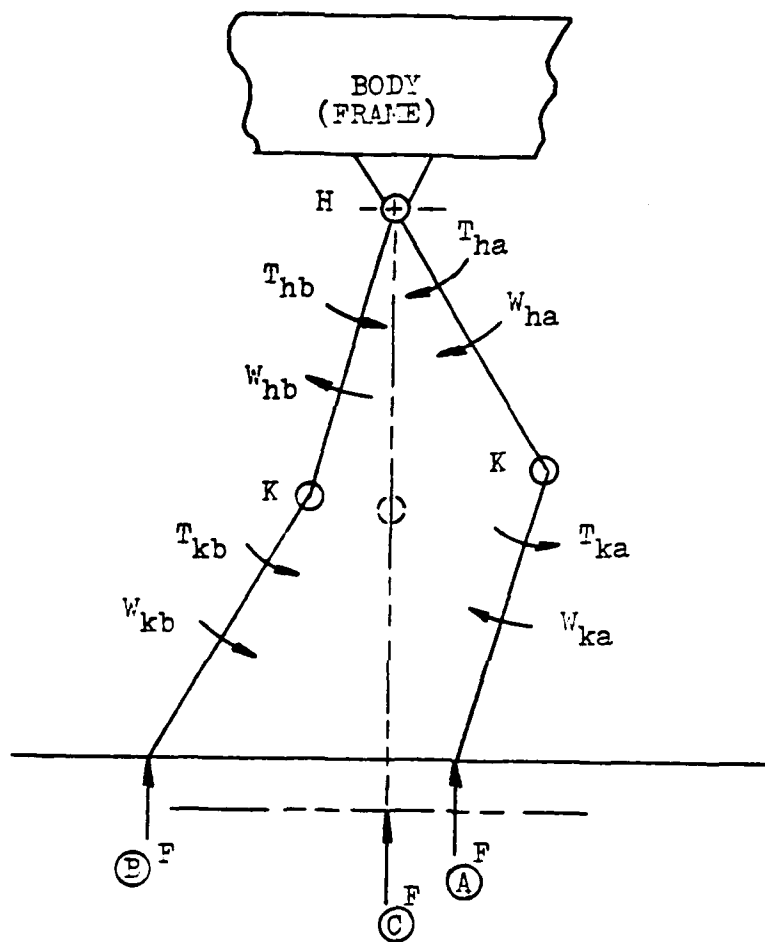


FIGURE 1.3 SIMPLIFIED LOADING OF
MAMMALIAN LEG

wise that nature has ever produced a long range ambulatory system, of a size similar to current land vehicles, which employ the insect type leg. However, nature has designed several multi-ton animals with mammal type legs including large dinosaurs (which may have also been cold blooded like modern reptiles).

In the larger mammals, in particular those which are the more efficient runners, the pendulating motion of the leg is apparent. This ability to establish a potential-kinetic energy exchange with the gravitational field is an important advantage to be considered for man made walking systems. It should be noted that, at least in the case of human locomotion, that this pendulation of the legs is not the only energy exchange mechanism used [26]. It does however, represent the most obvious and the easiest to implement in a robotic ambulator. As stated, it is a natural attribute of the joint orientation of a mammalian type leg.

Another attribute of the mammalian dyad can be, in theory, a major disadvantage. This disadvantage is also inherent in the joint arrangement and motion of the leg. Figure 1.3 is a schematic showing the mammalian dyad in three positions under a constant vertical ground reaction "F". A and B are arbitrary positions in the support phase of stride while C is the standing position. Assuming that the leg is controlled by input torques at hip joint "H" and knee joint K then it is apparent that required torques T_H and T_K must vary in magnitude and/or direction between A and B while no torque is required (ideally) in position C. Note that the joint torques and their rotation (ω_H , ω_K) do not always have the same sense. When the load torque at a joint has the same direction as the rotation about the joint the actuator does negative work on the leg. That is, it functions as a brake. This condition is often

termed back-driving. If the joint energy source were an ideal reversible process then a back-driven joint would be actually generating instead of absorbing power. In fact, with reference to Figure 1.4, if joints H and K had a common energy source and the motion was uniformly horizontal, then the energy required at H in Position A would be generated at K. In position B, the energy generated by the back driving of H would be completely used to drive K. This result simply restates the theorem of classical physics that no work is required to move, with constant velocity, a frictionless system along a plane, perpendicular to a gravitational field.

A problem arises when the torque generators at joints H and K are not capable of regeneration. This means that, at best, the back drive work is not available for use. Realistically, if the joints are driven directly by a servo motor then the back driven joints must be controlled with braking energy which has a positive cost in an energy audit.

To garner the inherent advantages of the mammalian type leg without paying the back drive energy cost, the leg must be designed to passively transmit the knee reactions to the hip and vice-versa. A careful study of the real mammal legs will show that nature has solved this problem by placing major locomotion muscles across more than one joint. This allows two simultaneous joint rotations by the action of one muscle. Consequently the real mammalian leg is a complex linkage system rather than a joint controlled dyad. Classical kinematics of planar mechanisms provide many possible mechanical analogues to the solution suggested by nature. Moreover, because of the ability of a linkage to maintain specific repeatable relationships between joint rotations, a certain amount of the coordination can be completely mechanical. In fact, the early investigations of suitable legs, in particular reference [4], concerned only link-

age mechanisms since even at this time (1961) computer control of three independent actuators was not feasible and leg control logic had to be essentially mechanical.

As has been mentioned, the major work of the past twenty years in walking vehicle technology has been directed toward solving the control problems uncovered by the early investigators. With the recent advances in digital computer technology, the control problems are being continually reduced and solved. However, mechanical logic can still play a significant role in ultimately solving the overall problem of a practical walking vehicle by minimizing low level servo control computation and execution times. It is significant that employing linkage mechanisms to increase the energy efficiency of a walking vehicle can also result in reducing the control problem. Representative of earlier thinking, reference [32] states that a major reason for choosing the insect dyad for the OSU Hexapod vehicle was that the mammalian leg apparently required more complex control since it only appeared on neurally more advanced animals.

1.4 Project Goals.

The object of the work documented by this thesis is to devise a leg mechanism that will demonstrate the advantages of a pendulating planar leg while avoiding the loss or penalty of back drive work. The advantages shall be demonstrated by showing that a significant reduction in power consumption can be realized by a leg designed from the theoretical considerations briefly discussed above. For purposes of power comparison the experimental leg has the same scale as the OSU Hexapod which will be used as the alternative arthropod machine with directly driven joints.

Formally this project can be divided into four sub tasks.

1. Kinematic synthesis and analysis of linkages to meet motion requirements.
2. Mechanical design of mechanism and actuator components based on kinematic and dynamic analysis such that frictional and inertial losses are held to a minimum.
3. Testing of the leg under load in various operating configuration and modes to assess the energy consumption.
4. Comparison and evaluation of energy/power data with respect to the OSU Hexapod vehicle.

Task 1 is discussed in Chapter 2, task 2 in Chapter 3, and tasks 3 and 4 in Chapter 7. Chapters 5 and 6 concern tasks essential to the completion of this project but for which the author was not primarily responsible. The discussion of the motor power control in Chapter 5 and the control program in Chapter 6 are included in this thesis principally for the sake of completeness. Wherever it is appropriate, the work of others will be acknowledged.

During the course of this project the mechanical leg systems under development has been referred to by various names. The leg linkage itself has been termed the "Planar Hexapod Leg". The leg-cart-control system has been given the name "Monopod" by those working on it. The official designation applied by the project sponsors (DARPA) is "Prototype Low-Power Leg" (PLPL). To avoid confusion, the prototype leg mechanism itself will be referred to as the planar leg while the leg-cart-control system will be referred to as the Monopod.

Chapter 2

KINEMATIC DESIGN OF LEG MECHANISM

2.1 Introduction

The initial scope of the project described in this thesis specified that a planar linkage leg be designed and constructed. It was decided that this leg should be on the same scale as the OSU Hexapod. Similarity in size between the Hexapod leg and the new linkage type leg would facilitate the required comparisons of energy consumption.

2.2 Choosing the 3rd degree of freedom.

A planar linkage has, by definitions, two dimensional motion only. This is not a problem if, as in the Shigley [4] or Aerojet General machines [5], turning is accomplished in a manner analogous to that of a tracked vehicle. However, much greater mobility and increased efficiency is attained if the vehicle can turn by changing its foot fall pattern in a direction transverse to the long axes of the body. All biological walking systems turn in some such manner. To accomplish this, the legs must each have a full three degrees of freedom. The third degree of freedom can be acquired by rotating the base link of the leg mechanisms with respect to the body. The orientation of the axis of this rotation dictates the dexterity with which the machine will be able to turn. It will also affect the complexity of the required control system.

The plane within which the axis of this third degree of freedom lies should be normal to the plane of the second degree of freedom to minimize actuator motion coupling. This restriction still leaves an infinite number of possible axis orientations. However, any orientation of the axis in the plane other than horizontal or vertical would disrupt the proper kinematic functioning of the leg mechanism. Carefull reexamination of Figures 1.1 and 1.2 will reveal that if the insect leg dyad were rotated 90° about joint 3, it would represent a planar leg with a vertical third axis. Thus the attitude of this axis with respect to the body is one of the essential differences between an insect type leg and a mammalian type leg. Intuitively this leads to the choice of parallel (abduction-adduction) axes since the planar leg mechanism is conceptually similar to the mammalian leg in operation. More rigorous reasoning also leads to this choice if the basic kinetics of each case is considered.

The required task of the leg regardless of axis orientation is to be able to generate any curvilinear foot path within its kinematic volume. In general, energy expended in generating a foot path is minimized if motion is concentrated, to the extent possible, in a single degree of freedom [18]. In a planar linkage leg the actuator activity is concentrated in the actuator driving the input crank. Thus motion about the third axis should be minimal. For this reason planar legs have a distinct advantage over an insect style, joint driven leg which uses two actuators to produce a straight line foot path. If vehicle motion is strictly straight ahead, the horizontal and vertical third axis orientations are equivalent. To perform a turning maneuver on level ground, vertical axes planar legs can only avoid using two actuators if the legs of the vehicle are coordinated as if they were wheels. This turning mode severely restricts the mobility of the vehicle.

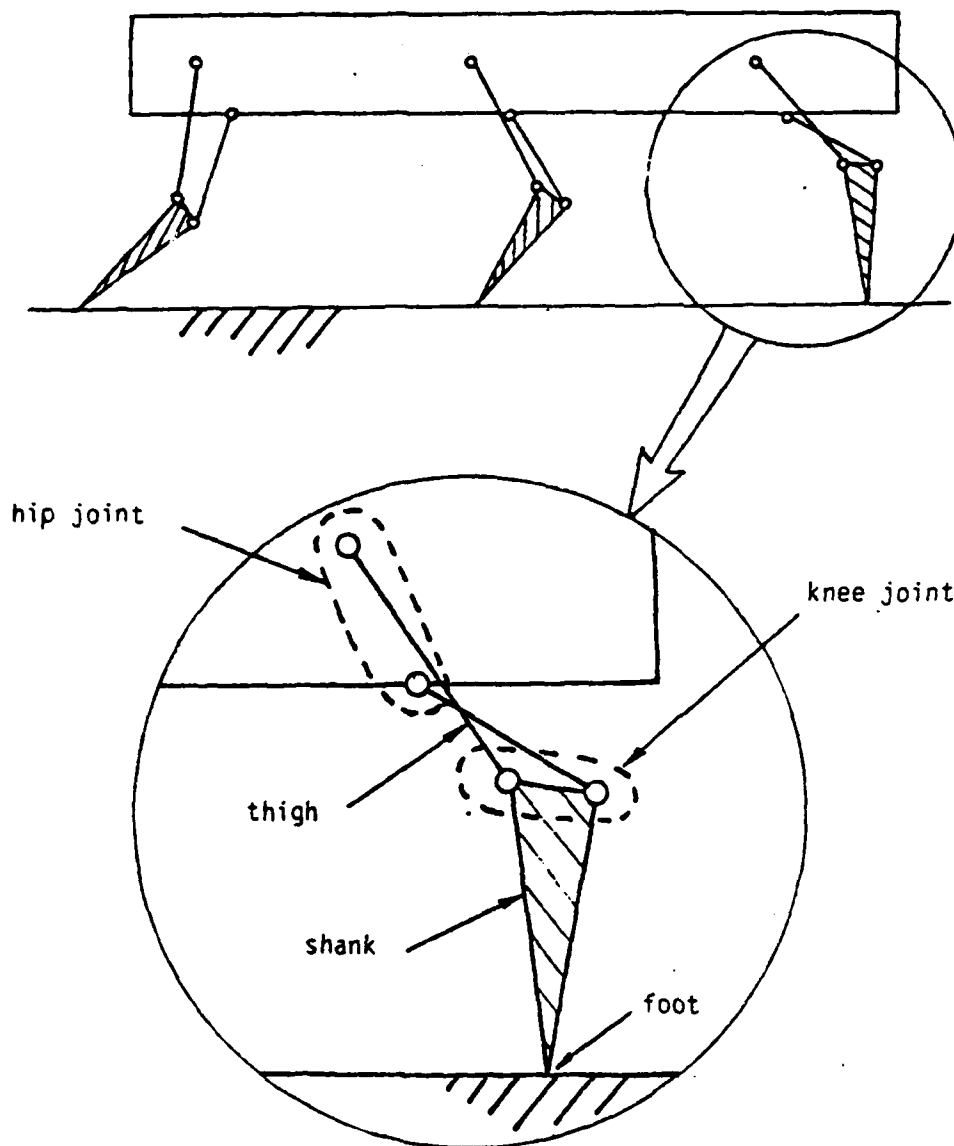


FIGURE 2.1 ANATOMY OF A FOUR BAR
LINKAGE LEG MECHANISM

A common operation for a walking system is to change stance width to suit a narrower path. This requires a foot path which is parallel to, but outside of the plane of the third degree of freedom. To trace this path a planar leg with a vertical third axis must rotate about it nearly 180° while servoing the "main" actuator to keep the foot on line in a manner exactly analogous to the insect type leg. For a planar linkage leg with a properly aligned abduction-adduction axis a foot path of this type can be generated using essentially only the "main" actuator in the same manner as for normal straight ahead walking. The only work done by the other two actuators is in positioning the leg before the start of the stride. Clearly this mode uses less energy since most of the motion is still confined to one actuator.

Acceptance of the above reasoning restricts the choice of the third axis to one that is parallel to the horizontal center line of the body and in the plane perpendicular to the plane of the second degree of freedom (hip joint). Unfortunately there are still an infinite number of possible axes. To narrow the field further, additional constraints can be applied by consideration of the required control algorithms.

To simplify the control program, the abduction-adduction axis should intersect the "hip" joint of the leg. This results in generally reducing the number of computations required and thus the execution time of a control program loop. In a four bar leg mechanism the "hip" joint is actually both of the fixed link joints (see Figure 2.1). It was decided only after the kinematic design was finalized to position the axis to intersect the crank center point farthest from the ground. This would allow the greatest abduction-adduction motion of the foot.

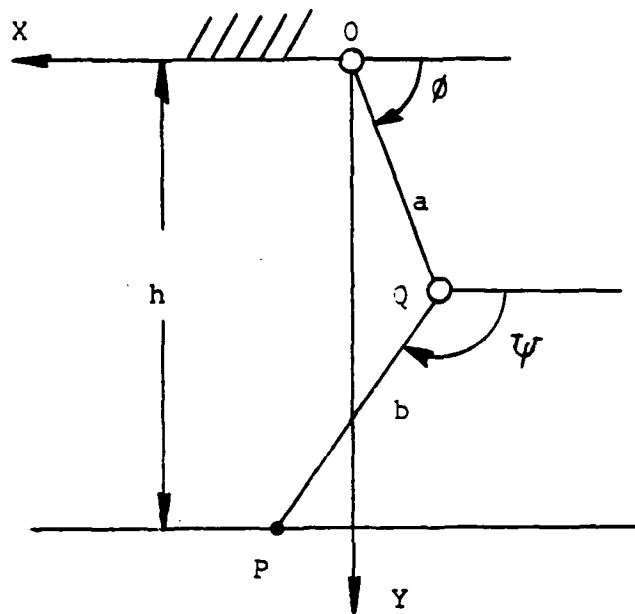


FIGURE 2.2 CONVENTIONS FOR KINEMATIC SYNTHESIS

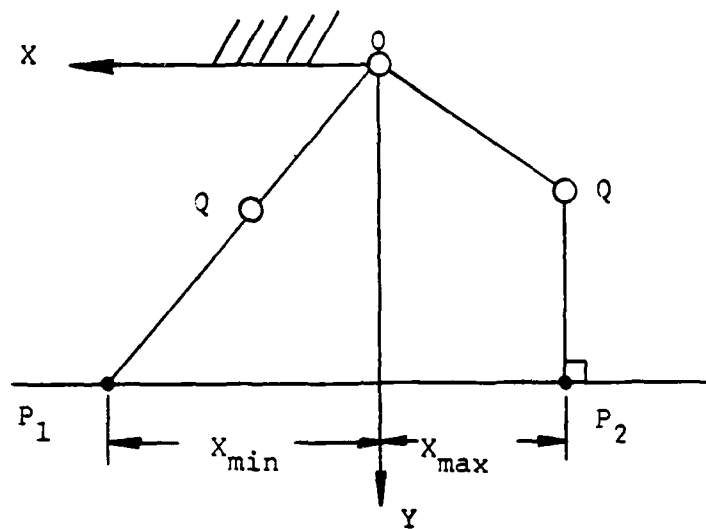


FIGURE 2.3 A FULL STEP OF THE WALKING MACHINE LEG

2.3 Synthesis of four bar leg mechanism.

The first step in producing a linkage leg is the kinematic synthesis of the various link lengths and joint positions from the motion requirements. The basic motion required of the leg was geometrically simple, a straight line. However, if curvilinear motion is specified as the input the problem becomes more difficult, as James Watt and others have previously acknowledged.

For a single rotary input and approximate straight line output motion, four bar mechanisms provide the simplest solutions. Graphical and analytic methods for finite position synthesis of four bar mechanisms can be found in any good applied kinematics text such as references [1] or [6].

Figure 2.2 shows a dyad model of the leg used to determine the design positions of the leg linkage. Referring to Figure 2.2, the origin "0" is fixed to the machine frame, h is the working height, a is one of the cranks, and b is a line on the coupler. Point P, the foot point, is constrained to move in a straight line parallel to the x axis. Figure 2.3 defines the required extent of motion of foot point P.

Given the restriction of the linkage geometry to four bar mechanisms, it is not possible to find a solution linkage that will generate a perfect straight line from x_{\max} to x_{\min} . In fact, the path generated will be a sixth order curve. It is only possible to constrain the linkage to pass point P through discrete points which lie on the ideal straight line thru P_1 and P_2 . Although more precision points can be used in theory[†], the existence of a real solution is guaranteed for a

[†] The greatest theoretical number of precision points that a four bar can be constrained to is 9 on a general curve and 6 on a straight line [1].

maximum of four points. This results from the fact that for five or fewer precision points, the point position problem can be solved as a rigid body guidance problem. The rigid body problem can be considered a subclass of the point position problem. In addition to specifying a set of points in the fixed plane that the coupler point must pass through, rigid body guidance requires a corresponding set of angular displacements of the coupler plane. For five specified positions of a rigid body, the synthesised four bar mechanism is unique, if it exists. For four or fewer positions there exists, in theory, an infinite number of solutions [1]. By using four positions rigid body guidance synthesis, added control over the physical size and working volume of the linkage is gained. The possible cost of this control is a degradation of straight line motion. It should be noted however that since this solution space is infinite, it is entirely possible to find a four bar linkage synthesized from four positions which will approximate the straight line between the designated precision points as well or better than a five or greater point synthesis (by point position reduction). Such a large solution space is difficult to adequately investigate without the aid of a computer and efficient programs.

The interactive program used to synthesize useful solutions is described in references [2] and [7]. The program, called RECSYN, greatly simplified the task of defining solution linkages. Further, RECSYN provided the opportunity to map and investigate the four bar solution space to this kinematic synthesis problem. Therefore crank-rocker solutions could be compared with the rocker-crank and double rocker solutions. This initial investigation was largely carried out by Mr. Shin Min Song and described in reference [3].

In order to use RECSYN the four design positions must be defined in a manner consistent with the input format, four points on directed line segments defined by the point coordinates and an angle measured counter clockwise from the horizontal axis. From Figure 2.2 the constraint equations are

$$h = a \sin \phi + b \sin \psi$$

$$-x = a \cos \phi + b \cos \psi$$

These equations can be solved for ϕ and ψ in terms of a , b , h , and x . the solutions are

$$\tan \frac{\phi}{2} = \frac{B + A^2 + B^2 - C^2}{A - C}$$

where

$$A = 2ax$$

$$B = -2ah$$

$$C = a^2 + h^2 - b^2 + x^2$$

and

$$\tan \frac{\phi}{2} = \frac{B' + A'^2 + B'^2 - C'^2}{A' - C'}$$

where

$$A' = 2bx$$

$$B' = -2bh$$

$$C' = b^2 + h^2 - a^2 + x^2$$

In an effort to reduce the path deviation between precision points, Chebychev spacing was used to pick four points in the range of x . Then a judgment was made concerning the length ratios between a , b , and h . It was decided to choose $a = b = 1.0$ as a starting point since this is approximately the porportion of the human leg (a proven efficient walking machine). The range of h was choosen to be between 1.3 and 1.9 ($1.3 < h < 1.9$).

2.4 Kinematic and force analysis of leg mechanism

From these parameters several candidate leg designs were defined. To further investigate these designs, a general four bar analysis interactive program was written. This program, called FORBAR, was necessary for precise coupler point curve comparisons along with angular velocity, acceleration, and force analysis of the various candidate mechanisms. Further, this program has the ability to selectively alter the length of any link in the mechanism so that off design behavior of the mechanism can be investigated without defining a new mechanism. This feature of the program was most essential since the return phase of the stride cycle requires that one of the link lengths change to provide ground clearance. It is also necessary that the leg be able to alter its working height for the negotiation of obstacles. Using this feature of the program the behavior of each candidate leg linkage in all probable modes of operation was investigated for comparison. Due to simple structural considerations the adjustability of the mechanism was restricted to the cranks.

The force analysis feature of the program was used to compare the required input drive torque for the specified drive crank and a constant load vector acting at the coupler point (foot) for each of the candidate linkages. The bearing reactions were also computed for comparison. By changing the direction of the load vector, the program was able, in a simplified way, to simulate the effect of the leg walking up or down different grades or accelerating the main frame. It should be noted that this force analysis ignored dynamic loads by considering the leg links massless. The actual leg weight was lumped with the body. This is justified for the case of the electric prototype leg due to the low design speed (12 in/sec). In fact, it can be justified for much higher

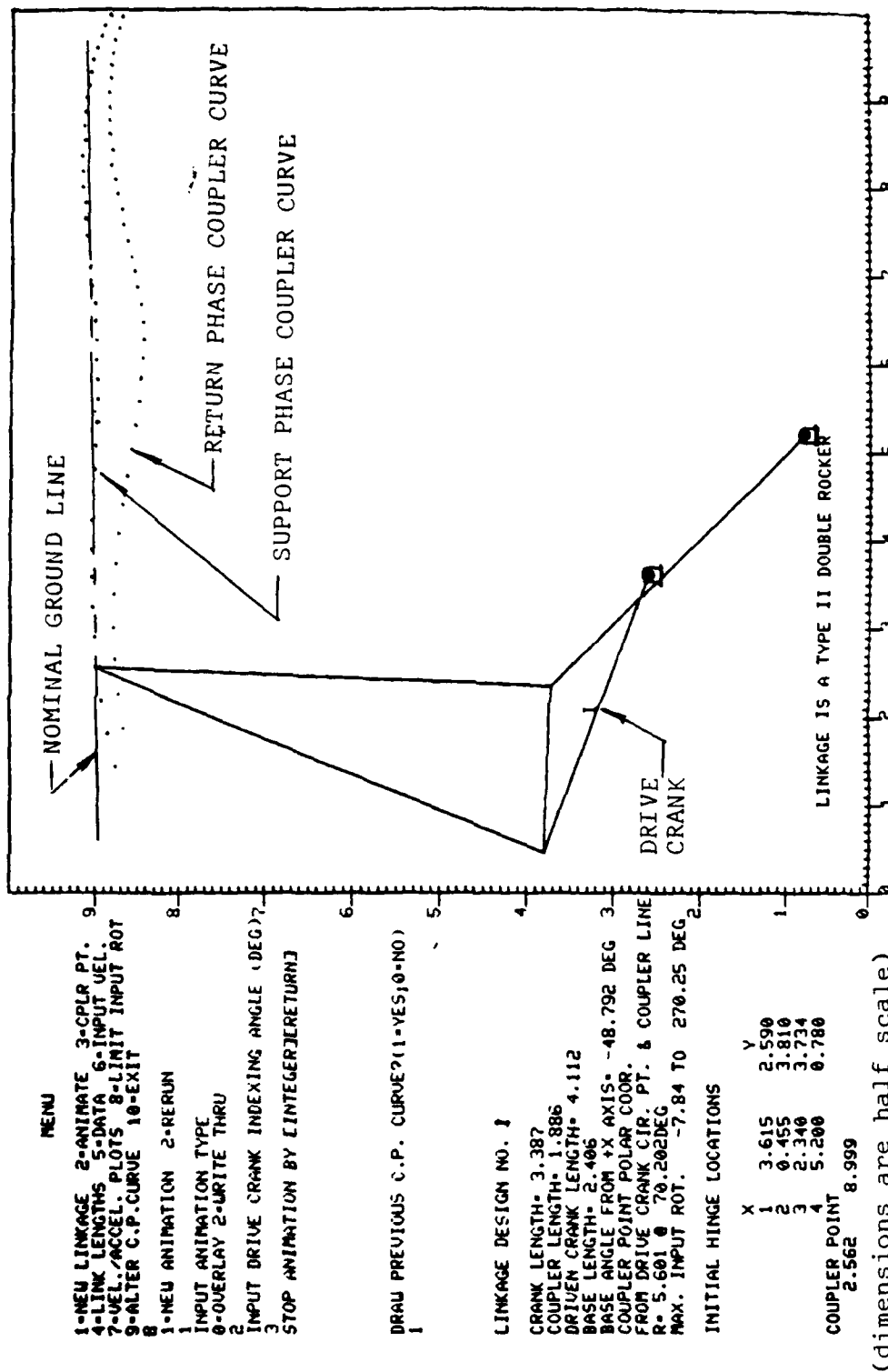


FIGURE 2.4a SCHEMATIC OF PLANAR LEG FROM FORBAR PROGRAM

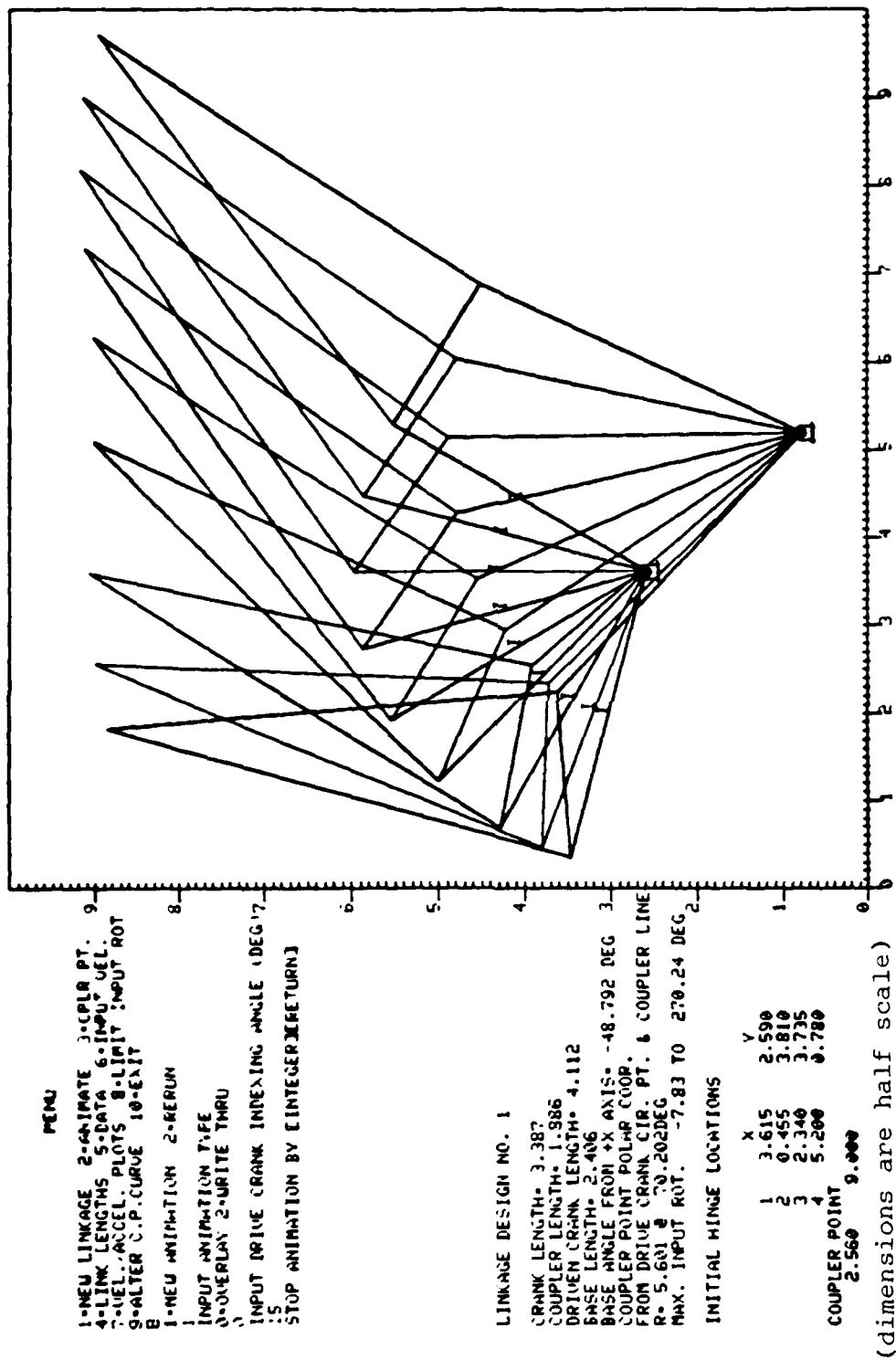
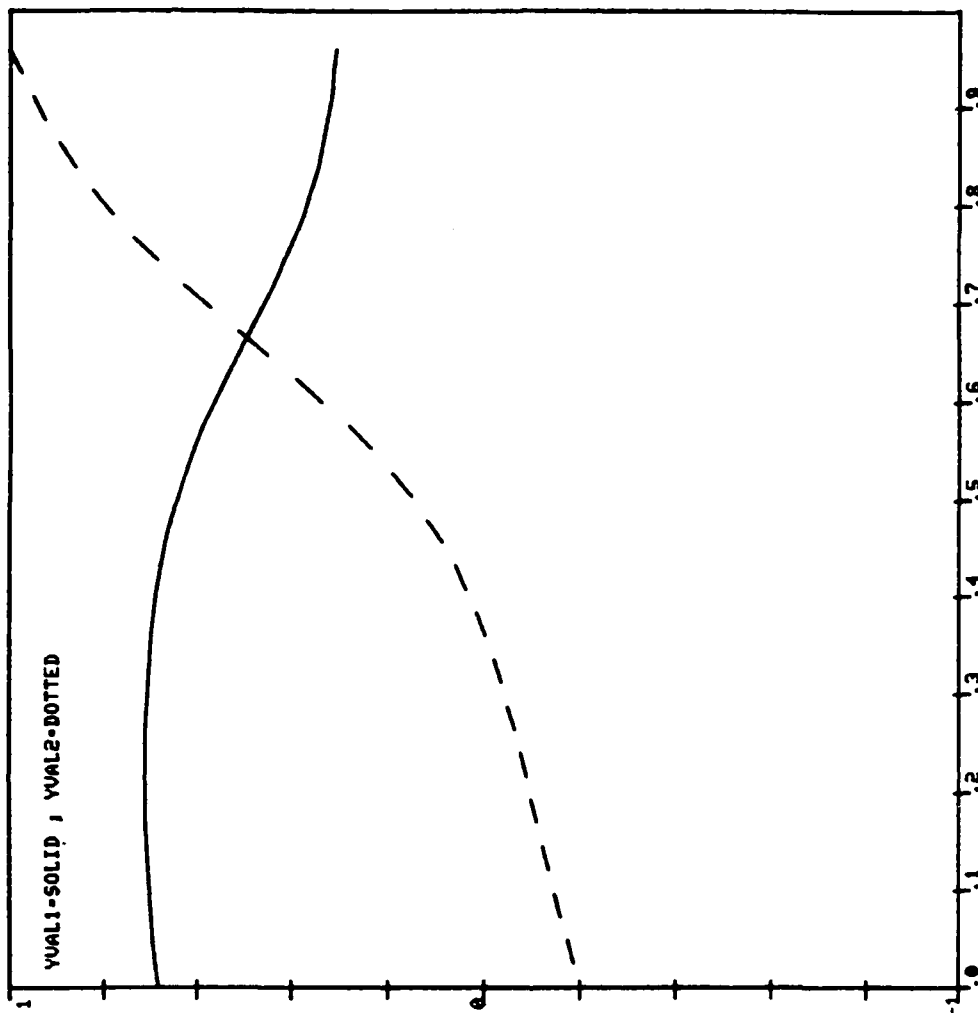


FIGURE 2.4b ROTATED SCHEMATICS OF PLANAR LEG FROM FORBAR PROGRAM

LINKAGE DESIGN NO. 1
YVAL1-DRIVEN CRANK ANGULAR VEL.(+CCU)
YVAL2-COUPLER ANGULAR VEL.(+CCU)
DRIVE CRANK VELOCITY- 1.000 RAD/SEC

DO YOU WANT TABULAR RESULTS?
0=NO 1=DISPLAY 2=DISPLAY/HARDCOPY

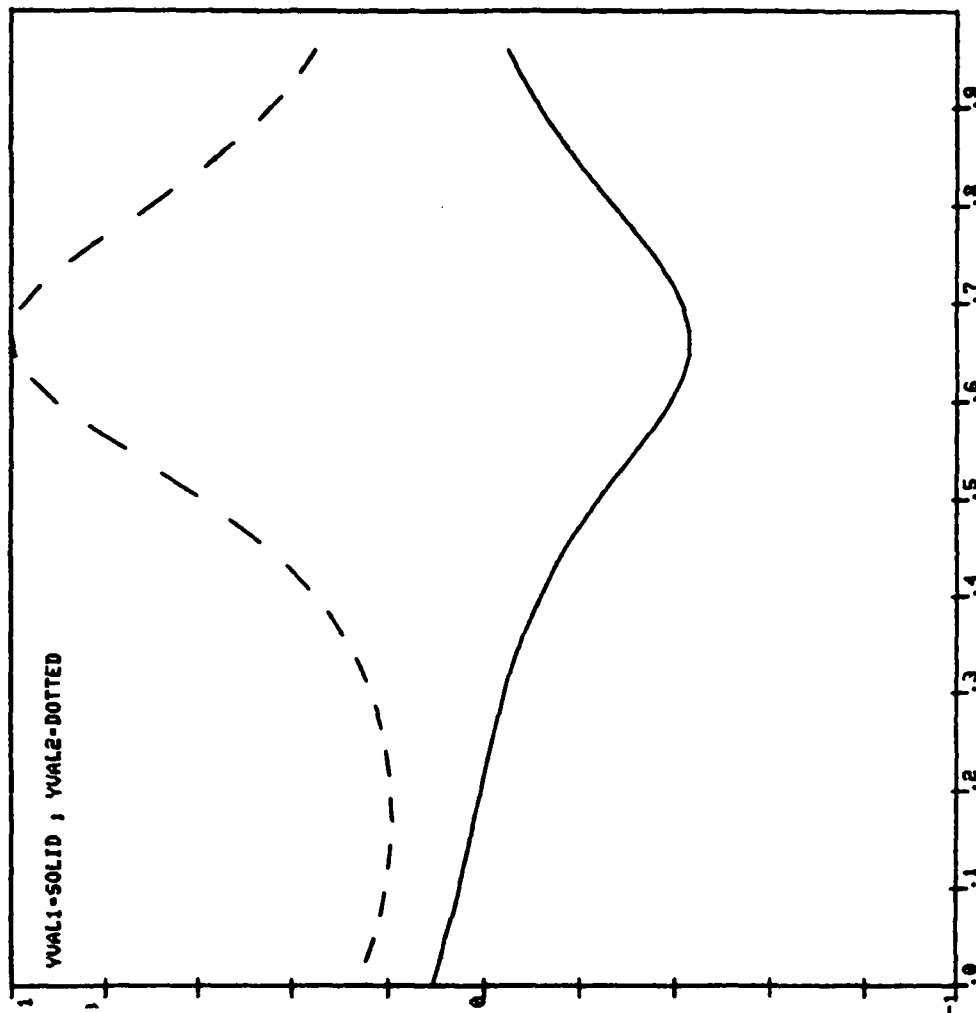


DIMENSIONLESS PLOT, Y/VMAX VS θ TOTAL DRIVE CRANK ROTATION
YMAX- 1.180; ROTATION- 45.000 TO 170.001 DEG

FIGURE 2.5
from FORBAR program
ROTATIONAL VELOCITY OF
DRIVEN CRANK AND COUPLER
BAR VERSES DRIVE CRANK
POSITION

LINKAGE DESIGN NO. 1
 YVAL1-DRIVEN CRANK ANGULAR ACCEL.(+CCU)
 YVAL2-COUPLER ANGULAR ACCEL.(+CCU)
 DRIVE CRANK VELOCITY- 1.000 RAD/SEC

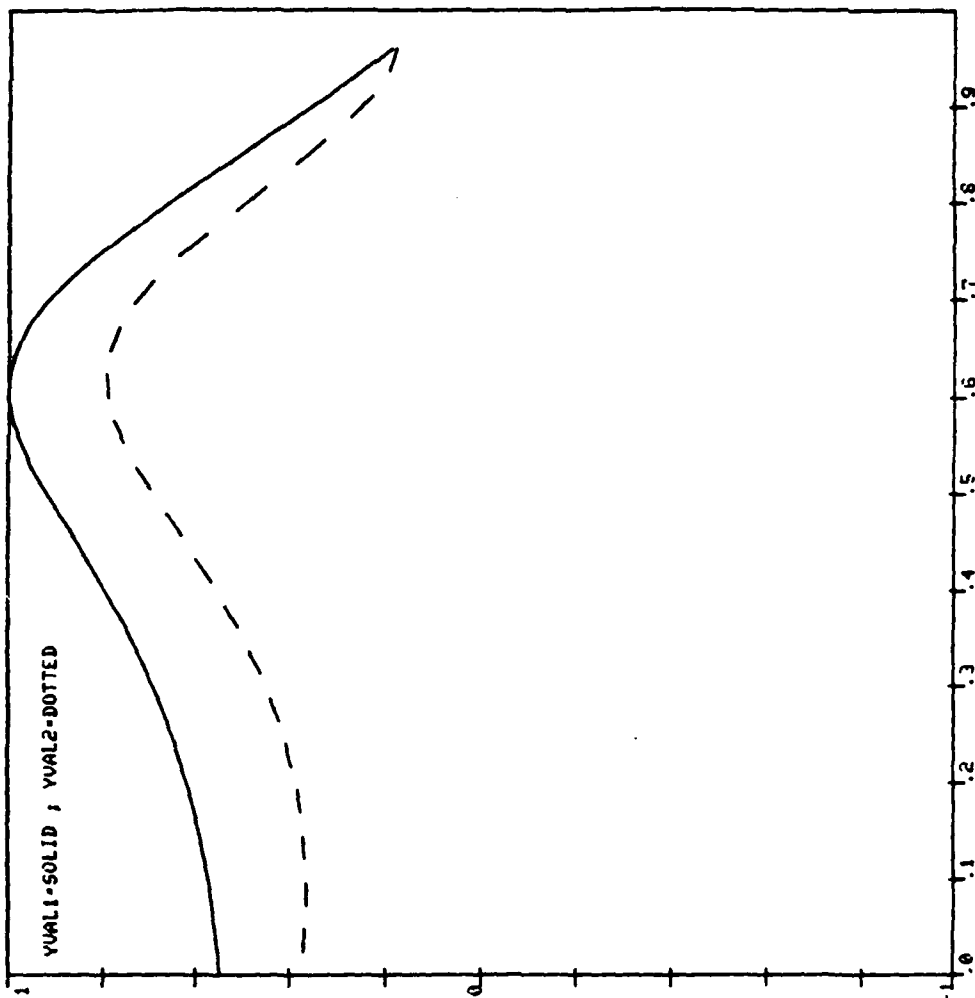
DO YOU WANT TABULAR RESULTS?
 0=NO 1-DISPLAY 2-DISPLAY/HARDCOPY



DIMENSIONLESS PLOT, Y/YMAX VS X TOTAL DRIVE CRANK ROTATION
 YMAX- 1.357, ROTATION- 45.000 TO 170.001 DEG

FIGURE 2.6
 from FORBAR program
 ROTATIONAL ACCELERATION
 OF DRIVEN CRANK AND
 COUPLER BAR VERSES DRIVE
 CRANK POSITION

LINKAGE DESIGN NO. 1
 LOAD AT COUPLER POINT
 FIX1= 0.000 F(Y)= -110.000
 VVAL1=DRIVEN CRANK BEARING LOAD
 VVAL2=DRIVE CRANK BEARING LOAD
 INPUT INTEGER FOR NEXT PLOT

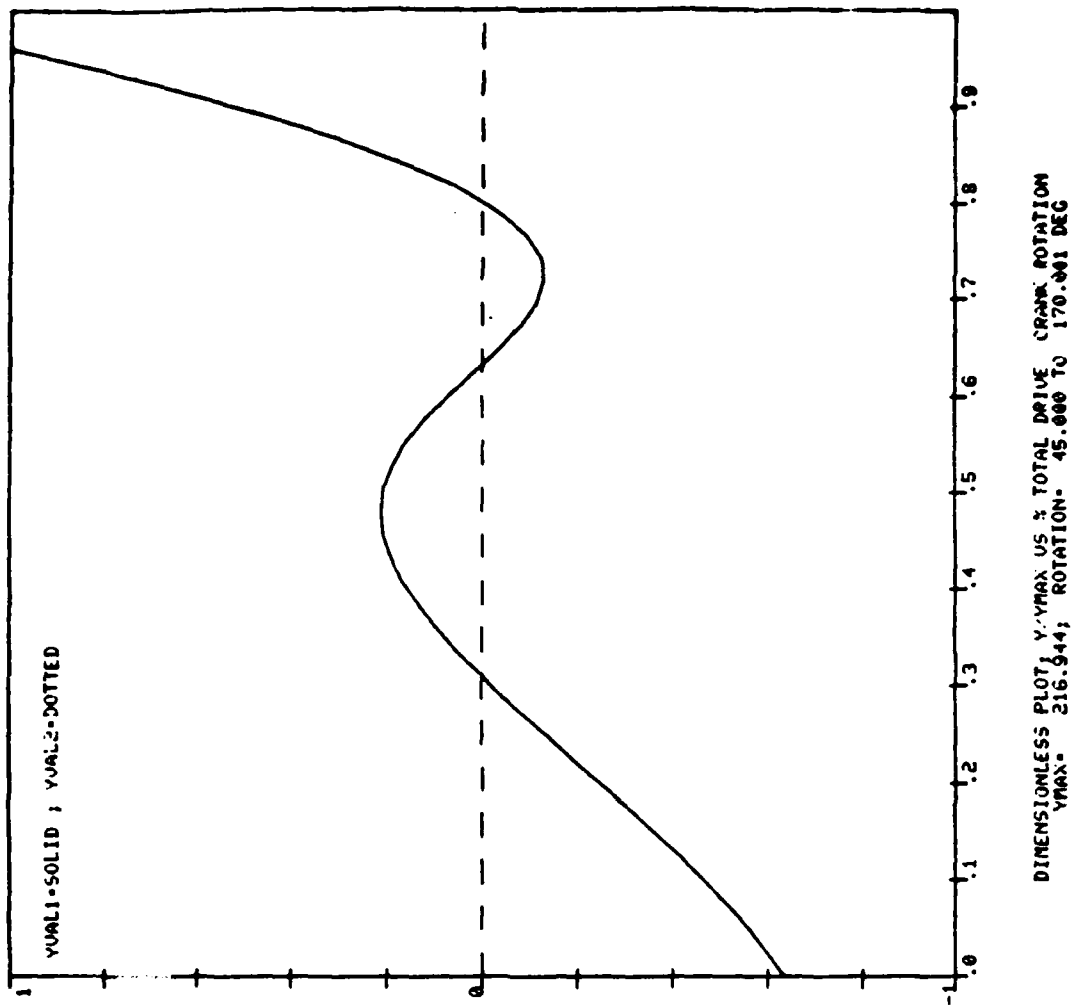


DIMENSIONLESS PLOT; V VMAX US % TOTAL DRIVE CRANK ROTATION
 VMAX= 454.270; ROTATION= 45.000 TO 170.001 DEG

FIGURE 2.7
 from FORBAR program
 DRIVE AND DRIVEN CRANK
 BEARING LOADS VERSES
 DRIVE CRANK POSITION

LINKAGE DESIGN NO. 1
 LOAD AT COUPLER POINT -110.000
 FIX: 0.000 FIV: -110.000
 YVAL1-REQUIRED TORQUE AT DRIVER
 DO YOU WANT TABULAR RESULTS?
 0-NO;1-YES...

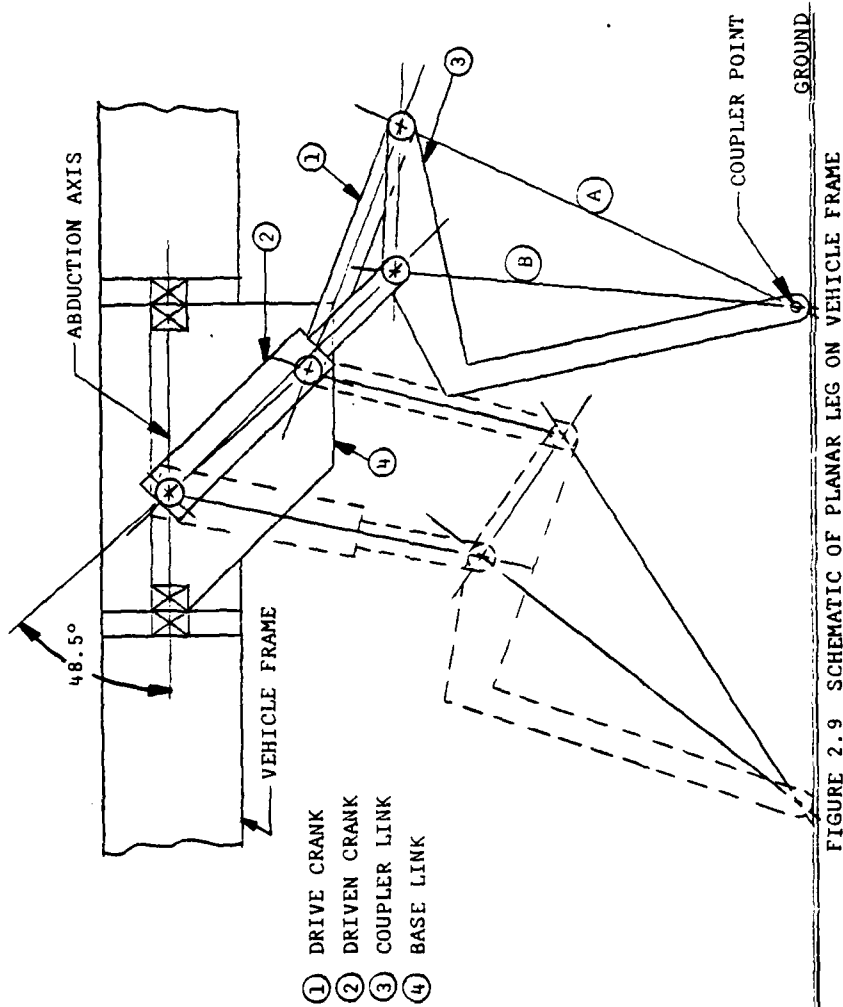
FIGURE 2.8
 from FORBAR program
 DRIVE CRANK TORQUE VERSES
 DRIVE CRANK POSITION



speeds or even larger legs by considering that the input load at the foot is always much greater than the inertial loads of the links and therefore governs the design.

It was decided for comparison purposes and for a mechanical design parameter to use an input coupler point (foot) load of 110 lb. This represents half of the OSU Hexapod weight. It was further decided to simulate the effect of the leg walking up and down 10% and 20% grades. These five cases (0, ± 10 , $\pm 20\%$ grade) were run for each of the candidate linkages. The final choice for the prototype leg was based on the peak drive torque required, bearing loads, and overall compactness as well as its ability to trace a straight line with the coupler point. Figure 2.4a and 2.4b shows a schematic of the final kinematic design for the electric prototype leg as drawn by the FORBAR analysis program. The link dimensions given on these figures are half scale. Figures 2.5, 2.6, 2.7, 2.8 are dimensionless plots of angular velocity, angular acceleration, bearing reactions, and input torque plots for this leg in level walking at 12 in/sec. Further investigations of this linkage resulted in choosing the shorter of the two cranks as the input. The longer crank was chosen as the adjustable link and the coupler point was shifted slightly which reduced the peak torque.

A secondary consideration in the choice of this design was the relatively smooth change in foot velocity during ground contact for a constant rotational velocity of the input crank. The coupler curve shown in Figure 2.4 as the dotted line qualitatively illustrates this since each dot represents equal angular increments of the drive crank (labeled "I" in the figure) and thus equal time increments if the crank is driven with constant velocity. Most desirable is a constant foot velocity for constant crank velocity. Excluding this, it is desirable to maintain a



monotonic change in foot velocity which avoids a sign change in the crank acceleration when the foot is required to move with constant velocity. This will tend to keep the drive actuator torque load from changing sign during the stride portion of the leg cycle. Under these conditions any backlash in the drive actuator will be unloaded only at the beginning and end of the stride. Consequently, the margin for instability in the motor velocity control feedback loops should be widened. Figure 2.9 is a more detailed schematic of the leg in its operating positions.

There are two general modes of operation of this linkage leg. One is that in which the adjustable crank is activated only for toe down and toe off. The other is that in which the adjustable link is active during the entire cycle so that some arbitrary foot trajectory (within the working volume of the leg) can be followed. This mode is needed for obstacle avoidance or vehicle attitude control. It was therefore necessary that the FORBAR program be able to accept some arbitrary coupler point curve and constrain the foot (coupler) point to follow this curve while calculating and recording the required change in adjustable crank length as a function of input crank position. This feature allowed investigation into the total mobility of the leg as well as providing data required later in the mechanical design of the linear actuator itself.

The final decision to be made concerning the kinematic design of the leg was the selection of the input crank operating range. The operating range of the crank is determined by that portion of the coupler curve selected as the nominal ground contact phase. The foot would be in contact during this phase for cruising over level terrain.

Referring again to Figure 2.3 the coupler curve appears relatively flat between .15 and .95 on the horizontal axis. This corresponds to

input crank position between 40° and 160° as measured counter clockwise from the right horizontal axis. With the nominal crank operating range thus defined, the last procedure was to determine the orientation of the leg with respect to the vehicle or more specifically the prototype test cart.

The orientation was fixed by establishing a line tangent to the coupler point curve at the two relative maxima which occur in the nominal ground contact phase (see Figure 2.4a). The angle between this line and the containing the two crank center points (base link center line) should be the same as between the base link center line and the vehicle center line. This choice of orientation minimizes the change in vehicle c.g. elevation due to the deviation of the coupler point curve from a straight line.

The full scale ideal center to center dimensions of the final kinematic design of the prototype leg (refer to Figure 2.9) are as follows:

1. Drive Crank	6.774"	3. Coupler Link	3.772"
2. Driven Crank	8.224"	4. Base Link	4.812"

Coupler Point

A - distance from drive crank circle point	11.202" .
B - distance from driven crank circle point	10.540" .

Angle between the base link center line and horizontal
(theoretical ground line) $\approx 48.5^\circ$.

The actual ground line is defined by the orientation of the leg in the test cart which is described in Chapter 4.

Chapter 3

MECHANICAL DESIGN OF LEG MECHANISM

3.1 Introduction

With the kinematic design frozen and the loading information obtained from the analysis program, the actual sizing and design of the various mechanism components could commence. Before the actual drawing started, some overall design criteria were formulated based on the performance requirements of the final system. The most pervasive design consideration limited the performance to concept verification and therefore the operation of the system to a laboratory environment. This significantly relaxed the requirements on components such as the bearing seals and the general need to protect precision surfaces or electrical circuitry from contamination. More importantly perhaps it allowed design simplicity to override reliability and thus reduce the total cost and manufacturing time required for the planar leg.

The decision to use electric motors as prime movers in the system also directly affected the final geometry. However, this was not a completely arbitrary decision but was based largely on the lack of small standard fluid power motors, control simplicity, and consideration of maintaining the laboratory environment. (Experimental hydraulic systems tend to leak.)

The total mechanical system design problem can be conveniently divided into two parts, the leg mechanism and the testing system. This chapter will deal only with the leg mechanism, including actuators.

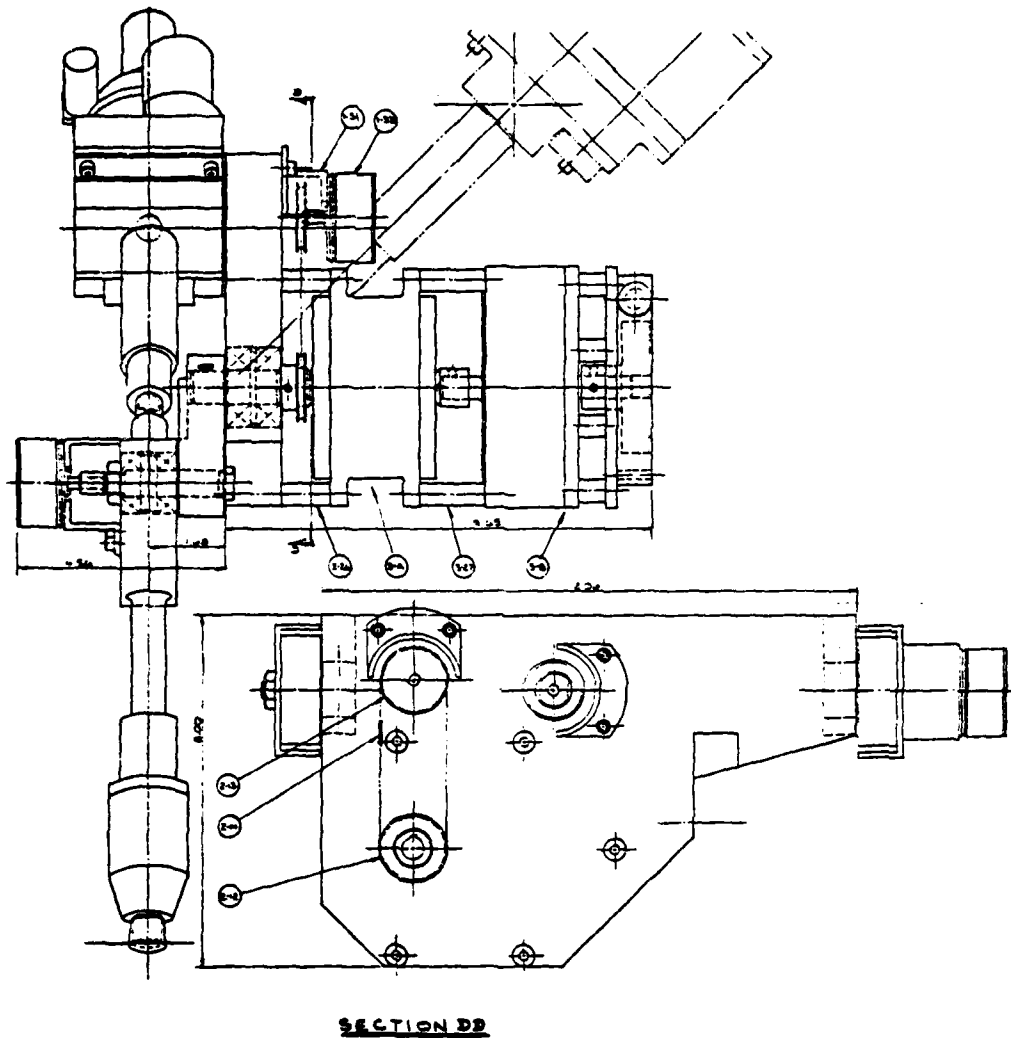


FIGURE 3.1B GENERAL ASSEMBLY OF
PLANAR LEG MECHANISM

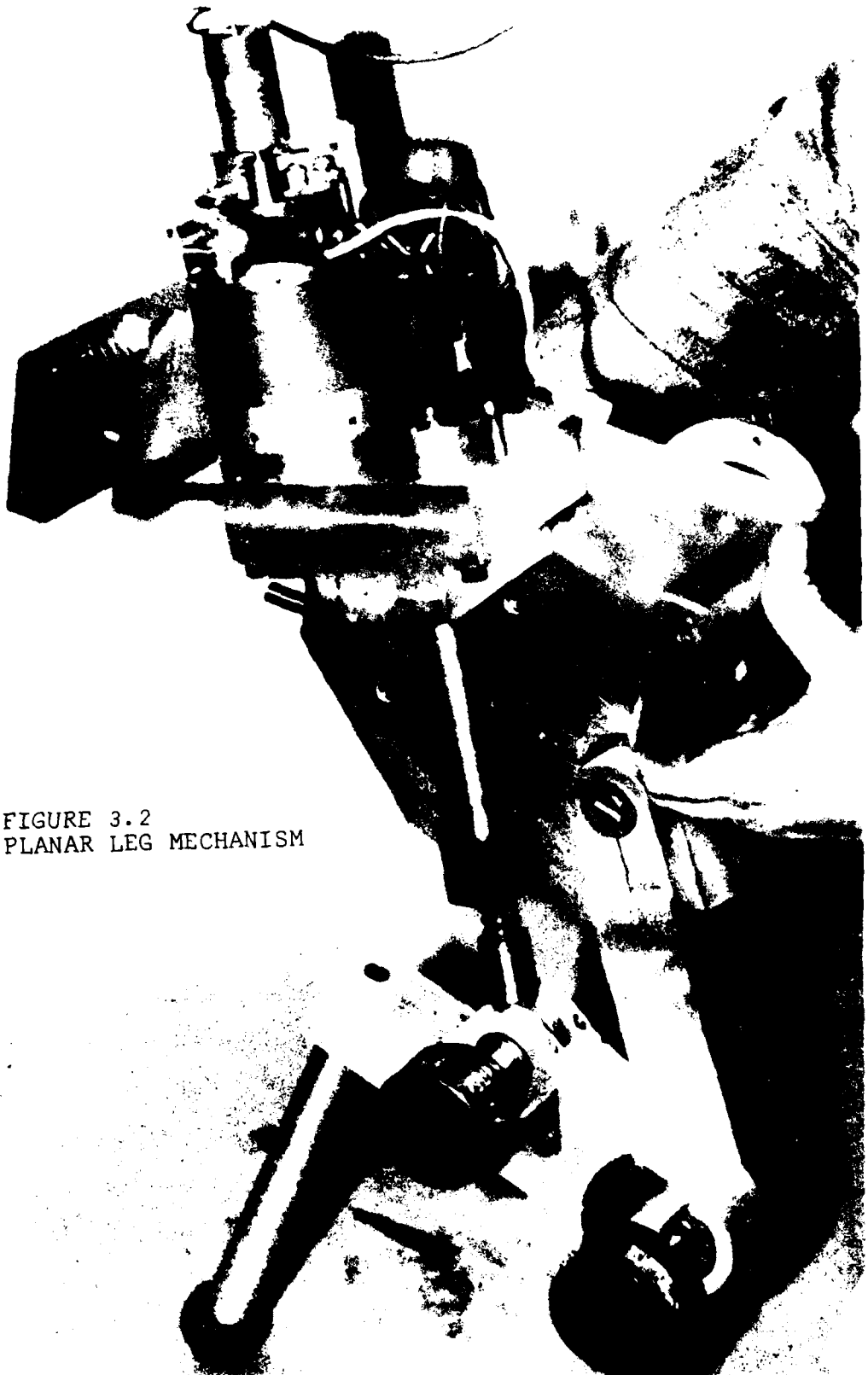


FIGURE 3.2
PLANAR LEG MECHANISM

Chapter 4 will deal with design of the testing systems for the leg mechanism.

As follows from good engineering practice, the design process was lead by the evolution of an accurate full scale assembly drawing of the leg mechanism. The assembly layout in machine design is the stage at which the various conflicting requirements such as strength, stiffness, weight, size, standard component availability and functions meet and are compromised to arrive at an acceptable if not optimum solution mechanism. Figures 3.1A and B are the final product of this process. Figure 3.2 is a photograph of the actual finished leg assembly before it was installed in the test cart. For the purposes of discussion the leg mechanism can be divided into a number of major components and subassemblies. In the order of decreasing complexity, these subsystems are linear actuator, main drive actuator, coupler, base link plate, drive crank and shaft. There are miscellaneous components such as bearing spacers, mounting brackets, etc which will not be described in any detail since their design is explicitly defined by their use.

3.2 Linear actuator.

Figure 3.3 is a photo copy of the linear actuator general assembly drawing. This actuator design was used for both the driven crank and the abduction-adduction actuator. Besides reducing the total amount of design work required, using identical actuators provided a backup for the heavily used driven crank. (The abduction-adduction actuator was not essential for the initial tests.) Because the driven crank had the more demanding performance requirements, the actuator was designed almost exclusively for this role. Obviously this means that the abduction-

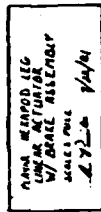


FIGURE 3.3 LINEAR ACTUATOR GENERAL ASSIMBLY

adduction actuator was over designed. This was, however, quite acceptable based on the time savings alone.

Throughout the entire design there was a constant need to reduce friction and stiction to the extent possible with standard bearing types. For this reason a ball screw and nut arrangement was used to transform motor rotation into linear motion. From the various manufacturers of ball screws the Sagnaw standard 5/8 x .200 rolled screw and single ball nut was chosen. They provided adequate accuracy and efficiency at a fraction of the cost of a precision ground set. The general arrangement of the actuator is of the screw-in-tube type used in many commercial screw actuators. The rather stringent geometry and performance criteria of the driven crank made the adaptation of a commercial unit impractical.

The basic design criteria for the drive crank were as follows:

1. Minimum of 2" travel
2. 550 lb axial load
3. servo rate under load .30in/sec minimum
4. less than 3.5" wide
5. position and rate sensors required
6. repeatable positioning to $\pm .010$ ".

The short travel required of the actuator allowed a blind tube design to be used which resulted in a more compact unit. The final design provides a maximum travel of 2.51" which is more travel than the mechanism can use without locking up.

The 550 lb axial load is the maximum driven crank bearing force computed by the Forbar program. This loading occurs once a cycle during 20% grade descent. No bending loads were considered since the drive crank was to carry any side loads on the leg. The maximum axial load can be

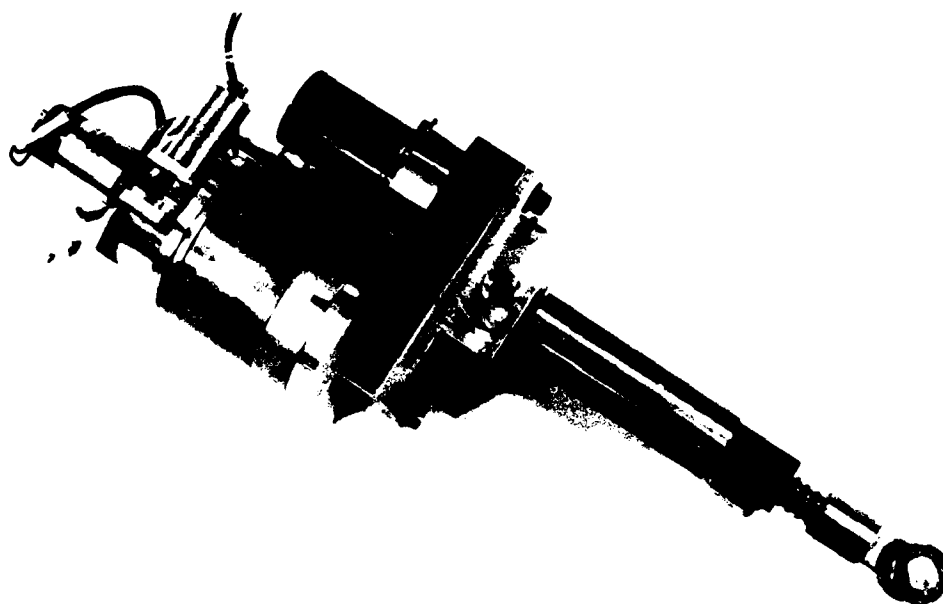


FIGURE 3.4 LINEAR ACTUATOR ASSEMBLY

translated into a maximum drive torque T_d by

$$T_d = \frac{Pl}{2\pi e}$$

where

p = axial load

l = screw pitch

e = screw efficiency

Ball screw efficiencies are commonly about 90% therefore the peak drive torque on the screw tube is 19.45 in lb. This assumes, of course, that the motor or brake have the required capacity. With maximum torque known and some estimate of the required servo rate, the drive motor and gear train could be sized.

The design servo rate was arrived at by using the average driven crank length change per degree of drive crank rotation over the nominal stride length to maintain a straight foot trajectory. This value was computed to be $\sim .001$ inch/degree. The average change in the x position (parallel to ground) of the foot over the nominal stride length per degree of drive crank rotation is $\sim .16$ inches/degree. The nominal design ground speed was chosen to be 12 in/sec. Therefore by simple ratios the average servo rate is calculated at .075 in/sec. To provide for the eventuality of requiring a more severe corrective action for some later test program, this rate was multiplied by a safety factor of 4.0 which places the design servo rate at .30 in/sec. With a ball screw pitch of .200 inches the required average drive spindle rotation under load is 90 RPM.

Optimally the spindle should be directly driven by the actuator motor. In this way the motor windage and bearing losses along with the

stored kinetic energy of the armature would be minimized. However this would demand an overly large motor due to the low-speed torque required. A single stage spur gear reduction was considered to provide sufficient freedom in motor selection with a minimum of efficiency loss. For the maximum actuator width allowed, a 5 to 1 single reduction gear set was designed using standard Boston 20 diametral pitch, 20° pressure angle steel gears. A 12 tooth pinion was used with a 60 tooth gear. The face widths were reduced to .350 inch from the standard .500in to increase the gear set efficiency. The AGMA factors of safety computed for this gear set are; 3.0 for strength and 1.0 for wear (see Appendix A).

The motor specifications were now sufficiently defined to make a selection. The minimum requirements were:

- Torque @ 450 RPM = 62 in/oz
- not over 3.0" diameter
- as light as possible

In general, the desired motor would be small, light weight, have high torque, and operate with minimum I^2R loss. This narrowed the search almost exclusively to permanent magnet direct current motors. Several domestic and foreign manufacturers were researched. The final selection was an Inertia Motors Corporation 03 series 24 VDC servo motor. The motor design and test data is given in Appendix B. Although the rated torque is listed at 40 oz/in., Inertia Motors Engineers assured us that the motor could easily produce the required torque for limited time periods. An approximate overload duty factor of .2 calculated for the actuator predicted that the motor could perform satisfactorily. The allowable overload time could be increased if needed by providing increased cooling capacity for the motor.

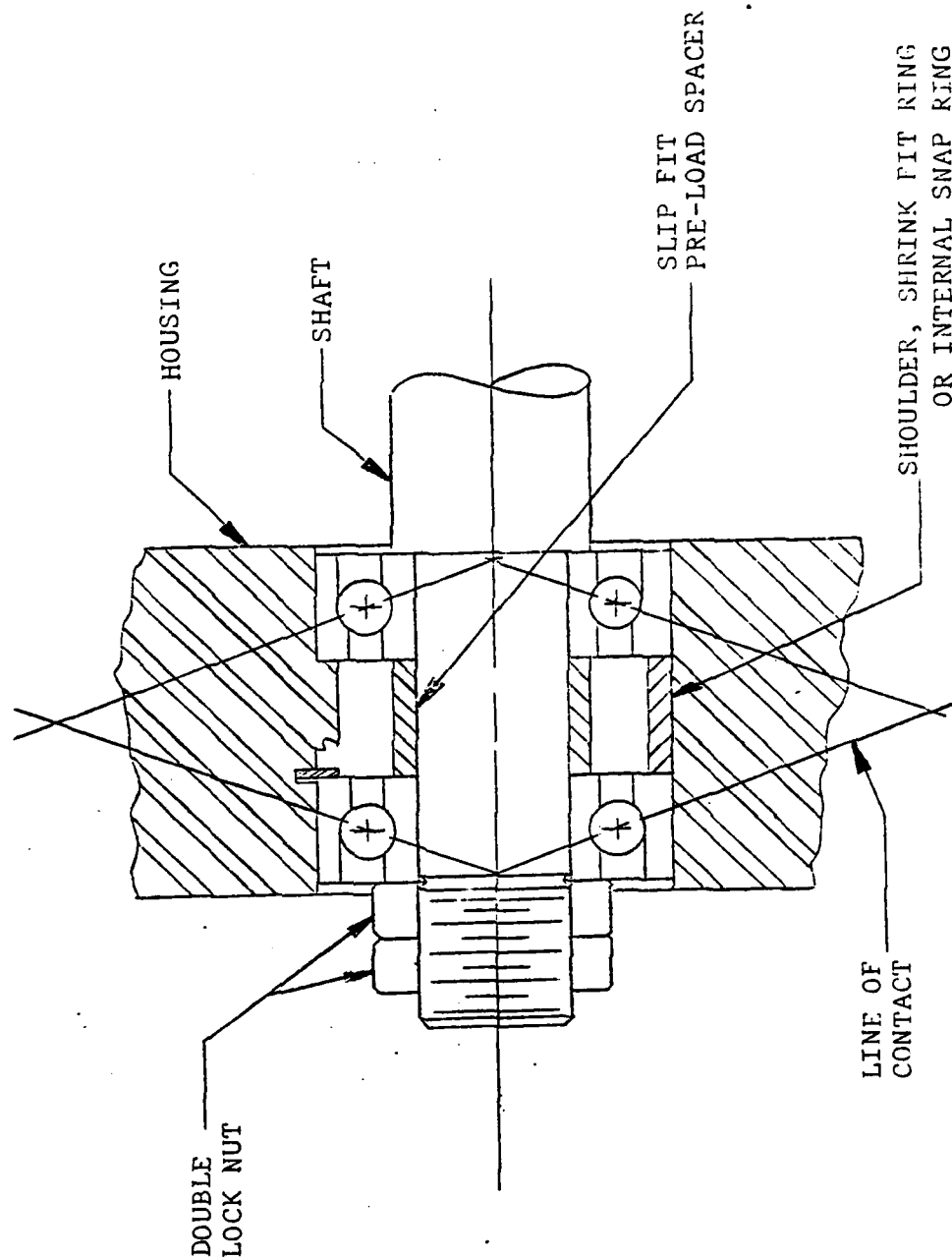


FIGURE 3.5 BALL BEARING DUPLEX ARRANGEMENT

To transmit the motor power to the ball nut, the gear was keyed to the drive spindle. Elementary shaft stress equations showed that a .500 dia shaft with standard .125" square key would be adequate. The choice of .500 in for the drive end eliminated the need to rebore the YA60 Boston Gear.

The drive spindle bearing mounted in the gear case had to absorb the thrust load of 550 lb while maintaining accurate spindle alignment with as little frictional drag as possible. These requirements lead directly to the choice of angular contact ball bearings. When this type of bearing is properly mounted in a duplex arrangement all backlash can be removed between the shaft and the housing by preloading. Figure 3.5 shows the general bearing mounting used for all duplex bearing sets in the mechanism. Fafner single-row, angular-contact, No. 7202W bearings were used for this duplex set. These 15 mm bearings have a 1500 hour thrust load rating of 1200 lb at 90 RPM which provides an adequate safety factor of 2.2 [17]. The bearing set is preloaded by the lock nut arrangement which also retains the drive gear. Preload force is in the range of 8 to 12 lb, which is just enough to remove the backlash. More preload than this begins to significantly increase bearing drag and also reduces load capacity.

Due to the high mechanical efficiency of the ball screw, ball bearings and spur gear set, a brake was required. Without a brake, the actuator motor would have to hold the commanded positions of the ball screw under load. None of this motor's stall current can perform useful work since the motor does not rotate. This power is, in fact, all dissipated in resistive heating.

The brake system for the actuator is designed so that it is spring loaded on and requires power only for release. In this way the energy consumed by the motor-brake system can be less than for the motor acting alone. This is especially true if the servo time for the linear actuator is much less than the total cycle time for the leg.

Before a custom brake system design was begun, there was an attempt to obtain a commercial brake system. The motor manufacturer could supply an electromagnetic disk brake made by the Electectoid Corp., however, this system would have nearly doubled the size and weight of the motor unit. Moreover it required a motor with a nonstandard rear shaft which was not readily available. For these reasons, it was decided to design a custom brake system.

The general assembly of the actuator (Figure 3.3) shows the brake assembly with the integral tachometer mounting. Figure 3.4 shows the actual brake-tachometer assembly in place on the motor.

As shown, the system is an external double shoe type. A small tension spring attached between the two shoes outboard of the solenoid mounting area maintains the brake load. The brake is released by energizing the small Ledex type 75 pusher solenoid. For a duty cycle of about .2, this solenoid will generate 16 ounces at a stroke length of .250 inches (see Appendix B). Standard inner tube butyl rubber was used as the brake lining. The high coefficient of friction between the rubber lining and the aluminum rotor allow a very light spring to be used (~ 4 oz.) thus ensuring the adequacy of this solenoid which was the largest permissible in terms of size.

The choice of butyl rubber, over other rubber-like elastomers, for the brake lining material was based on strength, resistance to abrasion, resistance to tearing, and resistance to heat. Of the common

"rubber" materials, only natural rubber is superior in these categories but was not as readily available.

Common 50-50 epoxy was used to bond the rubber lining to the aluminum shoes. The rated bond strength of this adhesive is 1000 PSI and given proper bonding technique should prove (and has proven) to be more than adequate.

To properly control the actuator under dynamic conditions, both position and rate information is required. The rate information is obtained from the rear motor shaft by a small Beckman tachometer-generator coupled directly thru the brake rotor hub. Extension or retraction of the ball screw is transduced to a voltage signal by a Spectrol 870-100 10-turn precision potentiometer. The potentiometer is driven thru a zero backlash pin type timing belt and sprocket arrangement from the gear end of the ball nut tube. Space and cost savings gained by the use of the rotory potentiometer instead of a linear motion type was somewhat offset by slightly degraded accuracy. Lead inaccuracies of the ball screw and ball nut backlash would both affect the rotory potentiometer reading. However, the required positioning accuracy of the actuator was low enough ($\pm .010$ ") to ignore these effects.

3.3 Main drive actuator.

The choice of a rotory actuator to power the drive crank was largely precipitated by the bulkiness of electric linear actuator having adequate power for this application. Although using a linear actuator to power the drive crank would avoid the problem of transmitting large oscillating torques thru shaft couplings it should be noted that the actuator described in section 3.2 as well as all commercial screw type linear actuators are not true electric linear actuators since rotory

electric motors are their prime movers. True electric linear actuators are essentially variations of an electric solenoid. Their output force is, in general, a nonlinear function of extension. Speed and position control of such electric prime movers is significantly more difficult than that of rotory electric motors.

A suitable electric linear actuator would not eliminate rotory motion and its inherent bearing, gearing, and windage losses, only a reduction in the shaft torque transmission problem, rather than its elimination problem, could be realized. Drive torque loads predicted by the analysis program were not large enough to cause any overwhelming design problems for a rotory type main drive actuator.

The major design criteria for the actuator were the following:

1. must be able to produce at least 400 in/lb of torque.
2. Maximum output speed of at least 13 RPM at 200 in/lb torque.
3. Bearing losses, gearing losses and inertia low enough to allow the leg to back drive the actuator.
4. compact and light enough to mount directly to the base link plate.

The design process for the actuator consisted, in general, of matching the right speed reducer with the right motor. Coupling and mounting were considered minor problems for any given motor-reducer set.

To start the procedure it was decided to choose a motor first since a custom design was out of the question. The qualitative selection criteria were generally the same as for the linear actuator motor, i.e., maximum torque, minimum inertia, and low speed power, all within the smallest possible volume. Although the speed reducer was to be designed

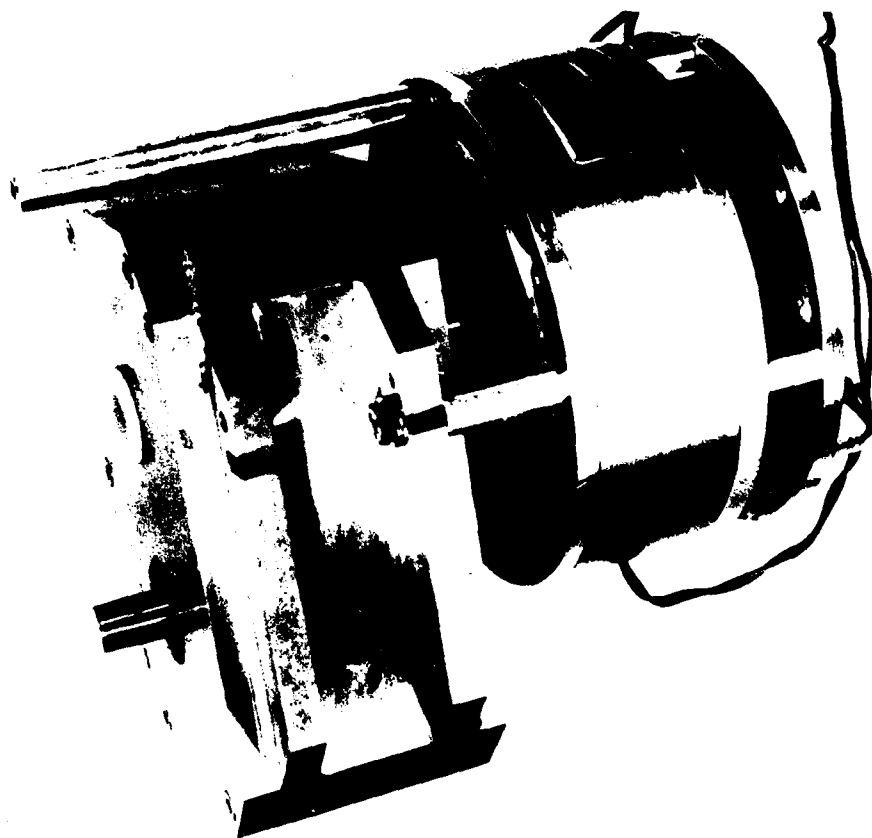


FIGURE 3.6 ROTORY ACTUATOR ASSEMBLY

or selected to match the motor, a preliminary decision on its reduction capacity was needed. Based on accepted gearing practice, the maximum reduction with back drive possibilities is approximately 125:1. This is arrived at by assuming a maximum of 3 gear meshes, 5:1 reduction per stage and a minimum mesh efficiency of .90 to produce an overall efficiency of about 70%. An efficiency of 70% was considered to be a minimum and equally applicable to nongear reduction systems as well.

Using the assumed reducer specifications, quantitative motor criteria were established from the results of the four bar analysis program. These requirements were as follows:

1. maximum output power of at least 100 watts
2. continuous output power of at least 50 watts
3. maximum torque of at least 75 oz/in
4. speed of at least 1625 rpm at 37 oz/in.

Several types of motor were considered. High performance servo motors, universal series motors, brushless d.c., and printed circuit motors were the most serious contenders. The final choice was a PMI standard model U12M4T built by Kollmorgen Corp. Figure 3.6 shows the PMI motor coupled with the actual speed reducer. Detailed electrical, mechanical performance data from the manufacturer is included in Appendix B. With a rated torque of 114.5 oz/in at 300 RPM (254 watts), this motor has a performance safety factor of 2.54. A motor of lesser capacity could have been used but the weight and size savings were not sufficient to override the performance gained with this motor.

With actual motor data the speed reducer selection or design could be finalized. Commercial gear speed reducers, in general, did not adequately meet all of the criteria. Gear boxes with the required

reduction ratio were either too heavy or not able to handle the maximum torque. A harmonic drive speed reducer was very promising with 125:1 reduction, adequate strength and very compact geometry. However, its efficiency was rated at only 70% and availability was, at the time, poor. It was then decided to design a compound gear reducer utilizing standard "off the shelf" hob cut gears. Transmission efficiencies for these types of gears is commonly 96% [11]. If three reductions are used the overall efficiency would be 88%. This could be improved by precise mounting and lapping.

Figure 3.7 is the general assembly of the gear box designed. Boston gears were used in the design because of their reputation for accuracy and availability.[†] The initial sizing of the gears was arrived at by approximate horse power rating charts supplied by the manufacturer [10]. Using a nominal horse power of .05 and an output speed of 13 RPM, a set of three 16 tooth pinions with 70 tooth gears of 20° DP and 20° pressure angle was selected. With these, the overall reduction would be 101.63:1. Extensive remachining of the gears was required to produce the compound pairs and to minimize rotational inertia. Thin bronze oil film bearings were used for the compound gears to allow the largest possible shaft diameter. Minimally the gear set would need to be run in an oil splash bath. To ensure that the compound gear bearings received an adequate supply of oil, four 0.35 inch diameter holes were drilled from the root land of the 16 tooth gear to the bearing at equal intervals about the pitch circle. The meshing actions of the teeth pumps oil from

[†] Before back driving was achieved, the axial machine marks from the hobbing process, had to be removed by lapping each gear against a master.

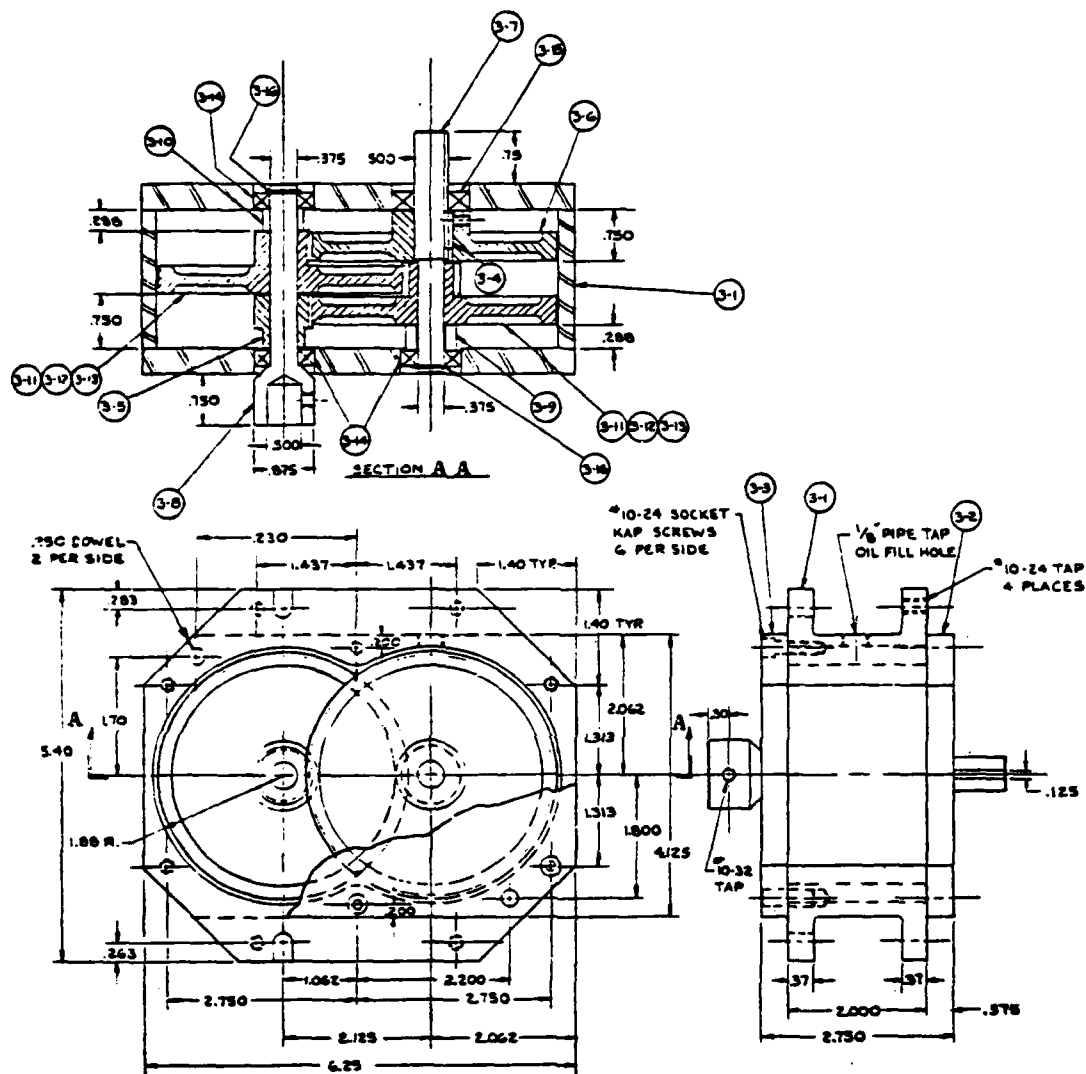


FIGURE 3.7 GENERAL ASSEMBLY OF ROTARY ACTUATOR SPEED REDUCER

from the bath through these holes into grooves cut into the bronze bearings surface then out along the shaft.

The shaft ends are supported by Fafner S3K and S5K precision radial ball bearings. The bearings are press fitted into holes precision line bored into the casing side plates. With the side plates located by dowel pins to the casing, the critical shaft spacing is accurately maintained and reproduced upon any reassembly of the gear box.

To provide the necessary axial clearance and reduce drag, the gear face widths were reduced from .500 to .400 inches.

The geometry and material specifications of this gear train were input into the equations for strength and wear from the American Gear Manufacturers Association . The resulting safety factor for strength and wear for an output of 400 in/lb at 13 RPM were:

Reductions Set	Strength	Wear
1	11.1	1.86
2	2.63	.91
3	.59	.43

Obviously the final reduction is significantly under size while the second set is marginal at best. The first set is perhaps over sized.

The use of larger coarser gears as a solution was unacceptable based on volume constraints. However, the problem can be solved within the initial design volume by increasing the face widths of the final reduction set and/or using a 4340 or similar alloy instead of 1020 steel. Using alloy steel the reduction sets could be optimized to a uniform safety factor for strength and wear. Although the last stage face width might increase, the first and second stage face widths should decrease enough to retain the same total volume. Reentering the AGMA equations with an alloy steel which has an bending endurance limit of at least 47500 PSI and a contact stress limit of at least 190,000 PSI, the face

widths required are as follows:

Alloy Gear Set

20 diametral pitch
20° pressure angle
15 tooth pinion
70 tooth gear

Infinite life safety factors; strength = 2.0 wear = 1.0.

Reduction Set	Minimum face width
1	.0403 inches
2	.170 inches
3	.563 inches

From the above results it is apparent that only the 3rd reduction set need be an alloy. The second and first set can be standard 1020 gears. The face width for the first stage can be reduced to .150 inches (min) while the second stage can be left the same with a slight reduction in the wear safety factor.

The factors and results from the gear analysis program for the various gear sets discussed is listed in the Appendix A.

Since gears made of the recommended alloy are not available "off the shelf", it was determine that the original design using only 1020 stock gears would be implemented. This decision was also based on a reevaluation of the operating conditions.

All the initial testing would be done in level walking. For this regime the maximum torque magnitude is 300 in/lb. Also, as explained in Chapter 2, the contact phase of the stride was generally limited to the region between the two height extremes of the coupler curve, which further reduced the maximum torque to 100 in/lb. At this loading the last stage has an AGMA strength safety factor of 2.37 and a wear safety factor of .86; adequate for the initial test program. For a more

rigorous test program, the last gear stage could be replaced by an alloy set as previously described. The only other alteration necessary would be to replace the end spacers on the input shaft.

To complete the design of the gear box, a computerized stress analysis of the shafts was performed. The program used employs the Mises-Henky failure theory for shafts as presented in ref. [13]. The results from this program indicate a minimum factor of safety of 9.5 for the input shaft and 1.9 for the output. These factors are based on the use of 4140 steel (untreated) and a 400 in/lb output torque. The bearing reactions calculated during this analysis have a maximum value of 70 lb which is well under the 1500 hr load rating for the Fafner S3K and S5K ball bearing specified.

To summarize, the speed reducer was produced according to the initial design specification despite an obviously undersized final drive gear for the maximum load expected. The proposed solutions to this problem can be easily implemented at a later time. However, inspection of the gears after preliminary tests revealed no visible signs of damage.

3.4 Coupler (Knee joint and shank).

In many four bar mechanisms, the coupler is simply a rod which connects the input and output crank circle-points together. It is often even referred to as the "connecting rod". However, in this application it is the output link of the mechanism. To make a rough analogy to the human leg, the coupler acts as the shank and half of the knee joint. The coupler point (leg support point) would be analogous to the ankle joint. (This leg actually has no foot.)

It was decided that the coupler should be designed as an assembly. The connecting link, containing the bearing mounting bores, would be



FIGURE 3.8 COUPLER BAR WITH FORCE TRANSDUCER SHANK

detachable from the shank bar. This arrangement would permit the coupler "foot" point to be adjusted with respect to the connecting link "knee" with minimal expense. Also different shank types could be easily tried. The value of this design was realized when it was decided to replace the solid tube shank with a force transducer shank. The coupler bar, with the force transducer shank is shown in Figure 3.8.

The design of the coupler bar was governed principally by the bearing mounting. To maintain adequate lateral stiffness at the drive crank center point, the axial distance between the angular contact ball bearings was to be maximized within the general size limitations of the leg. The final geometry of the coupler bar resulted directly from the above reasoning and the size of the Fafner 7202W ball bearings chosen. From a strength and stiffness view, the coupler bar is considerably over designed. The inherent weight penalty incurred by this was not deemed sufficiently excessive to warrant further design iteration.

Because the shank is an obvious place to locate a force transducer and because there would be a need for force information eventually, the solid bar shank was replaced by a three axis force transducer unit. The unit consists of two major parts: the bending load element and the axial load element. The disassembled transducer shank is shown in Figure 3.9 along with the solid shank.

A force applied at the foot point in any direction produces some combination of bending and axial strain in the shank. The bending strains are changed to proportional electric signals by four foil type strain gages bonded to the outside diameter of the bending element. By placing the gages at 90° intervals and adding the signals from diametrically opposite gages the sensitivity to bending is doubled while axial strain bias is eliminated. The geometry of the bending element is

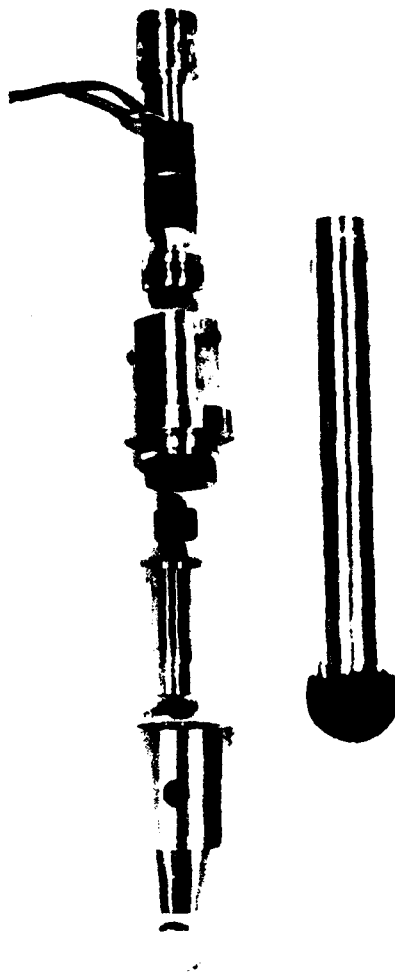


FIGURE 3.9 SOLID AND FORCE TRANSDUCER SHANKS

essentially a thin wall cylindrical tube. The dimensions of this aluminum tube were proportioned to provide as much elastic strain under the predicted loads and the foil gages could safely handle, thus maximizing the force resolution.

Axial shank loads are measured with a quartz piezoelectric load cell made by Kistler Instrument Corporation. The load cell is mounted inside an aluminum housing which is designed to maintain the loading surfaces of the cell parallel. Undesirable transverse and torsional loads are also eliminated by the housing. To avoid ground loop noise from distorting the cell output signal, the housing electrically isolates the load cell from the machine frame.

Specifications for the load cell and bending element are included in Appendix B and C.

3.5 Drive Crank and Shaft

The drive crank is geometrically the simplest component of the mechanism. Figure 3.10 shows that it is essentially a rectangular aluminum bar, 8.5 inches long, 1.5 inches wide and 1.0 in thick with shaft bore holes at each end. Because the driven crank is a ball screw and cannot be loaded in bending, the drive crank must handle any transverse foot loads. Transverse loads occur when the leg is operated out of the vertical plane. That is, when it is abducted or adducted for turning. The loading on the drive crank is rather complex. At most positions in the abducted or adducted mode, the crank experiences bending in both major planes plus twisting and axial loads. Additional complications arises from the fact that the loading varies significantly through the ground contact phase. Also there is the gross loading and unloading which occurs every cycle at toe down and toe off. To be rigorous, a predicted spectrum for each component load should be

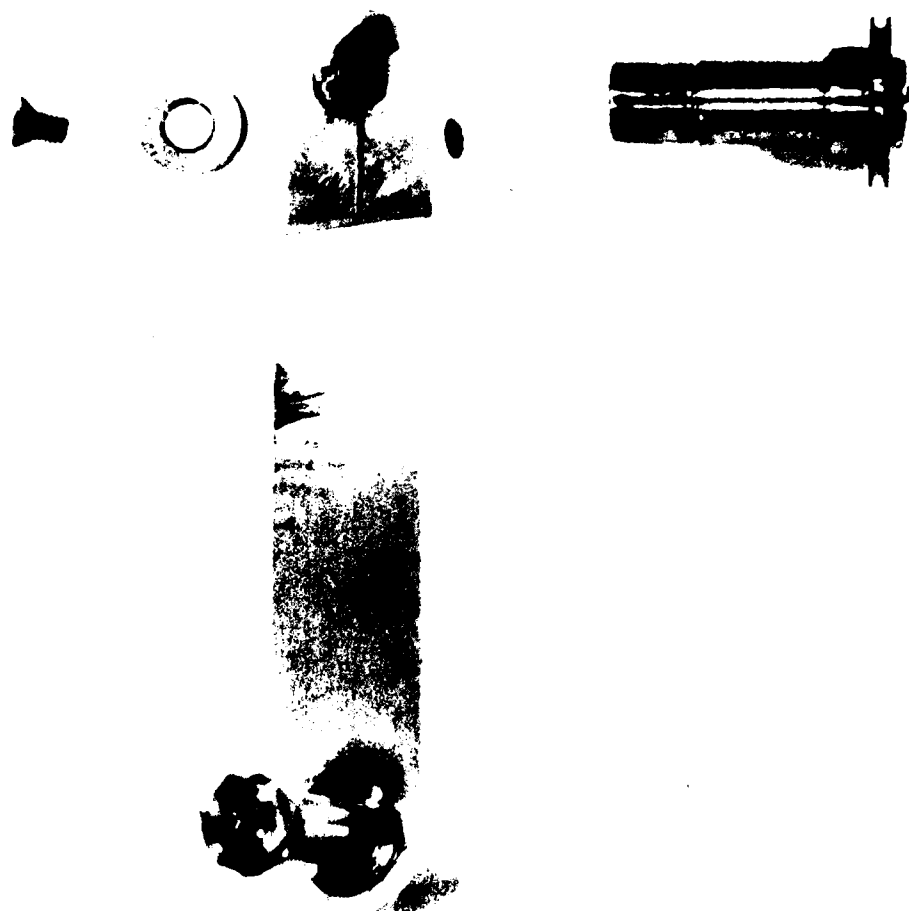


FIGURE 3.10 DRIVE CRANK AND SHAFT

I

assembled and used in a fatigue failure analyses. However, the laboratory prototype nature of the mechanism along with the relatively low cost of the component permitted a crank design based on a grossly simplified model.

From the total motion of the leg two positions representing extreme loading conditions were selected. One position was immediately after toe down when the twisting and torque were the greatest. The other was right before toe off when the transverse bending was the greatest. For all cases, the leg was assumed adducted at 30° to the vertical and at the standard extension. The critical cross section was determined to be through the center of the drive shaft bore containing the key way. To simplify the crank-drive shaft joint model, the worst case was assumed. The shaft was considered to be slightly loose in the crank bore. This allowable point reactions between the crank and the bore to be assumed. With a 400 in/lb torque at toe down[†], the twisting moment was estimated at 657 in/lb, the transverse bending moment was 11.2 in/lb and the axial load was 88 lb tension. This loading translated into a maximum tensile and shear stress in the critical sections of approximately 20 KSI and 19 KSI, respectively. At the toe off position, the torque load was 143 in/lb., the transverse bending was 648 in/lb, the twisting moment was 509 in/lb., and the axial load was 154 lb tension. Under this loading, the critical section through the keyway would experience a maximum normal stress of 21 KSI and a maximum shear stress of 16 KSI. According to the maximum shear stress of failure [12] this released loading can be continued for approximately 1 million cycles before failure [12]. These results were considered as sufficient indication of the crank structural integrity as initially designed.

[†] A constant vertical load at the foot of 110 lb was assumed.

The crank drive shaft (Figure 3.10) represents a less complex problem due to its simpler shape and limited motion. The function of the shaft is to transmit the drive torque from the main actuator and to accept the support loads transmitted through the crank. The shaft load is a combination of torsion and bending. The critical sections for the shaft is between the crank and the base link inboard bearing. From the crank analyses the maximum loads transferred through the drive shaft are 657 in/lb bending moment, 40 in/lb torsional moment and a 55 lb axial load. As previously stated for the crank these peak loads occur once a cycle with lesser fluctuations between occurrences. Choosing a .75 inch diameter crank end with a minimum bearing clearance fillet of .03 in radius and 4140 steel (untreated), an infinite life safety factor of 1.5 is predicted by the Mises-Henky equations [13]. With an infinite life safety factor greater than one for the peak load of the spectrum it can be assumed that lesser load fluctuations accumulate no damage and can be ignored.

In order to minimize the distance between the base link plate and the rotory actuator, the shaft coupler was integrated into the drive shaft. The coupling is accomplished by the keyed hole in the input end of the drive shaft. The output shaft from the main actuator fits snugly into this bore which is precisely located on the drive shaft center line. (The same coupling method is employed between the rotory actuator motor and speed reducer.) This coupler design has a draw back in that it can tolerate very little misalignment between the two shafts ($\pm .001$ in max) before significant bending loads are generated in the shafts. To avoid this, the mounting of the rotory actuator to the base link plate must be precisely repeatable and rigid. The process by which this was accomplished entailed first coupling the actuator to the drive shaft then cutting

precision spools for each mount location (5 total). It is therefore necessary that each spool retain its original location upon any reassembly of the base link-actuator unit.

3.6 Base link plate.

The base link plate is the largest single component of the leg. In the kinematic view it is the fixed link of the four bar leg mechanism. Its function is to provide an accurate rigid mounting for the crank center point bearings, abduction-adduction axis shafts, and the main drive actuator. Like the coupler bar, the base link geometry is governed principally by the required bearing positions and duplexing method. To save design time and machining costs, no attempt was made to optimize the weight of this component by selective material removal from the gross volume required by bearing locations. As a result the base link is essentially a piece of standard 1.250 inch thick 2024 rolled aluminum plate with the crank center point bearing bores and the appropriate screw holes for mounting the main drive actuator and abduction-adduction (AB-AD) axis shaft blocks. With maximum bearing loads not above 650 lb and AB-AD block reactions less than 110 lb with 172 in-lb moment, the base link strength is adequate by inspection. Both the drive and driven crank bearings are duplex sets of the type described in section 3.2 (refer to Figure 3.5). Fafner NO. 7202 W bearing are used for the driven crank circle point and Fafner No. 7204 W are used for the drive crank.

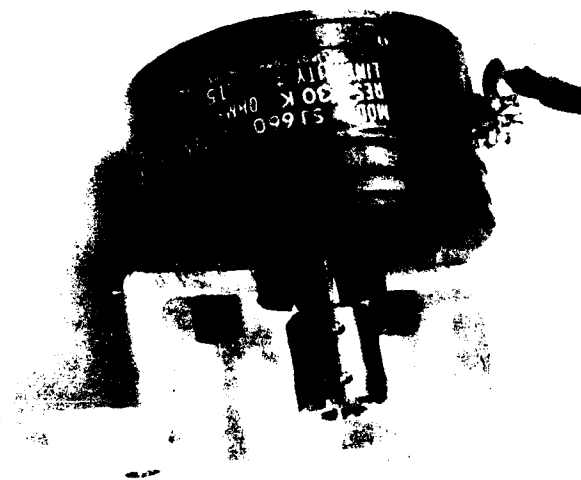


FIGURE 3.11 TYPICAL JOINT POTENTIOMETER MOUNTING

3.7 Leg instrumentation

Any control algorithms used on this mechanism will require position and rate information from some part of the system. The positions and rate devices used on the linear actuator have been described in Section 3.2. Since the exact method of control was unknown at the time of mechanical design, it was decided to instrument each joint with at least a position transducer. Consequently the leg mechanism has a total of six precision potentiometers and three tachometer generators in addition to the 3 axis force transducer. The theoretical maximum required for general three dimensional motion is one rate and one position transducer for each degree of freedom. This means that at least three of the potentiometers are redundant. This redundancy however serves to expand the number of possible control algorithms. The cost of the redundancy was minimized by using identical potentiometers and mounting brackets for each joint. Special attention was given to the mounting and coupling of the potentiometers because of problems encountered in the units used on the OSU Hexapod. Poor mounting design of the Hexapod joint potentiometers resulted in occasional rotation of a potentiometer with respect to its joint and subsequent loss of calibration. Figure 3.11 shows typical joint potentiometer for the planar leg mounted on a precision machined aluminum bracket with the straight sleeve coupler used.

The bracket is designed to provide a rigid non-rotating mount for the Helipot model SJ660 potentiometer used. The linearity of these pots is listed by the manufacturer at $\pm .15\%$.

A schematic of the analog signal conditioning circuit used to interface the potentiometers and tachometers with the analog to digital converter is included in Appendix C. Basically the circuit contains a

d.c. power source for the potentiometers and operational amplifiers for each analog channel. The operational amplifiers allow attenuation or amplification of the potentiometer or tachometer signal so that the full range of the analog to digital converter can be used to maximize resolutions.

AD-A115 600

OHIO STATE UNIV RESEARCH FOUNDATION COLUMBUS

F/G 13/6

DESIGN STUDY FOR AN ACTIVELY TERRAIN-ADAPTIVE OFF-ROAD VEHICLE. (U)

JUN 82 R B MCGHEE, K J WALDRON

MDA903-81-C-0138

NL

UNCLASSIFIED

2 OF 3

ADA
115600



Chapter 4

PLANAR LEG TEST SUPPORT SYSTEM

4.1 Introduction

With the possible exception of the Carnegie-Mellon "Hopper" [14], a single leg requires a support system to act in place of the actual multileg vehicle. There are two basic approaches to this problem. The more obvious one is a system in which the leg mount is fixed with respect to the ground and the leg is made to drive a tread mill which, in turn, would drive a dynamometer. With the calibrated dynamometer output of the leg and measurements of the electrical energy input, accurate power and efficiency data for the leg mechanism can be assembled. A stationary test bed of this type would be very convenient for photographic or video recording of the leg motion cycles. Moreover, various electric and electronic subsystem locations and interconnecting wiring, especially data links with the computer, would pose no additional problems. The major drawback of a stationary test system is cost. None of this equipment was available at the time of leg construction within a reasonable distance for data link hookup with the main frame computer. To design and build a specialized tread mill test stand in the computer room would be prohibitively expensive and time consuming. For these reasons the alternative approach was taken.

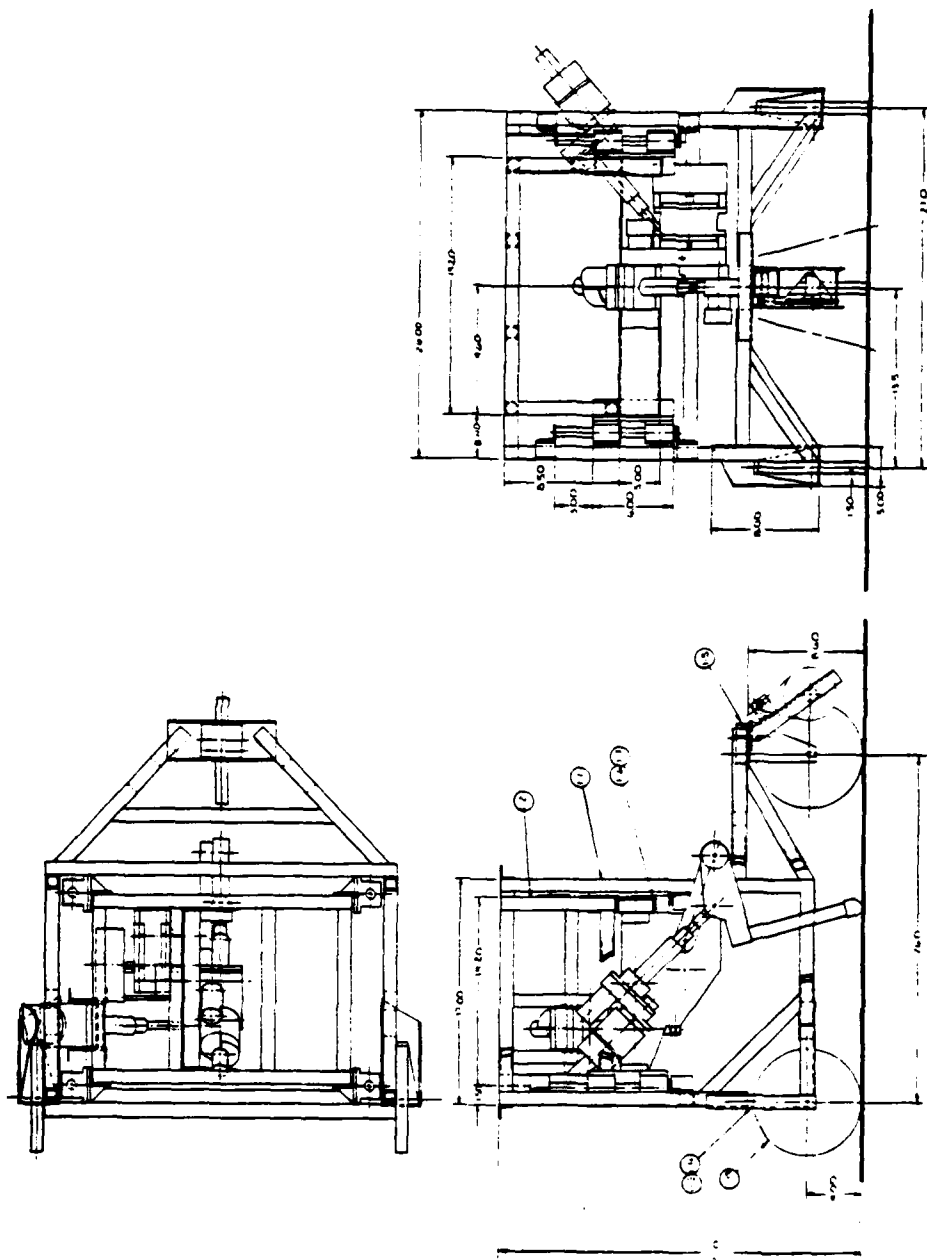


FIGURE 4.1 MONOPOD GENERAL ASSEMBLY

4.2 Test Cart Frame

The alternative to the fixed test stand is, of course, a moving test stand. To allow the leg to move without several other stabilizing companions, a wheeled double support frame was devised. Figure 4.1 is a photo reduction of the test cart-leg assembly. Figure 4.2 is a photograph of the actual assembly before any of the electronic components were mounted. The essential feature of the test cart is the inner and outer frame configurations. The leg mechanism, including the abduction-adduction actuator, is attached only to the inner frame. The inner frame is, in turn, attached to the outer frame through four sets of guide pins and ball bushing pillow blocks. This arrangement provides a passive degree of freedom for the leg in the vertical direction. The allowable motion between the two frames minimizes the tendency of the leg to lift the cart wheels off the ground and helps to isolate the leg loading from the outer frame.

The three wheel design of the cart is essentially for simplicity and cost reduction. An additional benefit of this design is avoidance of major wheel alignment problems. The third wheel is mounted in a caster frame to allow the leg to turn the cart by abducting or adducting. The initial tests do not require this mode of operation. Therefore, for strictly straight line operations, the caster wheel is locked in position.

The cart can operate with the caster wheel leading or following in both the locked or swivel mode. A preferred direction has not as yet been established. In the event that the preferred direction of cart motion is inconsistent with the original mounting of the leg in the cart frame (as illustrated in Figure 4.1), the symmetry of the guide pin

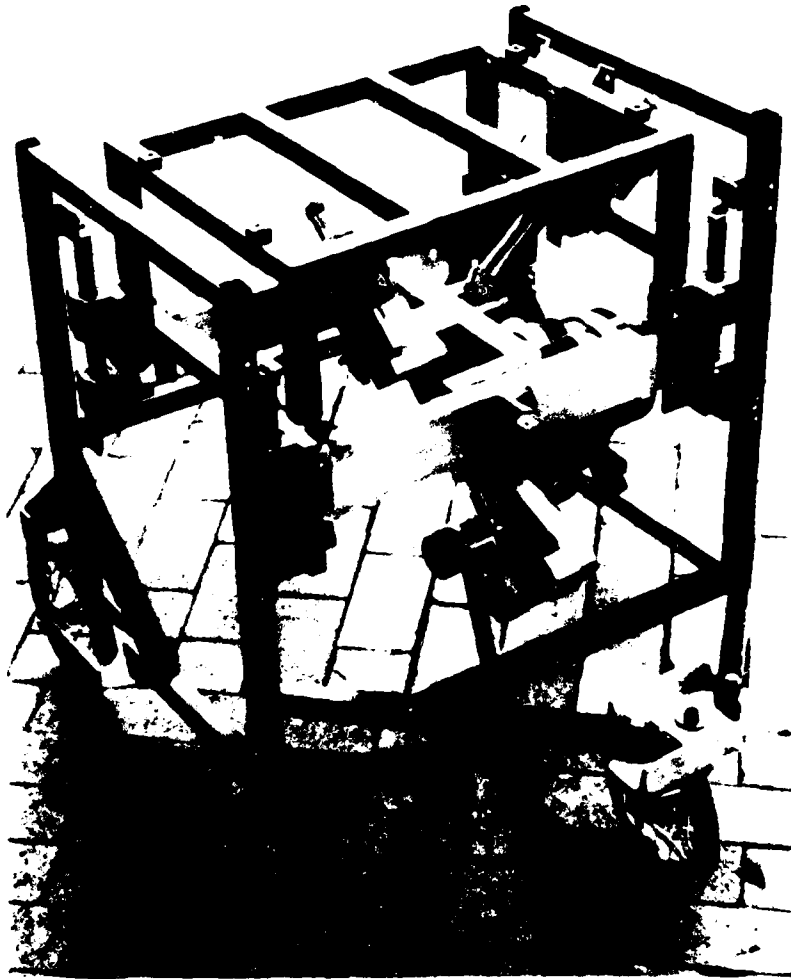


FIGURE 4.2 TEST CART WITH LEG INSTALLED

arrangement will allow the inner frame to be re-orientated 180° from its present position.

The inner frame is fitted with a set of adjustable stops which maintain the inner frame elevations when the leg is in the transfer (return) phase. By extending or retracting these stops, various walking heights of a multi-legged machine can be simulated.

The precision and ease with which the inner frame slides along the guide pins determines the ability of the system to maintain a uniform loading of the foot. Sliding friction and stiction between the guide pins and bushings allows the leg to see a portion of the weight of the outer frame in addition to the test load attached to the inner frame. Ball bearing bushings were employed in the design in an effort to minimize this effect. However, if the leg has force sensing capability, uniform loading of the leg is not a strict requirement.

The structural design criteria for the frames were not especially severe. The total leg and inner frame weight which the outer frame supports during the transfer phase was predetermined to be 110 lb (refer to Chapter 3). During the support phase of the leg cycle, the total cart frame assembly needs sufficient stiffness to resist distortion due to moments generated when the foot point is not directly beneath the center of support in the base link plate. Because of the generally light loads involved the frames could be constructed out of thin wall tubing. It was also deemed advantageous to minimize the weight of the frames so that the centers of gravity of the frames could be shifted, if necessary, with a minimal addition of dead weight. The material selected for the frame was standard 1.0 inch square, .032 inch wall, welded mild steel tubing. This material provided adequate mechanical properties and minimal welding problems. Most of the bolt on brackets, such as the wheel mounts and the

main leg support channels, were fabricated from 2024-T4 extruded aluminum shapes. Little attempt was made to predict frame deflections under load. The reason for this is that selective stiffening of the frame could be done, if necessary, after the leg was mounted and initial tests run.

During initial trials of the leg test system, it was found that the outer frame did indeed require counter balancing. To maintain all wheels in contact with the ground during the support phase, a 15 lb lead weight was attached near each fixed wheel, on the lower rails of the outer frame.

The cart wheels were chosen with some care since their behavior could effect the performance of the entire system. The wheels had to meet three basic requirements which were as follows:

1. Smooth running with relatively low friction.
2. Minimal concentricity run out between wheel periphery and bearing axis.
3. Minimal rotational inertia.

To meet these requirements, semi-pneumatic, 8 inch spoked wheels were purchased. The bearings supplied with the wheels proved to be substandard and had to be replaced with more expensive ball bearings. Radial run-out of the wheel would produce an undesirable vertical oscillation of the outer frame. To minimize this effect the wheels were mounted on a precision arbor in an engine lathe and their outside diameters were turned true to the bearing bore.

Besides holding the leg in position and allowing it to "walk" the cart frame also supplied structure to which various electronic hardware could be attached. To avoid noise generated in long analog signal lines, the motor control power circuits and analog transducer signal condition-

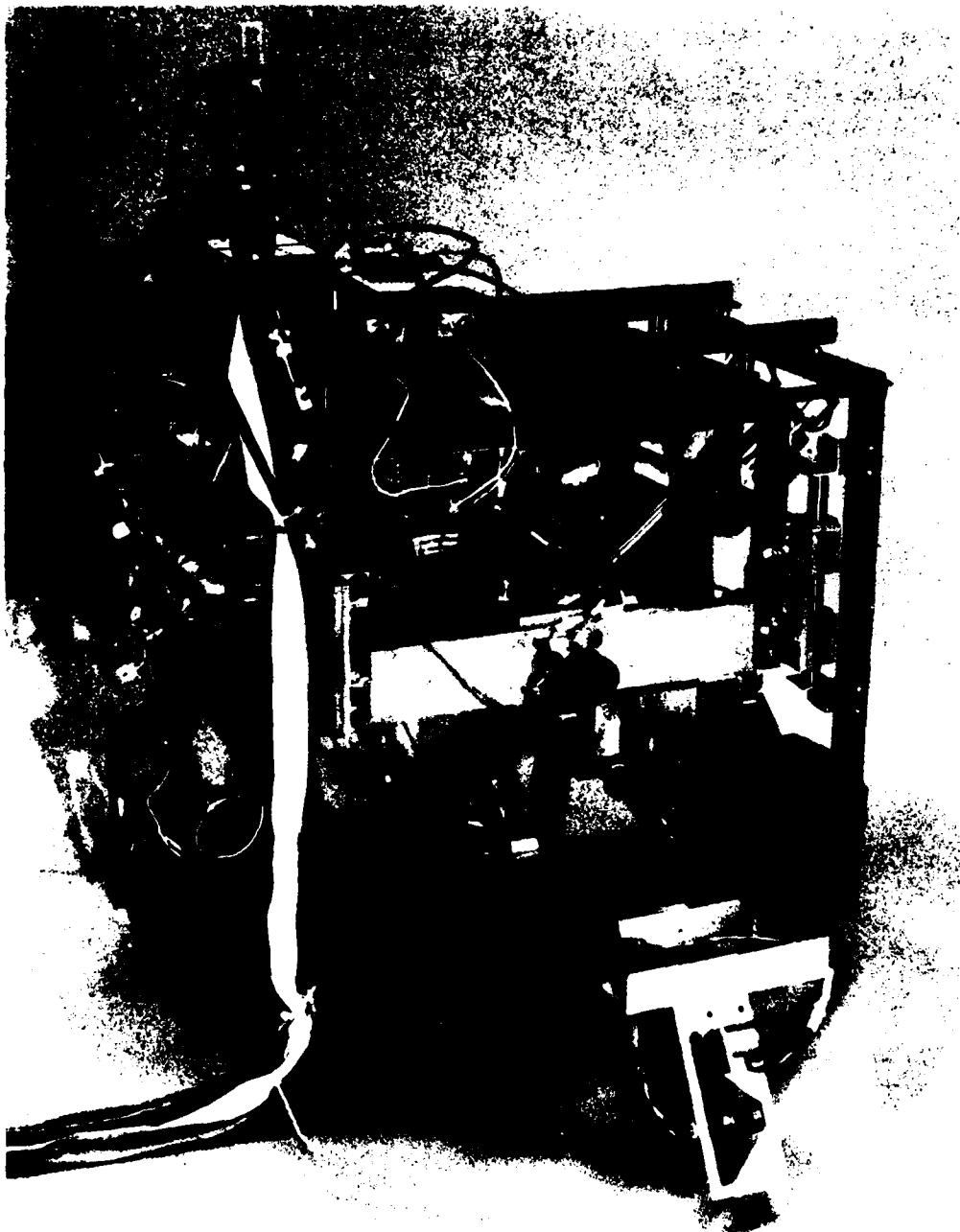


FIGURE 4.3 TEST CART WITH LEG AND ELECTRONICS
OSU MONOPOD VEHICLE

ing circuits had to be mounted on the test cart. As Figure 4.3 illustrates, the electronic hardware on board nearly obscures the leg.[†]

4.3 Cart instrumentation.

There are only three system parameters that are principal state variables of the test cart and are only implicitly defined by the state of the leg. These three are; the system ground speed, the direction of system motions and the vertical position of the leg center of gravity.^{††}

To measure ground speed independently of the calculated horizontal velocity of the foot point, a tachometer-generator system was attached to the caster wheel of the cart.. Figure 4.4 is a closeup photograph of the cart speed measuring system. The system is simply a small D.C. tachometer generator (Beckman Model 1150-5-3) driven by the caster wheel. An overdrive ratio of 1:23.632 is obtained by compounding a friction drive hub (1:7.877) with a pin timing belt (1:3.000). For a tachometer constant of .007 volt/RPM the theoretical constant is 2.478 in/sec/volt. Direct calibration agrees closely with this figure. Since the rubber wheel is subject to wear, the cart speed transducer should be recalibrated periodically.

The cart directions can be described by the angular displacement of the caster wheel plane from the centerline of the outer frame. This angular displacement can be easily sensed at the vertical caster truck axis with a rotary potentiometer. Because the initial test procedures

[†] This poses a potential problem for video recording of the leg motions. A future plan to mount an Intel 8086 microprocessor above the caster wheel will increase this problem.

^{††} In actuality it is the change in the position of the center of gravity of the imaginary vehicle that is of concern.

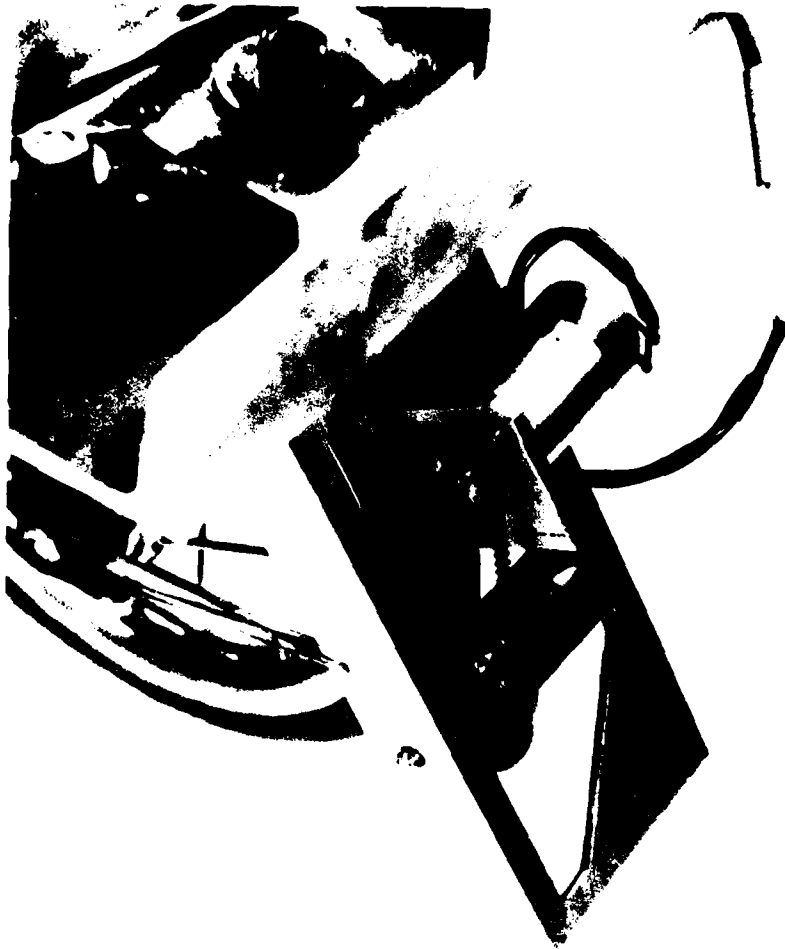


FIGURE 4.4 TACHOMETER/GENERATOR CART SPEED TRANSDUCER

did not include turning manoevers, this angle measurement transducer was not implemented.

To measure the vertical excursions of the imaginary vehicle body, a precision linear potentiometer was mounted between the inner and outer cart frames in the center line plane of the cart. This potentiometer actually measures the relative displacement of the inner and outer frames along the axis of the guide pins.

Data from the linear potentiometer can be translated into changes in potential energy of the system. In fact, the total mechanical energy of the test cart can be represented as functions of the cart tachometer output and linear potentiometer output.

Each wheel is mounted independently of the others to the outer frame of the cart and its position is somewhat adjustable. Using this adjustability the average axis of the guide pins can be brought into perpendicularity with the ground plane as defined by the three wheel contact patches. This is desirable if accurate potential energy measurements are required.

Chapter 5

ACTUATOR POWER CONTROL

5.1 Introduction

The effort expended in developing a leg mechanism with high mechanical efficiency as well as that expended in finding efficient electric motors can be, to a significant extent, lost if proper attention is not paid to the power regulation system. Some type of power control is necessary if the speed of an electric motor is to be varied on command. When the speed must be varied rapidly over a wide range, it is possible to throw away as much, or more, energy in the control circuit as is actually needed by the motor to produce useful work.

The circuitry needed to minimize the control losses of the permanent-magnet, direct-current (D.C.) motors used for the prototype leg was designed by Professor Karl Olson of the Electrical Engineering Department at The Ohio State University. The following sections of this chapter give a brief description of the circuits and the basic ideas behind them. This chapter is included only for the sake of completeness in the description of the Monopod system.

5.2 The resistor versus the switch

The speed of a direct current motor can be controlled by a very simple circuit. Figure 5.1a is a schematic for one such simple (and commonly used) motor control circuit. The direct current voltage, E , is a source or E.M.F. (electric motive force). The variable control resistor

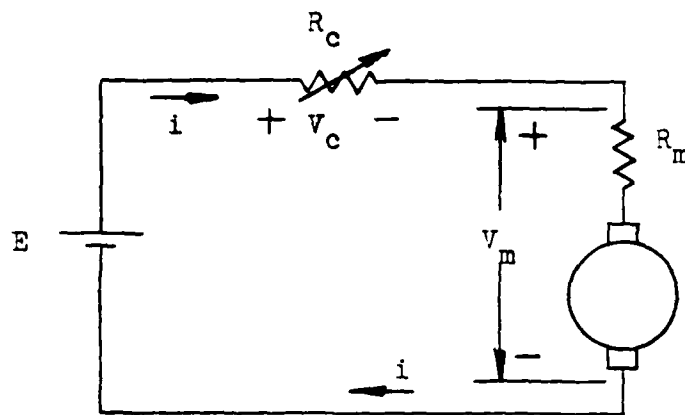


FIGURE 5.1a
VARIABLE RESISTOR
MOTOR POWER CONTROL

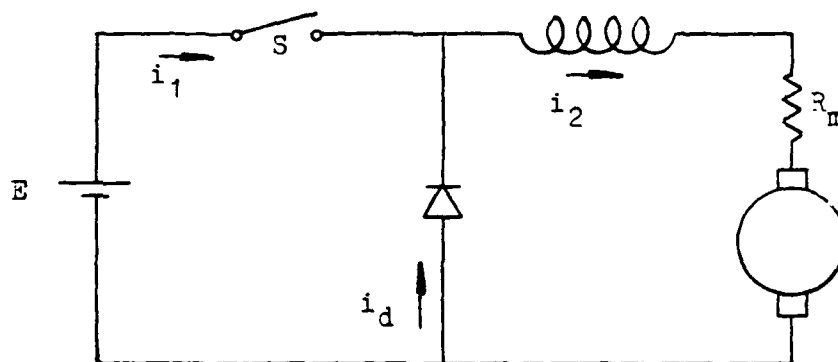


FIGURE 5.1b
PULSE WIDTH
MOTOR POWER CONTROL

is R_c and R_m is the internal motor resistance. The speed of the motor is proportional to the voltage across it. By elementary circuit analysis and D.C. motor theory

$$V_M = E - V_C = e_b + iR_m$$

where e_b is the back EMF produced by the motor rotation, and i is the current.

Of the total power used by the circuit, iE , the portion wasted in the control resistor is

$$iV_C = i^2R_c$$

The portion wasted by the motor is equal to i^2R_m . The remaining power is equal to ie_b which is available to produce torque.* Assuming that the motor losses are fixed, the only way to increase the efficiency of this circuit is to reduce R_c . This implies that the motor should always be run at full speed, which of course is contrary to the original motivation for developing the circuit. What is needed is a current or voltage control element which has zero resistance.

Only a little insight is required to recognize that a simple on/off switch has nearly zero resistance and can control both current and voltage quite effectively. Although there is an exact relation between the voltage across and the current through the resistive/inductive motor load, it is more common to consider the speed of a D.C. motor as a function of the voltage as stated above. By turning a switch on and off at a predetermined rate the average voltage supplied to the load can be varied anywhere between zero and the maximum supply voltage. From Figure 5.2a, it can be seen that opening the ideal switch for time T_0 seconds then closing it for T_c seconds generates a square wave train of voltage

* The actual shaft power is, of course, further reduced by frictional and eddy current losses.

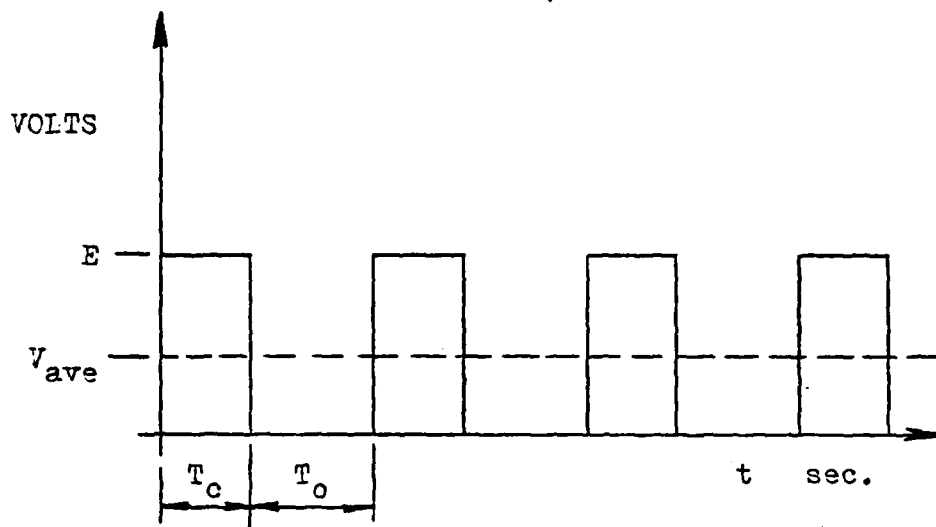


FIGURE 5.2a
PULSE TRAIN FROM IDEAL SWITCH

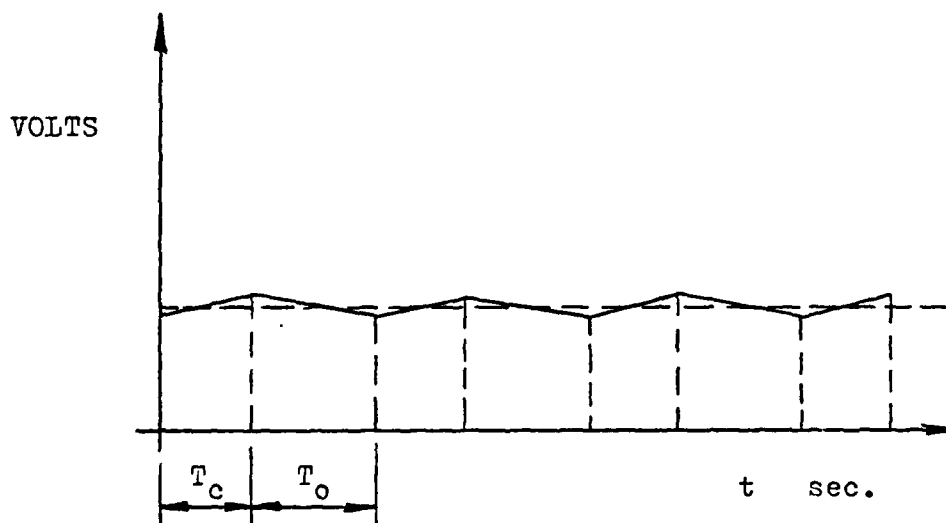


FIGURE 5.2b
PULSE TRAIN AFTER SMOOTHING INDUCTOR

with a frequency of $1/(T_0 + T_c)$ Hertz and amplitude E . The average voltage across the motor load is simply

$$V_M = \frac{T_c}{(T_c + T_0)} E$$

Figure 5.1b is a simplified schematic of a circuit which controls motor speed by pulse width modulation. The figure shows not only the replacement of the control resistor " R_c " by the ideal switch " S " but also the additions of an inductor in series with the motor and a diode in parallel. The inductor and diode are necessary for the physical realization of such a circuit.

Permanent magnet, D.C. motors have little internal resistance. For this reason, if applied voltage is of a pulsatory nature (as in Figure 5.2a) the armature current will have large peaks since back EMF does not have time to establish itself. Correspondingly, the output torque will also have undesirable pulsation. Moreover, the large current spikes produce large resistive losses in the armature and require a greatly over designed switching circuit. By placing a sufficiently large inductor in series with the motor, the pulses generated by the switch are smoothed to nearly the average D.C. value. The diode supplies a path for the induced current when the switch is opened. As a result the switch opens against only the average motor current. The total effect is that the no load motor speed becomes proportional to the switching duty cycle,

$\frac{T_c}{(T_0 + T_c)}$ as shown in Figure 5.2b.

5.3 Motor power bridge circuit.

The actual circuitry required to realize the concepts outlined in Section 5.2 can be conveniently divided into two parts. The first part is the power bridge which is able to change the direction of the current through the motor and thus the direction of motor rotation. The second part, which will be described in the next section, is the circuit needed to change a digital command from the computer into the appropriate train of switch pulses.

Figure 5.3 is a simplified schematic of the motor power bridge circuit. Each actuator motor is wired directly into a circuit of this type. Switches A_1 , A_2 , B_1 , and B_2 are actually power transistors. A_2 and B_2 are driven by the pulse generating circuit to produce the required square wave train. If the rotation directions of the motor are designated A and B, then the circuit operates as follows:

To rotate the motor in direction A, switch A_1 is closed and switches B_1 and B_2 are open. Switch A_2 is then opened and closed by the pulse generator with a duty cycle sufficient to produce the desired speed of the motor in direction A. While A_2 is closed the current flows from the power source through switch A_1 , then through the motor and smoothing inductor and finally through A_2 back to the source. While A_2 is open the current continues to flow in the same direction, through the motor due to the collapsing magnetic field in the inductor. The current path is now through diode D_A and switch A_1 which remains closed as long as rotation in the A direction is desired. Rotation in the B direction is accomplished through the bridge in a completely analogous manner using switches B_1 and B_2 in conjunction with diode D_B .

A photo-reduction of the design schematic for this circuit is included in Appendix C.

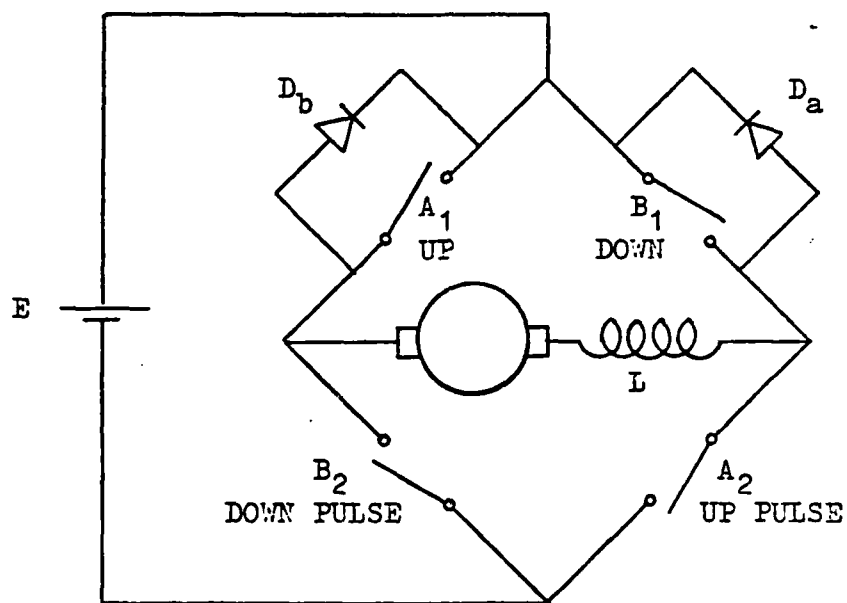


FIGURE 5.3
MOTOR POWER
BRIDGE CIRCUIT

5.4 Digital word to pulse width conversion

It is entirely possible to have the control computer generate the pulse train required to operate the A₂ and B₂ power transistors (see Figure 5.3). However this would take an inordinate amount of computer time which is better spent on performing feed back control calculations. A much more efficient method is to design a circuit which will accept a digital (binary) word, proportional to a desired motor speed and output a pulse train whose duty cycle will produce the required speed when applied to the motor power bridge circuit. Because bidirectional rotation is required, the input command word is a signed 2's complement number.* Using the 2's complement number allows an up/down counter to be used to determine the pulse width.

Figure 5.4 is a block diagram of the converter circuit. A 1.0 Mhz clock signal is reduced to a frequency of 976.6 hz to establish the fixed pulse frequency. This pulse tells the up/down counter when to load the digital command from the command word register. The register is loaded directly by the computer with a signed 2's complement binary number which represents the desired length of time the pulse switch (A₂ or B₂) is to remain closed. The most significant bit of the binary word determines which side of the motor bridge (A or B) is to be activated and thereby the direction of rotation. Also this bit tells the counter to count up to zero or down to zero.

While the count is proceeding to zero, the output from the circuit is high on either up (A) or down (B) channels depending on the direction bit. When the count reaches zero, the pulse switch (A or B) is opened.

* The 2's complement number is distinguished by a weighting of the sign bit of -2^N where N is the total number of bits in the word [19].

The circuit remains in this state until another load pulse is received by the counter at which time the process is repeated.

A design schematic, with all of the devices for this circuit specified, is included in Appendix C. Examination of this schematic will reveal that included in this circuit is the logic for operating the brake solenoids. Since these solenoids operate in strictly an on-off mode, the required control circuitry is much simpler than for the servo-motor. Basically, the circuit receives a command word from the computer whose least significant bit is either 0 or 1 corresponding to the desired state of the brake. The circuit reads only this bit and outputs a drive voltage if it is not zero.

Chapter 6

Control Program for Leg Mechanism

6.1 Introduction

The walking vehicle control problem has been under study at various universities and research institutions in several different countries. The Ohio State University has been among these institutions for several years. The Digital Systems Laboratory in the Department of Electrical Engineering has been the center for the work on the various aspects of the walking machine control problem. Up to this point the sole test bed for the digital control techniques developed has been the OSU Hexapod mentioned in Chapter 1. The Hexapod has been in operation since 1976.

As stated in Chapter 1, the Hexapod uses an insect type leg configuration with each joint driven by a separate actuator. The significant fundamental kinematic and mechanical differences between the Hexapod leg and the linkage leg described in this thesis are such that only some of the generalized control strategies used on the hexapod legs can possibly be applied to the new leg. For the most part, new control schemes are required. Reference [37] describes the initial work done at Ohio State toward this end by presenting an efficient method of calculating actuator forces and torques which can be applied to closed chain leg mechanisms as well as the more common open chain legs.

Due to the fact that this prototype linkage leg is essentially a four bar mechanism, its equations of motion are both non-linear and coupled. The consequence of the significant nonlinearity and coupling effects to efficient dynamic control of this linkage leg is addressed in detail in reference [38]. This reference includes proposed control schemes and results from their implementation on a dynamic computer model based directly on the leg mechanism of this thesis. No attempt will be made here to explain this work since the initial testing of the leg did not require a control program of this scope.

With the awareness that ignoring the inherent nonlinearities of the system would result in degraded dynamic performance, it was proposed that, for the sake of expedience, the initial energy consumption tests be run using a significantly simplified control scheme. This simplified control program would operate the leg in a manner which made best use of the mechanical logic of the mechanism. It follows that this would also be the most energy efficient mode since the least amount of corrective action is required by the servomotors. For this reason it is apparent that this would be the preferred control mode for cruising in a walking vehicle employing this leg. The author has been directly involved in formulating the concepts and requirement for this simplified control program. However, the actual details of program structure and implementation has been largely the work of Mr. Chi-Keng Tsai and to a lesser extent Dr. K. Olson both of the Electrical Engineering Department at The Ohio State University. This chapter is included essentially to complete the description of the "Monopod" system rather than document the work of the author.

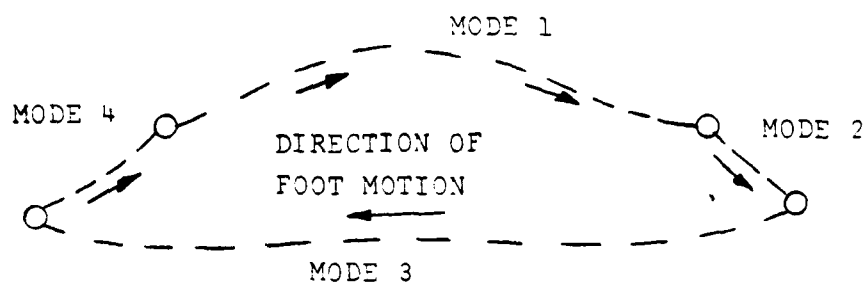


FIGURE 6.1a FOOT TRAJECTORY WITH
REFERENCE TO VEHICLE FRAME

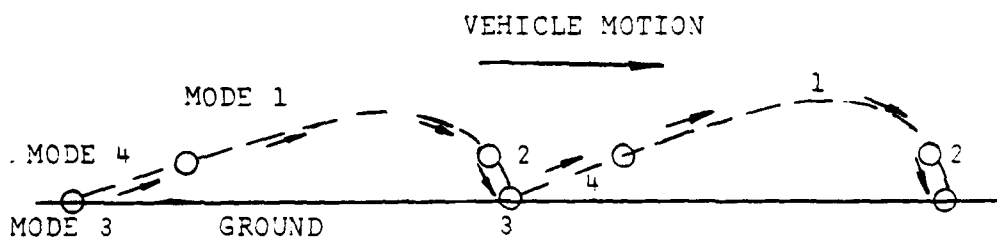


FIGURE 6.1b FOOT TRAJECTORY WITH
REFERENCE TO GROUND

6.2 Simplified Control Scheme; Mode Control.

In the most general sense any leg in any system has basically only two conditions, one in which it is supporting some portion of body weight and one in which it is not. When a leg is not supporting the body during walking it is retracting, extending or transferring in preparation for extension. Therefore, the two basic conditions can be further divided into four distinct phases of leg motion. To a certain degree the planar leg was kinematically designed to decouple the actuators such that the four basic phases or modes of any planar stride cycle could be effected by a single actuator. This condition enables a type of finite state control to be used so long as the active gait control required is minimal. The leg cycle for any fixed stride length was consequently divided into four discrete modes. These modes were termed and arbitrarily numbered as follows:

Mode 1 ; transfer phase

Mode 2 ; toe-down / off phase

Mode 3 ; support phase

Mode 4 ; toe-down / off phase .

Note that model 2 and 4 exchange functions depending on the direction of cart motion. For forward cart motion,* mode 2 is toe-down and mode 4 is toe-off. When the cart travels backward, the functions are reversed.

The state of the linear and main rotory actuators in each mode , for forward cart motion, is given in Table 6.1 where the three possible conditions of motor rotation are indicated by +, -, 0.

* Forward motion of the cart was arbitrarily defined as proceeding with the caster wheel foremost.

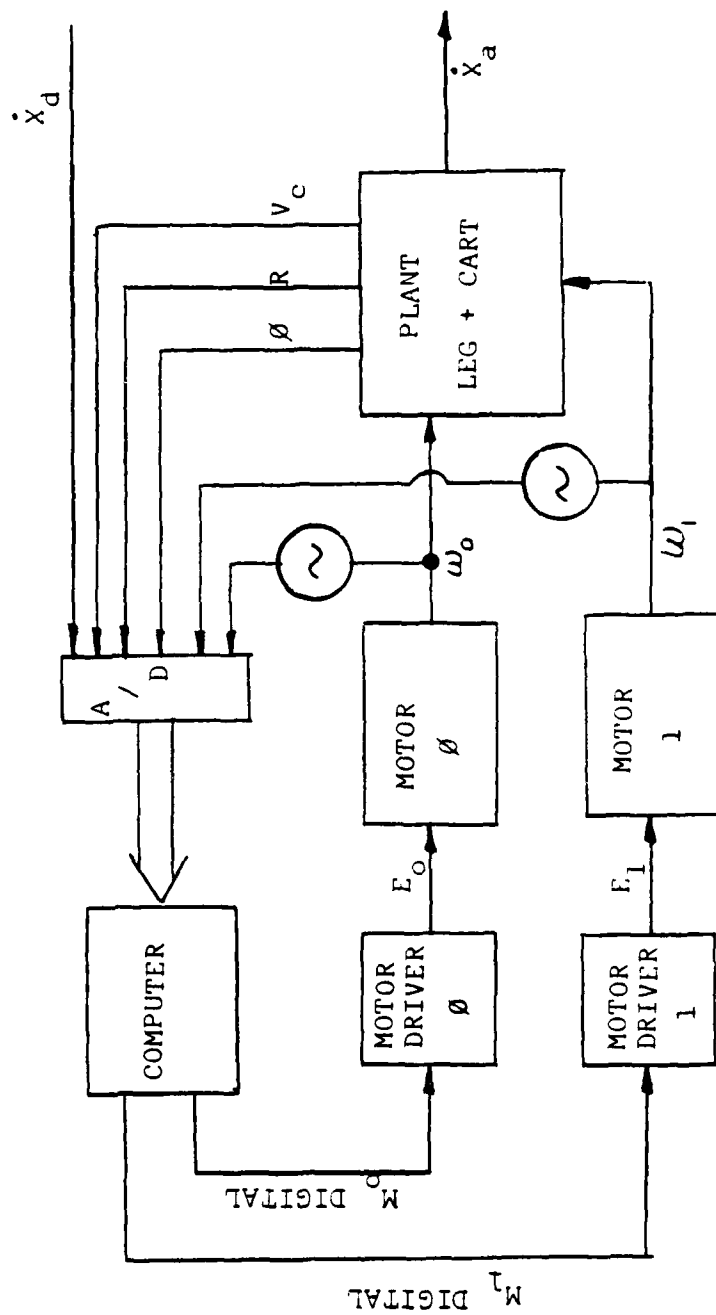


FIGURE 6.2 BLOCK DIAGRAM OF TOTAL LEG SYSTEM

Table 6.1

<u>Mode</u>	<u>Rotory</u>	<u>Linear</u>
1	-	0
2	0	+
3	+	0
4	0	-

Even for a very simple control scheme the desired rates of rotation for the motor should be included. However it is possible to employ a straight on/off motor control method with this linkage leg and produce crude but usable output motion. The added effort needed to implement simple proportional velocity feedback in the motor control loop is quite minimal and results in considerable improvement in the dynamic behavior of the system.

The minimum requirements for a control program can be stated as follows:

1. must be able to determine the state of the leg at any time.
2. must accept a command signal representing the desired velocity vector.
3. Using the system state information the program must be able to drive the motors such that the command condition is met.

Figure 6.2 is a block diagram of the basic system to be controlled. Note that θ and R can be any two of the five position transducer outputs mentioned in Chapter 4. V_c is the cart tachometer/generator signal and therefore represents the actual horizontal velocity of the leg. The command signal is from a joy stick and represents the desired horizontal velocity. The blocks labeled "motor driver" represent

both the "Digital-Word-to-Pulse Width Converter" and "Power Switching" circuit described in Chapter 5. From the computer system standpoint, these motor drivers are essentially Digital-to-Analog converters. The use of more sophisticated control schemes will not change the basic configuration represented by Figure 6.2 except for the possible addition of more state variables. Complete three degree motion of the leg would require only that another motor and motor driver be added to the systems of Figure 6.2 along with one additional state variable.

For simple velocity feedback control, the digital motor commands M_0 and M_1 are calculated by the computer in the general form of

$$M = K(\dot{\phi}_d - \dot{\phi}_a)$$

where $\dot{\phi}_d$ is the desired velocity of the motor, $\dot{\phi}_a$ is the actual velocity and K is the system gain. Both the gain K and the desired motor rotational velocity $\dot{\phi}_d$ would be nonlinear functions of the command input and the system state if high dynamic performance was required. However, for simplified control, $\dot{\phi}_d$ can be replaced by a measurable quantity which represents the general trend of $\dot{\phi}_d$ such as the input command $\dot{\lambda}$. The gain K can then be found experimentally. A single satisfactory gain constant for the entire cycle may not be found. In this case a different constant for each mode could be used. The modes could be further subdivided with a different gain constant found for each division. However before implementing extensive subdivision of the modes, the more generalized nonlinear control schemes should be investigated.

In lieu of defining different velocity gains for various portions of the cycle it may be possible to obtain a required dynamic performance improvement by adding a positional feed back term. The general form of motion command would then be

$$M = K_1(\ddot{\phi}_d - \ddot{\phi}_a) + K_2(\dot{\phi}_d - \dot{\phi}_a)$$

where for the simplified case, ϕ_d could be obtained by integrating whatever parameter is used for $\dot{\phi}_d$. As for the velocity case, ϕ_a is a representative measurable parameter and K_2 is an experimentally determined constant.

6.3 Actual Control Programs

Figure 6.3 is the simplified flow chart for the basic control program written for the leg system. The basic program has four variations dependent on the input command and the type of feedback used. The command input is either from a joystick or directly from the cart tachometer/generator which measures actual ground speed. When the cart tachometer signal is used as an input, the cart is pulled along by hand and the control program, in effect, seeks to match the foot and ground velocities. Operating the system in this manner simulates the condition the leg would experience in a multilegged vehicle. If the control program performs adequately then little or no traction force is generated at the foot tip which is the condition during uniform horizontal motion.

Initially only velocity feedback was employed. Simple position feedback was then added in an attempt to improve the dynamic performance. It should be noted here that for the purposes of this project, only that dynamic performance improvement which resulted in significant reduction of power consumption was sought.

The program determines the desired rates for the actuator by first determining the allowable elapsed time for each mode T_1 , T_2 , T_3 , T_4 . First the elapsed time for support phase (Mode 3) is defined by

$$T_3 = \frac{L}{|\dot{X}|}$$

where L is the stride length, which is constant, and \dot{X} is derived from either the joystick or cart tachometer inputs. The total cycle time, T , is given by

$$T = T_3/B$$

where B is the duty factor for the leg. In a multi-legged system the duty factor is dependent on the gait required. For this single leg test system B is a constant in the control program and was chosen to be 0.50. The elapsed time allowed for the transfer phase (Mode 1) is one-half the remaining cycle time. The other half is divided evenly between the toe-down and toe-off phases (Modes 3 and 4). Therefore T_1 , T_2 , and T_4 are given by

$$T_1 = 0.5(T - T_3)$$

$$T_2 = T_4 = 0.25(T - T_3)$$

The desired servo rates are then established as average velocities for each mode. As an example $\dot{\phi}_d$ for Mode 1 is given by

$$\dot{\phi}_d = \sigma \frac{(\phi_1 - \phi_2)}{T_1}$$

where ϕ_1 and ϕ_2 are the end points of Mode 1. σ is the direction of the input command and can be represented as

$$\sigma = \frac{\dot{X}}{|\dot{X}|} \quad \text{or} \quad \sigma = \text{sign}(\dot{X})$$

The program forms the proportional signal for each motor in each mode by multiplying the difference between the desired rate and actual

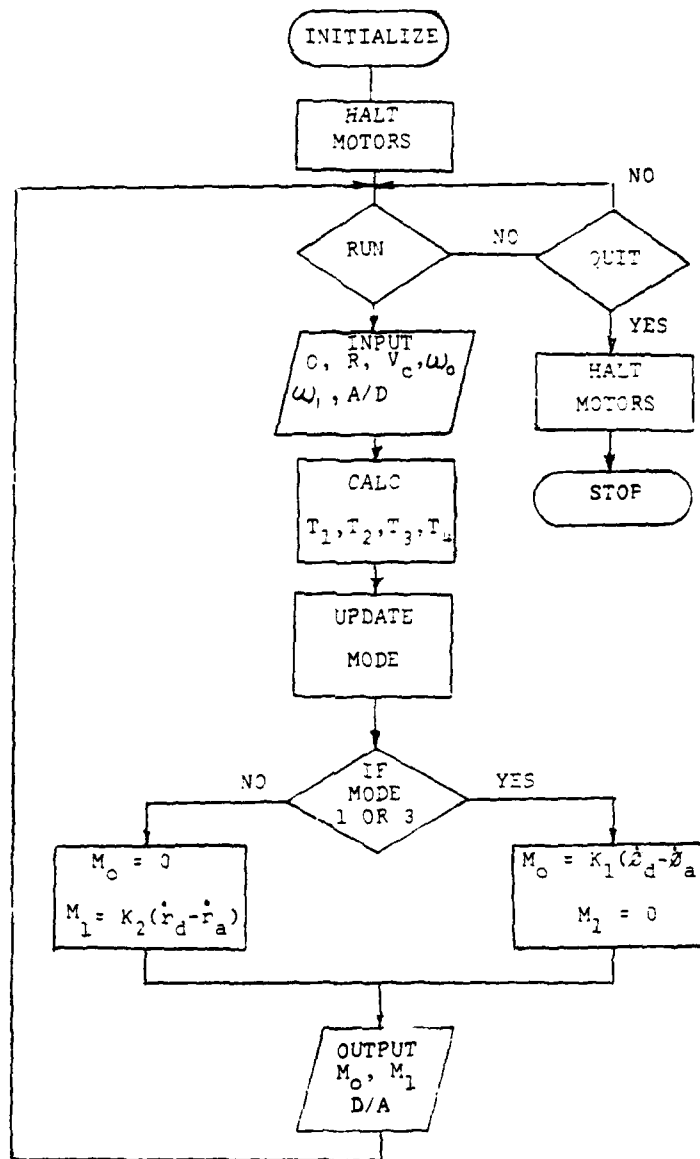


FIGURE 6.3
FLOW CHART OF SIMPLIFIED CONTROL PROGRAM

by rate some constant gain. Since all system parameters are supplied to the computer from the analog-to-digital converter as an integer number between -512 and 512, dimensional similarity in forming the error signal is not absolutely necessary. However, it was felt that maintaining correct scale and dimension would avoid problems with significant digits by keeping all values in the feedback equations similar in magnitude.

The gains used were determined by trial and error to be the highest allowable without instability effects. Velocity feedback alone proved to be sufficient for the initial energy tests despite the fact that there was a rather large steady state error.

Software lag compensators were used to reduce the steady state error but also reduced the response time to an unacceptable level. Positional error terms were added to the feedback equations but their effectiveness has not, at the time of this writing, been fully investigated.

The main control program outlined by Figure 6.3 was coded in PASCAL. PASCAL has several advantages over FORTRAN especially in control application. The major advantage is its readability. More specifically, it allows user selected memory locations and direct manipulation of stored data. Another advantage is that PASCAL can use FORTRAN subprograms. Several FORTRAN subroutines were called by the main program, in particular, for off-line data manipulation and output.

This simplified control program is short enough so that the sampling rate effect was deemed negligible. No program interrupts are used to update data during the main program loops. Unfortunately it was discovered that this assumption is valid only when the computer was lightly loaded with other user requests for C.P.U. time. The "Monopod" leg system was generally undependable due to sample rate instability

whenever the average execution time for the control program loop exceeded 50 milliseconds. The Monopod could only be run at full speed if the loop execution times were less than 20 msec. The degradation of performance between 20 and 50 milliseconds is rather subtle since the initial effect is overshooting of the limits which delineate the modes. As the execution time increases, the foot trajectory becomes visibly distorted. If the minimum execution time exceeds 50 milliseconds the system is usually completely uncontrollable.

6.4 Control hardware.

Figure 6.4 represents the Monopod control system hardware configuration. The major component is the PDP 11/70 digital computer. To interface the computer with the Monopod, an analog to digital (A/D) converter, digital to analog (D/A) converter, and two DR11-C general purpose 16-bit parallel transform interface devices are used.

The A/D converter is a standard 16 channel SDM835 unit. The basic characteristics of the unit are as follows:

input	10 mV to 10V
output	10 digital bits
accuracy	$\pm .25\%$
sample rate	3.3×10^4 C.P.S.*

The D/A converter is actually the "Digital-Word-to-Pulse-Width-Converter" designed by Dr. K. Olson and described in Chapter 5. There are currently only two output channels available, one for each motor. When the abduction-adduction actuator is required, another D/A circuit will be added.

* The conversion time assumed in the design of the overall control system was 20 μ sec.

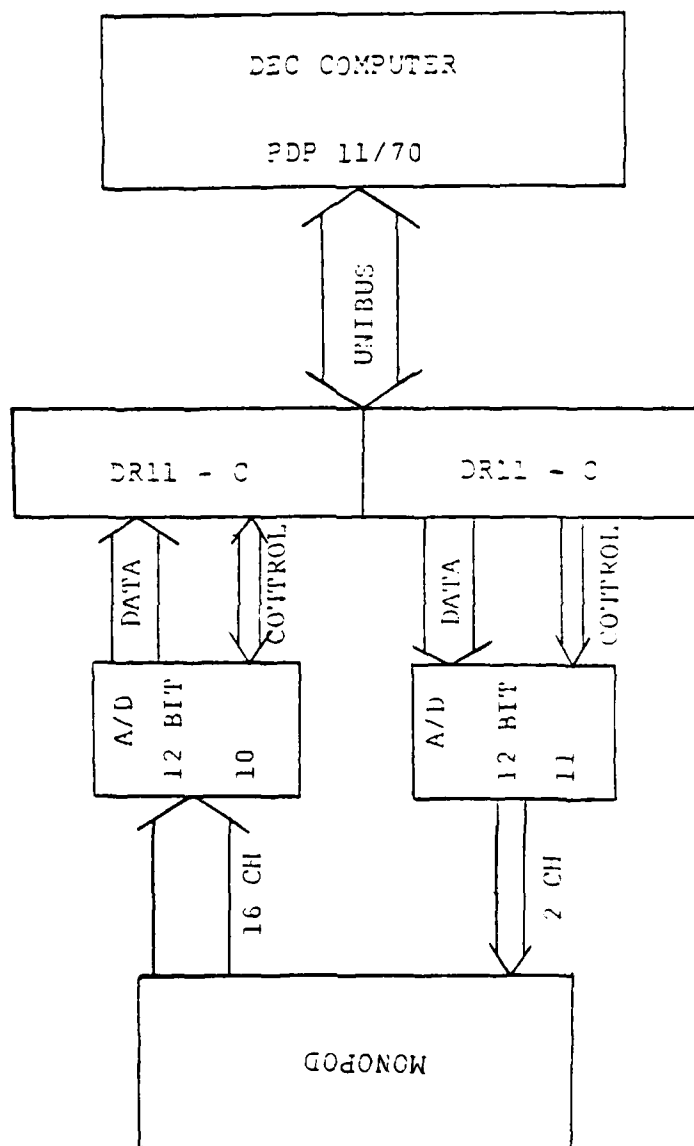


FIGURE 6.4 MONOPOD CONTROL SYSTEM HARDWARE CONFIGURATION

The DR11-C interface devices are required to effect the parallel data transforms between the PDP 11 Unibus and the A/D:D/A converters. Each DR11-C has an input, output and status register. Interrupt, command, and monitoring bits in the status register are controlled either by the computer program or the converters.

This hardware configuration may be replaced by a selfcontained micro computer system which could be mounted directly on the Monopod cart. The current system is slightly cumbersome in a strictly physical sense due to the trailing data lines between the various components. However, the PDP 11/70 is an excellent system with which to develop new control schemes. Its off line data reduction and I/O capabilities make it especially well suited to energy consumption tests.

Chapter 7

Energy/Power Tests of the Monopod System

7.1 Introduction

The goal of the project, on which this thesis reports, was to design an energy efficient leg mechanism. Specifically, a ten fold improvement over the OSU Hexapod was sought. To ascertain the extent to which this primary objective was met, a series of tests were performed with the Monopod. The tests essentially consisted of running the Monopod on a level floor forward and backward at various speeds. During each run 16 system variables were sampled and stored at a rate of approximately a 30 Hz. This real time data was then analyzed off line. The major system variables recorded along with the time provided by the internal clock of the computer included the total 20 V D.C. power, rotory actuator power, linear actuator power, cart velocity, actuator speeds, and actuator positions. With this data the instantaneous power consumed could be related to the cart speed and leg position throughout each cycle. Numerical integration of the power and velocity data was performed to obtain energy consumption and stride length. The programs used to control the Monopod were discussed in the previous chapter. Although there were three different programs, the data presented in this chapter were obtained under simple velocity feedback control. As a result of using this

control program for the energy/power tests two important points should be kept in mind.

- 1) The behavior of the planar leg in the cart system does not model exactly the behavior of the leg in a multi-leg vehicle.
- 2) As a consequence of point (1), the Monopod operated with a energy penalty handicap.

The principle reason for the disparity between the leg in the cart and in an actual six-legged walking machine is that the Monopod, under the simple velocity feedback/joystick control, cannot maintain a uniform velocity. This is caused partially by the fact that the cart must coast while the leg is in the transfer phase. Also, the leg linkage requires a monotonic change in drive crank rotational velocity in order to produce a uniform horizontal velocity of the foot. Point two above is thus validated since the Monopod system under these conditions must pay the energy cost of accelerating its 200 lb mass each cycle. In comparison, the Hexapod power consumption data from reference [36], which will be used as a base line, is for uniform horizontal motion.

7.2 Methods for Comparing Monopod Data to Hexapod Data

Obviously a direct comparison of the power requirement for a six-legged free walking vehicle and a single leg in a wheeled frame is not valid even through the total vehicle weights differ by only 10%. The simplest correlation function to use is a constant scale factor. To use a constant, the speeds of both vehicles should be the same as should the leg duty factors. The leg duty factor, β , is defined as the amount of

time a leg is in contact with the ground divided by the total leg cycle time.

For multilegged systems in creeping gait locomotion, optimum static stability is maintained by varying the leg duty factor with speed. The Hexapod duty factor changes β from .8511 at 1.0 m/sec to .5 at 6 in/sec. The Monopod system was run, for these preliminary tests, using a constant duty factor of .5. (In actuality the duty factors calculated from the real time data ranged from .46 to .56.) It was believed that a valid comparison could still be made notwithstanding the different duty factors at speeds less than 6 in/sec. An argument could be made to restrict the comparison to only the tripod speed of the Hexapod since the use of a scale factor correlation is truly appropriate only for a tripod gait. To restrict these preliminary tests to a single speed would make it impossible to identify any trends in the energy/power/speed characteristics of the Monopod. Future tests under more sophisticated control programs should be able to discover any significant error in the conclusions derived from these tests due to the tripod gait assumption.

In the tripod gait ($\beta = .5$) sets of three legs move in unison. Since the sets are approximately 180° out of phase with each other, one set is in transfer while the other is in support. Therefore the energy used by the Hexapod in 12 inches of motion (approximately one stride) is equivalent to the energy used by three Hexapod legs completing a full cycle. On this basis, the scale factor for comparing the Hexapod to the Monopod is 3.0. Using this scale factor still implies a penalty against the Monopod due to the different leg loadings. For the Hexapod in a tripod gait, the two legs in contact with the ground on the same side each carry a load of about 55 lbs while only the leg on the opposite side of the vehicle carries the 110 lb load that the Monopod was designed for.

In order to reduce this penalty somewhat, the Monopod leg load was reduced to 95 lb. This is greater than the average load with vehicle weight difference compensation included, i.e.,

$$\text{Monopod leg load} = \text{Avg Hexapod leg load} \times \frac{\text{Hexapod weight}}{\text{Monopod weight}}$$

For the tripod gait, the average leg load is 82.5 lb. Also the Hexapod weight is 220 lb and the Monopod weight is 200 lb. Therefore, the Monopod leg load is 91 lb. Hence 95 lb was used since it allowed better balancing of the inner frame while still being slightly conservative.

A more accurate comparison which would reduce the Monopod penalty would be to test the planar leg with both 55 and 110 lb loads at the Hexapod tripod speed. The Hexapod equivalent average power or energy would be formed by the linear relation.

$$\text{Hexpod equivalent} = 2(Q_{55}) + Q_{110}$$

where

$$Q_{55} = \text{Monopod results at 55 lb load}$$

and

$$Q_{110} = \text{Monopod results at 110 lb load.}$$

This linear summation method was not used because it would have required rather elaborate counter balancing of the inner frame. With electronics on board, the inner frame and leg weighs about 70 lbs.

There is another approach to the Hexapod/Monopod comparison problem. This approach uses the dimensionless motion resistance coefficient defined by Gabbrelle and Von Karman in reference [40]. The coefficient was formulated in order to compare all types of locomotion systems, both biological and mechanical, on a uniform basis. The only stipulation is that for comparing any two systems, the ratio of the

useful load to the gross weight should be the same. The coefficient was termed Specific Resistance or Coefficient of Specific Tractive Force, and is defined as

$$\epsilon = \frac{P}{WV}$$

where P = maximum power required (ft-lb/sec)

W = system gross weight (lb)

and

V = velocity produced by P (ft/sec).

Here, P and V are defined for horizontal motion.

It should be apparent that, using the dimensions given, ϵ is a pure number indeed. Specific resistance can also be viewed as the ratio of the total drag, both direct environmental and internal, to the gross weight. Garbrielle and Von Karmon have, in fact, referred to it as a "global coefficient of drag" for a vehicle. Some care must be exercised when applying ϵ to the Monopod or Hexapod especially if one wishes to compare the Hexapod or Monopod with the vehicles plotted by Gabbrielli and Von Karman. The difficulty is that both the Monopod and Hexapod do not carry their own power supply or sufficient electronics to perform the required control tasks for locomotion.* They are thus fundamentally unlike the rest of vehicles plotted (with the possible exception of electric trains). However, because the most important comparison to be made here is between the Monopod and the Hexapod, the fundamental differences with other vehicles need not be addressed rigorously.

It is appropriate to restate an important point concerning these tests. Note that the comparison we wish to make is not between the

*The Monopod can possibly become completely "energy autonomous" after installation of the 8086 microcomputer on board. Seven small 6 volt wet cell batteries should provide enough energy for a few hours of operation.

Monopod and the Hexapod but between an imaginary machine having six planar legs, of the Monopod design, and the Hexapod. To ensure a valid comparison or at least error on the conservative side, the weight term of ϵ for the Monopod was taken to be just the leg load of 95 lb and not the full Monopod weight of 200 lb. However, the full weight of 220 lb was used in the calculations of ϵ for the Hexapod.

7.3 Comparison of Monopod and Hexapod in terms of power and energy usage

Tables 7.1 thru 7.3 contain the gross results of the Monopod energy tests. The average cart velocities listed in the first column of each table represent the time average velocity of the cart during the support phase of the leg cycle. The assumption is that the next set of legs would be in place by the end of each support phase and would maintain the indicated average cart velocity. The power from the regulated 20 VDC supply was obtained by measuring the output current by means of a precision shunt and by multiplying the converted digital output in the computer by the constant source voltage of 20.0. The 20 VDC source supplied the power to the rotory actuator, linear actuator and linear actuator brake solenoid. The 5 VDC source supplied the power to activate the power transistors in the motor control bridge circuits described in Chapter 5. This power was not measured directly but calculated from the digital motor voltage pulse width command and the measured current required to bias the transistors. Due to the well defined behavior of the transistors this method of obtaining the control circuit power cost was considered acceptable. The only energy use not accounted for in the data was the power needed for the potentiometers.

AVERAGE CART SPEED (M/SEC) (IN/SEC)	SUPPORT TIME (SEC)	CYCLE ELAPSE TIME (SEC)	20 VDC SUPPLY		5 VDC SUPPLY		TOTAL	
			AVE. PWR* (WATTS)	ENERGY (JOULES)	AVE. PWR (WATTS)	ENERGY (JOULES)	AVE. PWR (WATTS)	ENERGY (JOULES)
.074 2.9	5.85	11.95	11.3	135.5	14.2	169.8	25.6	305.4
.097 3.8	4.27	8.23	12.0	99.0	14.5	119.3	26.5	218.3
.141 5.6	2.90	5.63	17.4	97.8	15.2	85.4	32.5	183.6
.211 8.3	1.93	3.98	39.0	155.5	16.6	66.3	55.7	221.8
.245 9.6	1.65	3.55	44.6	158.5	17.5	62.0	62.1	220.5
.267 10.5	1.45	3.18	57.5	183.1	18.2	57.8	75.7	240.9

* AVE. PWR = AVERAGE POWER

TABLE 7.1 MONOPOD POWER/ENERGY USE; ONE CYCLE, FORWARD STRIDE

AVERAGE CART SPEED (M/SEC) (IN/SEC)	SUPPORT TIME (SEC)	CYCLE ELAPSE TIME (SEC)	20 VDC SUPPLY		5 VDC SUPPLY		TOTAL	
			AVE PWR [*] (WATTS)	ENERGY (JOULES)	AVE PWR (WATTS)	ENERGY (JOULES)	AVE PWR (WATTS)	ENERGY (JOULES)
0.039 1.5	10.81	22.52	11.7	263.5	13.3	300.6	25.0	564.1
0.071 2.8	5.90	11.60	10.6	122.8	13.7	158.5	24.3	281.3
0.137 5.4	2.90	6.23	17.6	109.6	14.5	90.4	32.1	200.0
0.182 7.2	1.92	4.03	28.9	116.6	17.4	70.0	46.3	186.6
0.239 9.4	1.82	3.54	29.0	102.5	16.3	57.5	45.2	160.0
0.296 11.7	1.47	3.10	45.1	139.9	17.3	53.6	62.4	193.5

* AVE PWR = AVERAGE POWER

TABLE 7.2 MOJOPOD POWER/ENERGY USE; ONE CYCLE, REVERSE STRIDE

AVERAGE CART SPEED (M/SEC) (IN/SEC)	SUPPORT TIME (SEC)	CYCLE ELAPSE TIME (SEC)	20 VDC SUPPLY		5 VDC SUPPLY	TOTAL	
			AVE PWR [*] (WATTS)	ENERGY (JOULES)	AVE PWR (WATTS)	ENERGY (JOULES)	ENERGY (JOULES)
0.089 3.5	4.54	9.458	9.1	85.2	14.1	132.6	217.8
0.149 5.9	2.72	5.440	13.7	74.3	15.0	81.4	155.7
0.201 7.9	2.02	4.040	20.1	80.3	15.8	63.3	143.6
-0.123 -4.9	3.29	5.880	13.3	77.8	14.6	85.3	163.1
-0.187 -7.4	2.17	4.090	19.8	81.1	15.5	63.7	144.7
-0.229 -9.0	1.77	3.470	27.1	93.4	16.4	56.7	150.0

* AVE PWR = AVERAGE POWER

TABLE 7.3 POWER/ENERGY COST FOR MONOPOD, ONE LEG CYCLE; NO LOAD

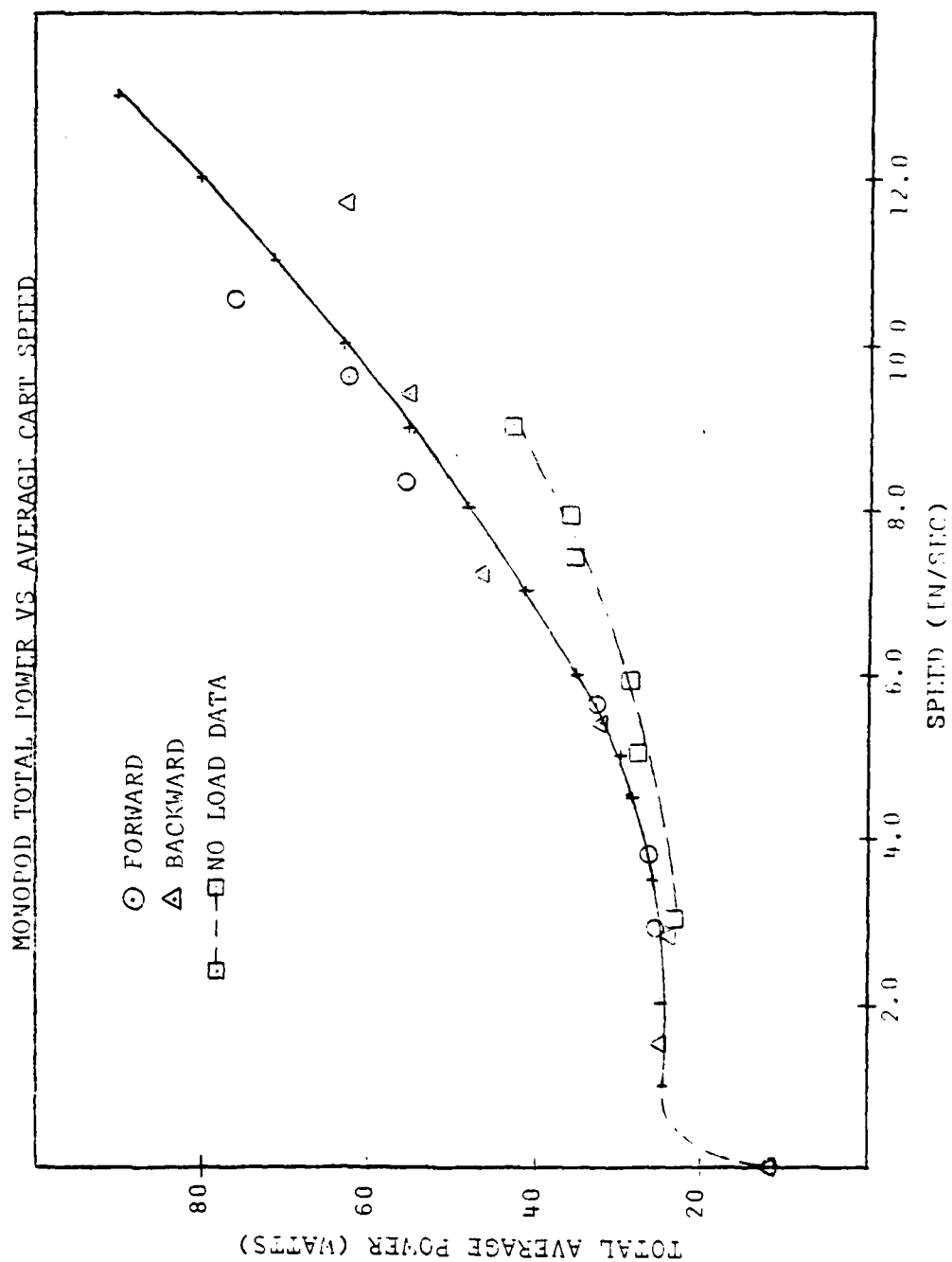


FIGURE 7.1 RELATIONSHIP BETWEEN MONOPOD AVERAGE POWER AND SPEED

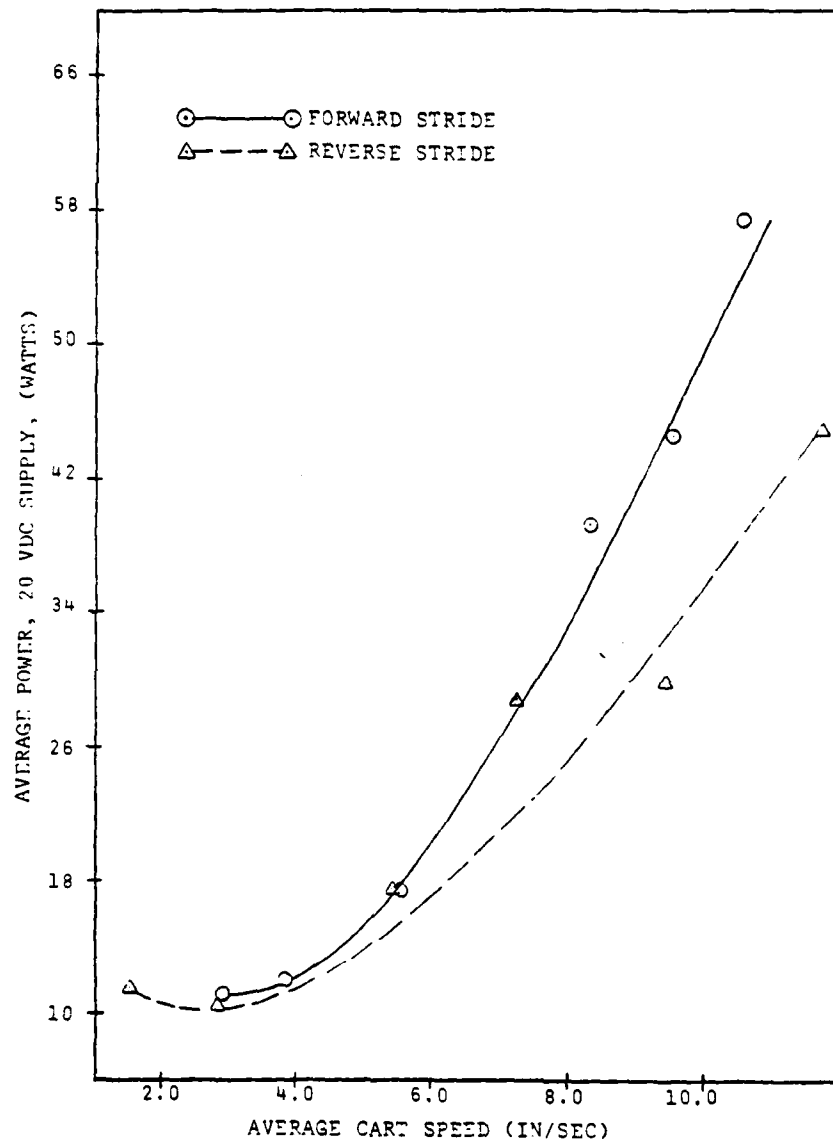


FIGURE 7.2 ACTUATOR AVERAGE POWER VS CART SPEED

The high resistance of the potentiometers used maintained the power requirement below .25 watts which was deemed negligible.

Figure 7.1 shows graphically the relationship between average power and speed. The curves through the data were graphically determined to minimize the perpendicular distance between the data points and the tangent to the curve. Three important points are immediately apparent from inspection of Figure 7.1.

- 1) For speeds up to about 4.0 in/sec the average power required is essentially independent of speed.
- 2) For speeds above 7 in/sec the average power required is related to cart speed in a nearly linear fashion.
- 3) For speeds up to 5 in/sec. the power required for locomotion seems to be largely independent of leg load.

The data point at zero speed represents the constant power overhead introduced by the use of power transistor instead of Silicon Control Rectifiers (SCR's) in the actuator motor bridges. Simply replacing the two power transistors in each bridge which control motor rotational direction, with SCR's would in fact lower the curves of Figure 7.1 by 12.2 watts. The significance of this potential power saving is discussed later.

Figure 7.2 is a plot of average power from the 20 VDC supply verses average cart speed. Since this supply powers just the actuators, the curves of Figure 7.2 suggest a preferred direction of motion from the energy standpoint, for speeds greater than 6.0 in/sec.

The lower average power for higher speeds in the reverse direction is explainable from a kinematic viewpoint. Referring to Figure 2.8 it is seen that the static torque requirement is greatest for toe-down in the

forward mode (crank angle of 160°). Moreover for a constant crank rotation, the horizontal velocity of foot monotonically decreases from toe-down to toe-off in the forward direction. These related characteristics of the leg linkage are a disadvantage at toe down in the forward direction since, during these tests, the cart had to accelerate its full mass from zero velocity at the beginning of each stride. Conversely, in the reverse direction the kinematics of the linkage gives the rotor actuator a better mechanical advantage with which to start the cart mass moving. In the reverse case, the maximum cart velocity always occurs at the end of the cycle as opposed to the middle of the cycle for a forward stride. In retrospect this result is fairly obvious from the data generated by the FORBAR program discussed in Chapter 2. It must be admitted that the apparent preferred direction of stride motion was overlooked due to a predisposition to view the preferred leg motion as originally defined during the synthesis process as being the forward direction. However, for slower speeds Figure 7.2 shows the direction of motion to have only minimal affect. This is largely due to the simple fact that the required acceleration is small. A multi-legged vehicle travelling at a relatively uniform horizontal velocity will also experience minimal acceleration. The preferred direction of leg motion under these circumstances may prove to have little benefit even for the higher leg speeds. The no-load data curve of Figure 7.1 seems to support this since the data has much less vertical spread even at the higher speeds.

The main curve of Figure 7.1 was used to interpolate the Monopod data for comparison with the Hexapod data from reference [36]. A copy of the pertinent sections from this reference are included in Appendix C. Table 7.6 contains the final results of the Monopod/Hexapod Power energy comparison. Note that the energy values given are for one foot of

AVERAGE CART SPEED (M/SEC) (IN/SEC)	DUTY FACTOR β	ROTOR ACT. MOTOR		LINEAR ACT. MOTOR		BRAKE SOLENOID		MOTOR DRIVE CIRCUITS	
		AVE PWR (WATTS)	ENERGY (JOULES)	AVE PWR (WATTS)	ENERGY (JOULES)	AVE PWR (WATTS)	ENERGY (JOULES)	AVE PWR (WATTS)	ENERGY (JOULES)
0.074 2.9	0.50	4.9	58.7	1.2	14.65	3.2	37.0	16.3	195.3
0.097 3.8	0.52	5.8	48.0	1.4	11.90	2.7	21.9	16.6	137.4
0.141 5.6	0.52	9.2	52.0	2.3	12.70	2.5	14.2	18.5	104.6
0.211 8.3	0.49	21.0	83.7	4.7	18.60	2.4	9.6	27.6	109.8
0.245 9.6	0.47	24.7	87.6	3.5	12.40	2.9	10.5	31.0	110.0
0.267 10.5	0.46	29.2	92.8	7.2	22.90	2.2	6.9	37.1	118.3

* AVE PWR = AVERAGE POWER

TABLE 7.4 MONOPOD ENERGY AUDIT; ONE CYCLE, FORWARD STRIDE

AVERAGE CART SPEED (M/SEC) (IN/SEC)	DUTY FACTOR <i>B</i>	ROTARY ACT. MOTOR		LINEAR ACT. MOTOR		BRAKE SOLENOID		MOTOR DRIVE CIRCUITS	
		AVE PWR (WATTS)	ENERGY (JOULES)	AVE PWR (WATTS)	ENERGY (JOULES)	AVE PWR (WATTS)	ENERGY (JOULES)	AVE PWR (WATTS)	ENERGY (JOULES)
0.039 1.5	0.48	2.8	62.4	1.6	34.9	5.0	113.3	15.6	351.2
0.071 2.8	0.51	4.0	46.9	1.3	15.4	3.3	38.7	15.7	182.0
0.137 5.4	0.47	8.7	54.2	1.5	9.5	4.2	26.0	17.7	110.3
0.182 7.2	0.48	17.9	72.3	2.5	9.9	4.0	16.1	21.9	88.2
0.239 9.4	0.51	17.0	60.2	5.1	18.2	2.3	8.2	20.9	74.0
0.296 11.7	0.47	26.4	82.0	7.6	23.8	2.2	6.9	26.2	81.3

* AVE PWR = AVERAGE POWER

TABLE 7.5 MONOPOD ENERGY AUDIT; ONE CYCLE, REVERSE STRIDE

AVERAGE CART SPEED (M/SEC) (IN/SEC)	MONOPOD TOTAL		SPECIFIC RESIST. ϵ_M	HEXAPOD TOTAL		SPECIFIC RESIST. ϵ_H	POWER RATIO $\bar{P}_H/3\bar{P}_M$	SPECIFIC RESIST. RATIO ϵ_H/ϵ_M
	AVE PWR (WATTS)	ENERGY (JOULES)		AVE PWR (WATTS)	ENERGY (JOULES)			
0.025 1.0	# 25.0	# 610.0	2.33	756.3	9076.0	30.4	10.08	13.04
0.051 2.0	25.0	305.0	1.17	926.1	5556.0	18.7	12.35	15.98
0.076 3.0	25.3	202.0	0.789	1103.0	4412.0	14.8	14.53	18.76
0.102 4.0	26.8	161.0	0.624	1499.0	4496.0	15.0	18.64	24.04
0.127 5.0	30.0	146.0	0.559	1556.0	3375.0	12.5	17.29	22.36
0.152 6.0	35.0	143.0	0.544	2136.0	4272.0	14.3	20.34	26.29
0.178 7.0	41.0	143.0	0.546	# 2660.0	# 9120.0	15.3	21.63	27.96

LINEAR EXTRAPOLATION

* AVE PWR = AVERAGE POWER

TABLE 7.6 COMPARISON OF MONOPOD TO HEXAPOD POWER/ENERGY REQUIREMENTS
FOR ONE FOOT OF LEVEL LOCOMOTION

AVERAGE CART SPEED (M/SEC) (IN/SEC)	MONOPOD WITH SCR CONTROLLERS		SPECIFIC RESIST. ϵ	POWER RATIO $\bar{P}_H/3\times\bar{P}_M$	SPECIFIC RESIST. RATIO ϵ_H/ϵ
	AVE PWR *	ENERGY			
0.025 1.0	12.8	307.0	1.19	19.7	25.5
0.051 2.0	12.8	153.0	0.596	23.6	31.4
0.076 3.0	13.1	105.0	0.407	25.2	36.4
0.102 4.0	14.6	87.3	0.340	34.2	44.1
0.127 5.0	17.8	85.4	0.332	29.1	37.6
0.152 6.0	22.8	91.0	0.354	31.2	40.4
0.178 7.0	28.8	98.6	0.383	30.8	39.9
0.203 8.0	35.9	108.0	0.418	---	---
0.229 9.0	42.8	114.0	0.443	---	---
0.254	50.8	122.0	0.473	---	---

* AVE PWR = AVERAGE POWER

TABLE 7.7 ESTIMATED MONOPOD POWER/ENERGY USAGE WITH
SCR MOTOR DRIVERS; ONE FOOT OF LEVEL LOCOMOTION

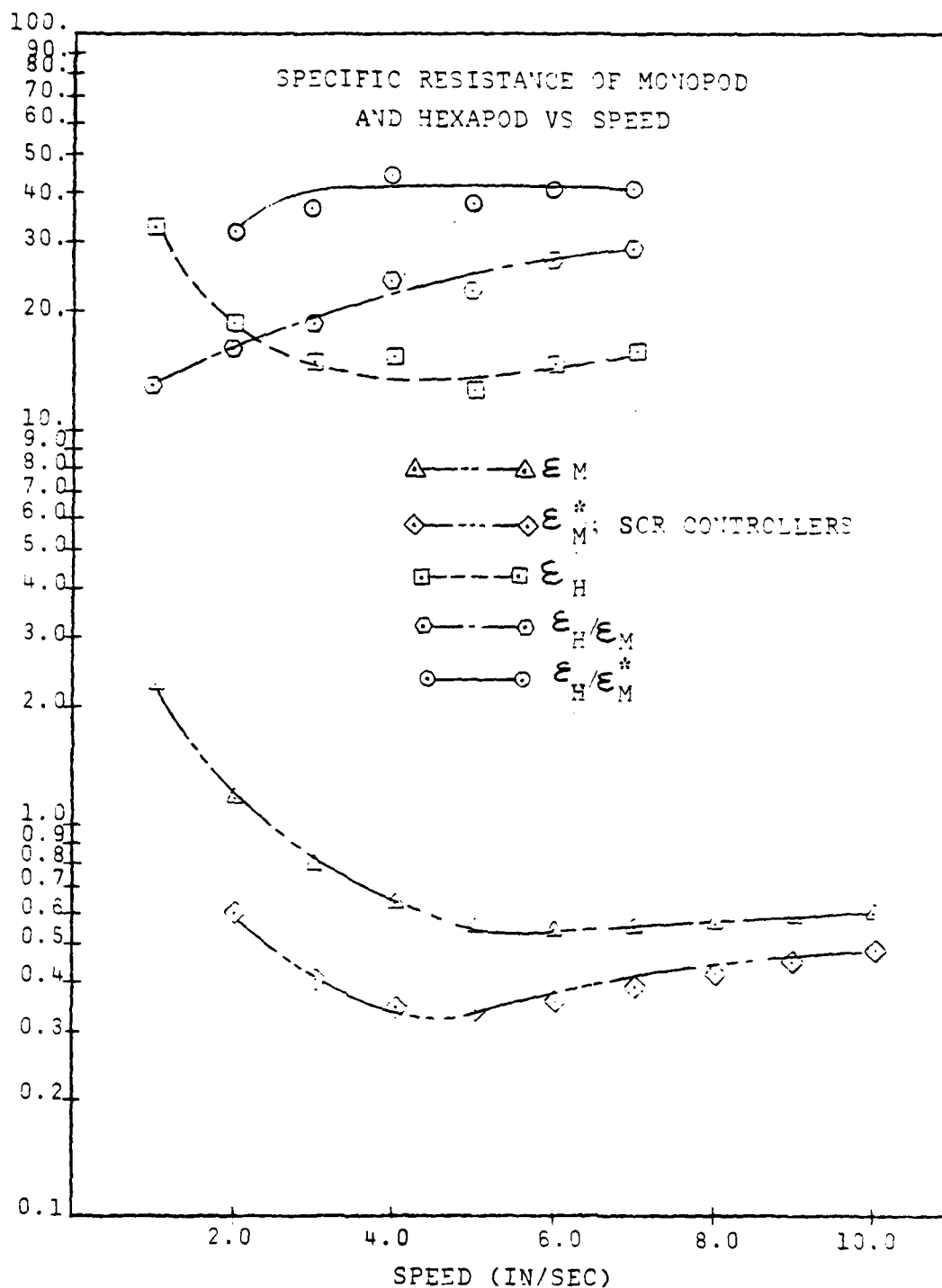


FIGURE 7.3 GRAPHICAL REPRESENTATION
OF SPECIFIC RESISTANCE
AND RESISTANCE RATIOS
BETWEEN MONOPOD AND HEXAPOD

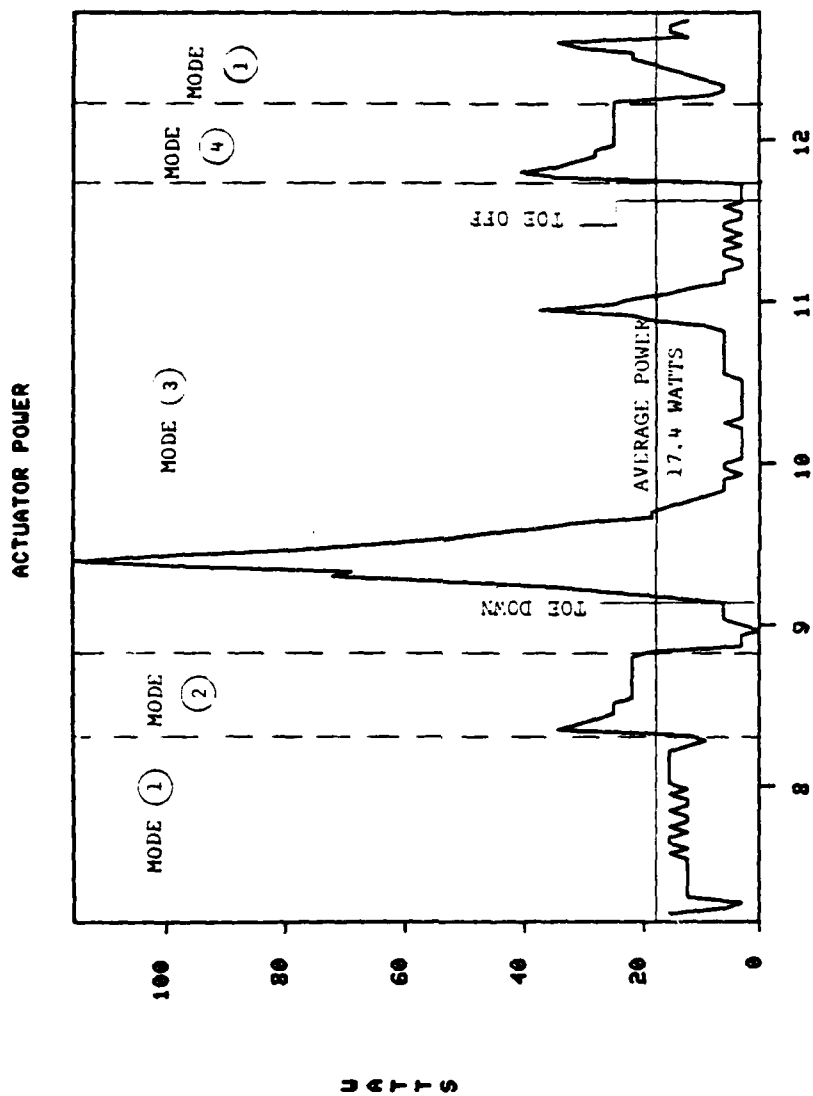


FIGURE 7.4 ACTUATOR POWER VS. REAL TIME.
 LEG LOAD = 95.0 LBS AVERAGE VELOCITY = 5.6 IN/SEC

ACTUATOR POWER

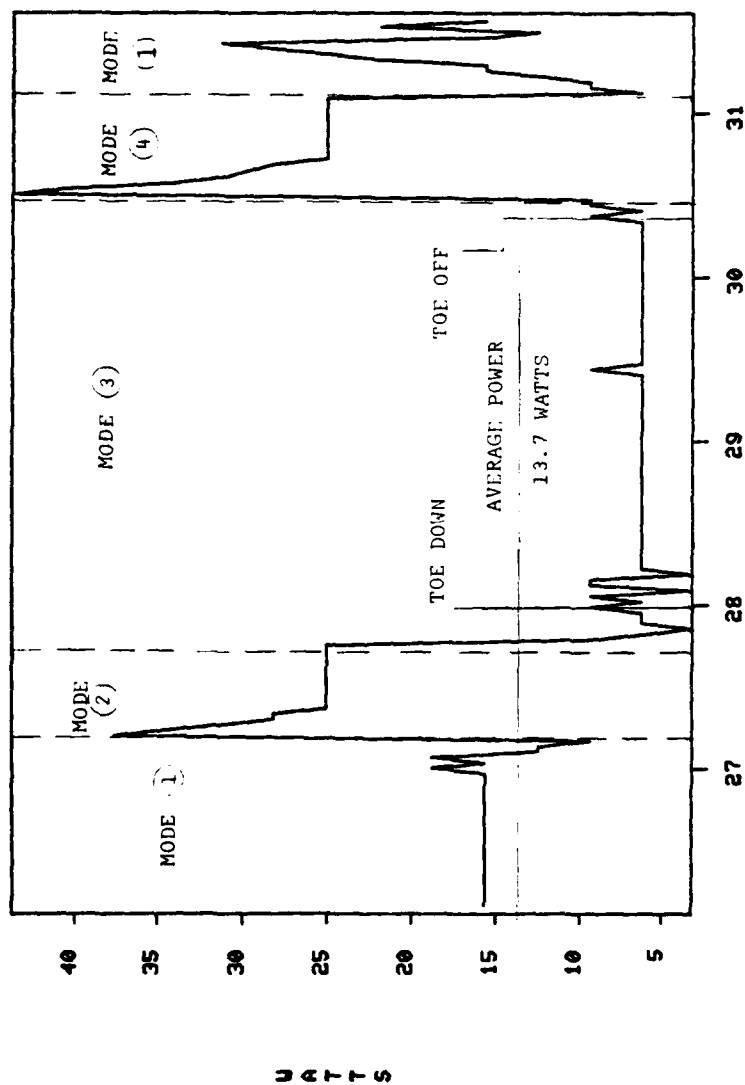


FIGURE 7.5 ACTUATOR POWER VERSUS REAL TIME
 LUG LOAD = 0.0 LBS AVERAGE VELOCITY = 5.9 IN/SEC

motion. The Monopod average stride is, however, 16.1 inches. The energy data for the Monopod was consequently generated from the average speed and power data. The correlation between average power or specific resistance is expressed simply as a ratio and is listed in the last two columns of Table 7.6. The ratio of average hexapod power to three times the average monopod power varies from 10.08 at 1.0 in/sec to a maximum 21.63 at 7.0 in/sec. The mean power ratio is 16.41 which is well beyond the specified order of magnitude power reduction. The ratio of the specific resistances, listed in the last column of Table 7.6, provides a basis for comparison independent of possible scale factor errors. According to this criterion, the average multiple of improvement for the Monopod system is 21.20. Again, this is well beyond the projected goal of 10X improvement. Through the primary design goal of the Monopod system has clearly been met and exceeded, the magnitude of the improvement can rather easily be further increased.

As has been mentioned, there is a constant 12.25 watt energy cost associated with the present power transistor, motor bridge circuit design (see Figure 5.3 and Appendix C). By replacing the power transistors, represented by A1 and B1 of Figure 5.3, with silicon control rectifiers, (SCR's) the 12.25 watt biasing power can be eliminated. In fact, the switches A2 and B2 could also be realized with SCR's but not without significantly more complex circuitry. Table 7.7 contains the estimated average power for the monopod with the top half of each motor bridge implemented with SCR's in place of the currently used power transistors. Table 7.8 summarizes the added improvement possible with SCR motor controllers. The data from Tables 7.6 and 7.7 is illustrated graphically in Figure 7.3. Inspections of these curves reveal an asymptotic nature in ϵ_m as speed increases.

Table 7.8

	<u>Transistor</u>	<u>SCR</u>	<u>Improvement</u>
Mean Power Ratio ($\bar{P}_H/3\bar{P}_M$)	16.41	27.69	69%
Mean Specific Resistance Ratio (ϵ_H/ϵ_M)	21.20	36.48	72%

This indicates that the non-linear losses, both mechanical and electrical, have stabilized at some constant value. Thus the ratio of power to velocity can only approach a constant if the internal losses contained in the power term and the external losses embedded in the velocity term are nearly linear. The ϵ_M curve in Figure 7.3 indicates a minimum specific resistance at about 6.0 in/sec. Correspondingly this point represents an optimum operational speed from an energy view point. The curve ϵ_M^* displays a more distinct minimum at about 5.0 in/sec. This probably more nearly represents the optimum speed of the leg mechanism itself since ϵ_M^* does not contain the known electrical losses of the up-down power transistors. As cart speed increases beyond 5.0 in/sec the advantage of the SCR controlled motors reduces. Though ϵ_M^* will always be less than ϵ_M , both should approach a common curve as speed increases by virtue of the fact that the SCR's eliminate a constant loss rather than one proportional to power.

Interestingly, the no-load curve of Figure 7.1 is quite close to the 95 lb leg load curve for speeds between 3.0 and 6.0 in/sec. The percentage increase in power for full load motion is only 8.5% at 3 in/sec and 17% at 6 in/sec. This is, at least in part, due to the relatively constant power requirements of the motor driver circuits.

Figures 7.4 and 7.5 are plots of the instantaneous power required for all the actuators versus real cycle time. Figure 7.4 is for a fully loaded leg cycle whereas Figure 7.5 displays the actuator power for the leg cycled in mid air. The increase in average power shown in Figure 7.4 is 27% over the no load case of Figure 7.5. Note that the average velocities are about the same. The increase in peak power is however considerably greater, about 160%. The large power peak which occurs at about 9.5 second in Figure 7.4 corresponds to the acceleration of the Monopod from zero velocity and the raising of the inner frame center of gravity as discussed in Chapters 2 and 4. The second smaller peak which occurs at about 11 seconds corresponds to the second hump in the coupler point curve for the leg mechanism (see Figure 2.4a). As may be expected, the power curves for modes 1,2, and 4 are quite similar in both figures. This is completely reasonable since in these modes the only loads are inertial and frictional constants.

Study of Figures 7.4, 7.5 and similar plots for other speeds lead to the conclusion that a significant reduction in total energy cost for the monopod system could be realized by reducing the various rotational inertia terms in the mechanisms. Specifically, the linear actuator energy requirements could be reduced by trimming the mass of its rotating components.

Figure 7.6 illustrates how the Hexapod and Monopod compare to other locomotion systems in Terms of Specific Resistance. It should be kept in mind that, as previously mentioned, neither the Monopod or Hexapod carry their own power supply and are therefore unlike the rest of the locomotion systems represented in the figure. The value of ϵ for the Monopod shown in Figure 7.6 is based on the full vehicle weight of 200 lbs. Not only is this more consistent with the other systems but also

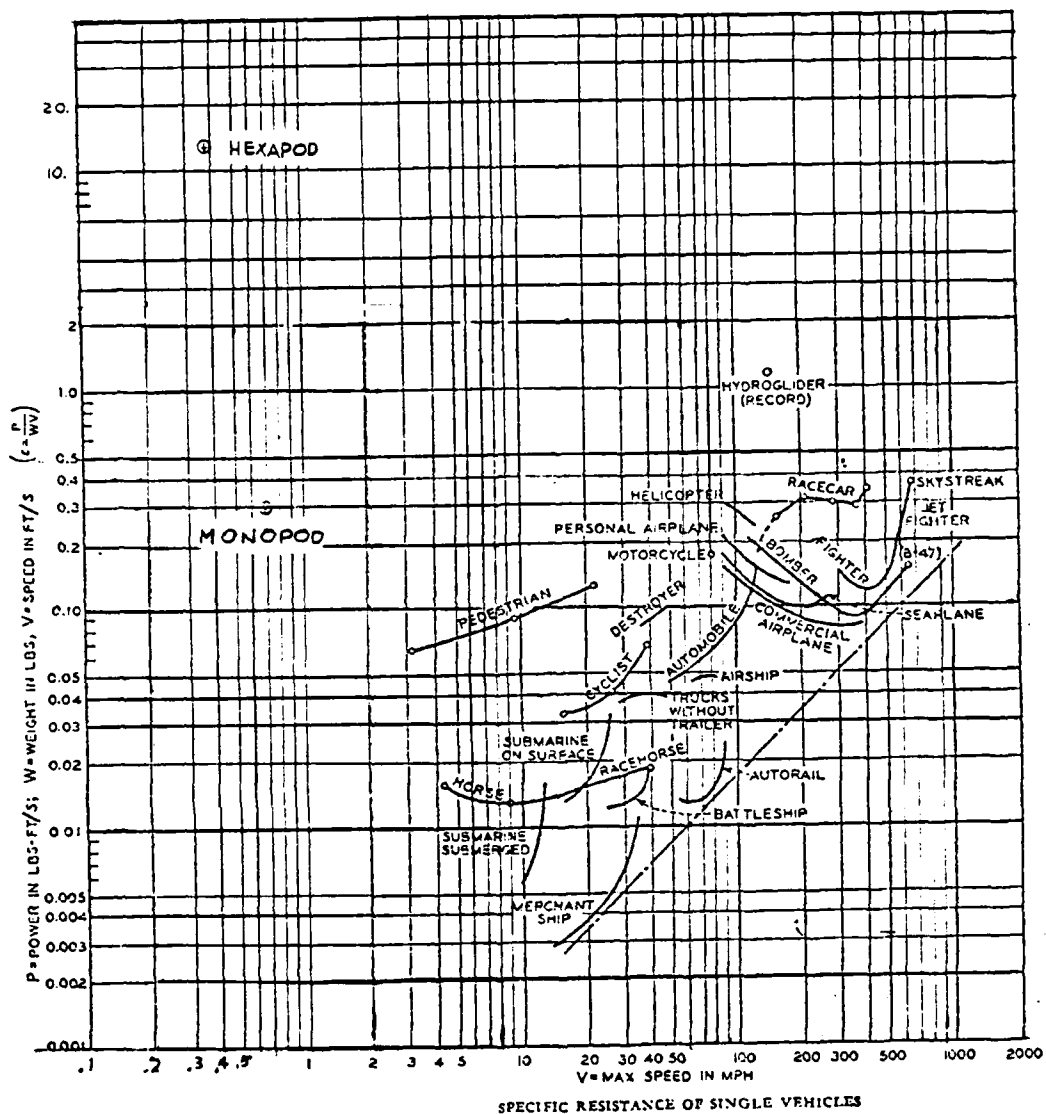


FIGURE 7.6 SPECIFIC RESISTANCE (ϵ) VS MAXIMUM VEHICLE SPEED
 ADAPTED FROM GABRIELLI AND VON KARMEN
 "WHAT PRICE SPEED" REF. [40]

represents a reasonable approximation of the gross weight of the Monopod with batteries and a selfcontained microprocessor on board.

At the present time the Monopod operates with about 50 lbs of lead and iron ballast. This ballast will be removed if the Monopod is made self propellable. Along with the reduction in size and weight of various other non-optimum components, the autonomous Monopod should not weigh much over 200 lbs. Irrespective of this estimate, Figure 7.6 clearly shows that the Monopod system is significantly closer than the Hexapod pointing the way to the ultimate specific resistance goal for any practical legged vehicle , namely, the graph area directly above the curve representing human locomotion.

Chapter 8

Discussion, Conclusions, and Extensions

The Monopod system has successfully demonstrated an order of magnitude reduction in energy cost in comparison with the OSU Hexapod. This conclusion was based on two different methods of comparison. Care has been taken to ensure that errors in these methods due to simplifying assumptions tended to penalize the Monopod system. It is therefore felt that the results presented are fundamentally correct. Improvements made in subsequent test procedures and control programs should serve to increase the margin of improvement established here. It should be kept in mind that the Hexapod data used from reference [36] was the best available at the time of this writing but was compiled in 1979. Before 1983 there will be new Hexapod energy data available generated with a significantly more sophisticated control program. This program will eliminate self generated loads in the Hexapod. However, the energy savings from this improvement is estimated to be only one percent [42].

The single design goal not clearly verified by the test results presented in Chapter 7 was the original maximum average velocity of 12 in/sec. Table 7.5 shows the highest average cart speed to be only 11.7 in/sec. Actually average cart speeds in excess of 12 in/sec. were recorded. However, for these speeds the duty factor (β) for the leg dropped below .45 due to saturation of the rotory actuator during the return phase (Mode 1). This saturation problem can be easily overcome

and higher average cart speeds, without motor saturation, can be obtained by simply raising the maximum supply voltage. Currently the maximum motor voltage is 20 VDC. The rotory and linear actuator motors are both nominally rated for 24 VDC. Data provided in Appendix B verifies that the motors can be run at even higher voltage levels. The initial testing of the Monopod was done at 20 VDC for reasons of conservation.

During the course of the test program, certain deficiencies in the Monopod system were discovered which had not been anticipated during the design process. The principle mechanical deficiency is the backlash in the rotary actuator. A certain amount of backlash is difficult to avoid if a conventional spur gear reducer is used. However it was found that the simple key coupler used between the actuator and drive crank shaft could not remain tight under the shock loading at toe down. Typically the coupling would begin to loosen after a dozen or so steps unless run very slowly. The coupler never failed completely but loosened by deforming the soft steel key until enough slip was generated to smooth the torque peaks by frictional energy dissipation. The excessive backlash in the drive crank generated in this way leads to problems in motor control stability, especially when a position feedback term is added to the control loop. This instability is due principally to the nonlinear unpredictable nature of this type of compliance. A possible solution to this problem would be to design a compliant coupler to interface the drive crank and rotary actuator. This coupler would be designed to smooth the torsional shock loads in a predictable manner. With a predictable compliance the motor control feedback loop can be compensated using classical control algorithms.

The energy power audit of the Monopod presented in Chapter 7 reveals that the brake solenoid on the linear actuator uses a considerable

amount of energy. In fact Tables 7.4 and 7.5 indicate that the brake solenoid uses more energy than the actuator motor for speeds up to approximately 6 in/sec.. This condition could be alleviated by redesigning the brake actuator system. By employing two electro magnetic solenoids in conjunction with a toggle mechanism, an actuation system with two nonenergized states could be devised. The solenoids in this case would be pulsed to change the brake state from "on" to "off" or vice-versa. Without the need for the brake solenoid to remain "on" while the brake is "off", the brake energy consumption would be reduced to a fraction of its present value especially at the lower speeds.

The only other significant improvement to the mechanical side of the Monopod system would be a lengthening of the coupler. It was found during further investigation into the kinematics of the planar leg mechanism that lengthening the coupler from 3.772 in to 4.055 in. would result in a flatter foot trajectory and lower torque requirements. Unfortunately this discovery came after the planar leg had been built. It would not, however, be difficult or expensive to alter the coupler bar to obtain this improvement.

By far the greatest work to be done in the future on the Monopod system will be concerned with the control programs. Much of the desirable additional control sophistication has already been investigated by Cheng in reference [38]. A logical extension to the implementation of these suggested control schemes is to employ the currently unused abduction-adduction actuator. With full three degrees of freedom the Monopod system can become a useful tool for investigating general motion control of planar type legs. The control techniques developed with the Monopod are not necessarily confined only to the four bar mechanism of

the Monopod. Actually much of the generalized control schemes would be applicable to any type of planar linkage leg.

References

1. Hane, Kurt, Applied Kinematics, McGraw-Hill Book Co., New York, NY 1967.
2. Song, Shin-Min, Theoretical and Numerical Improvements to Computer Aided Linkage Design, M.S. Thesis, The Ohio State University, Columbus, Ohio 1981.
3. Song, S.M., Johnout, V.J., Waldron, K., Kinzel, G., "Computer Aided Design of a Leg for an Energy Efficient Walking Machine", Proc. 7th Applied Mechanisms Conference, Kansas City, Mo., Dec. 1981.
4. Shigley, Joseph E., "The Mechanics of Walking Vehicles", Proc. 1st International Conference on Mechanics of Soil-Vehicle Systems, Torino, Italy 1961.
5. Morris, R.A. "Iron Mule Train", Space Division Aerojet-General Corp., El Monte, California 1967.
6. Hall, Allen S., Jr., Kinematics and Linkage Design, Balt Publishers, West Lafayette, Indiana 1966.
7. Chuang, Jo-Chick, Geometric Theory and Numerical Analysis for Interactive Mechanism Design, Ph.D. Dissertation, University of Houston, Houston, Texas 1980.
8. Duetschman, Michele and Wilson, Machine Design: Theory and Practice, Macmillan Publishing Co., Inc., New York, N.Y. 1975.

9. Juvinal, R.C., Stress, Strain, and Strength, McGraw-Hill Book Co., New York, N.Y. 1967.
10. Boston Gear Catalogue MC80, Incon, International Inc. 1979.
11. Mark's Mechanical Engineering Handbook, Eighth Edition, McGraw Hill Book Co., New York, N.Y. 1978.
12. Collins, J.A., Failure of Materials in Mechanical Design, John Wiley and Sons, New York, N.Y. 1981.
13. Spotts, M.F. Design of Machine Elements, 5th Edition, Prentice-Hall Inc., Englewood Cliffs, N.J. 1978.
14. Bekker, M.G., Off Road Locomotion, The University of Michigan Press, Ann Arbor, Mich. 196.?
15. Bekker, M.G., Introduction to Terrain-Vehicle Systems, University of Michigan Press, Ann Arbor, Michigan 1969.
16. Von Sybel, Hans, and Grosse-Scharmann, Franz, "Increased draft for Wheeled Vehicles Operating Outside the Roadway by the Thrust-Stride-System" Proc. 1st International Conference on Mechanics of Soil-Vehicle Systems, Torino, Italy 1961.
17. Fafner Ball Bearing Catalog 68, The Fafner Ball Bearing Co., New Britain, Conn.
18. Waldron, K. and Kinzel, G., "The Relationship Between Actuator Geometry and Mechanical Efficiency in Robots," Proc. Ro Man Sy 81, Warsaw, Poland 1981.
19. Gibson, Glen and Liu, Yu-cheng, Micro Computers for Engineers and Scientists, Prentice-Hall, Inc., Englewood Cliffs, New Jersey 1980.

20. Saunder, B.C., "The Major Determinants in Normal and Pathological Gait", Journal of Bone Surgery 35-A, 1953.
21. McGhee, R.B., "Some Finite State Aspects of Legged Locomotion", Mathematical Biosciences, Vol. 2, No. 1/2, Feb 1968.
22. McGhee, R.B., Frank, A.A., "On Stability of Quadruped Creeping Gaits", Mathematical Biosciences, Vol. 3, No. 3/4, Oct 1968.
23. McKenney, John D., "Investigation for a Walking Device for High Efficiency Lunar Locomotion", Proc. American Rocket Society Space Flight Report to the Nation, Oct. 1961.
24. "Development of the Quadruped Walking Truck," General Electric Co. Progress Report #10, June 1966.
25. Ronald A. Liston, "Increasing Vehicle Agility By Legs: The Quadruped Transporters", Proc. 38th National Meeting of the Operations Research Society of America, U.S. Army Cold Regions Research and Engineering Laboratory, Hanover, NH, 1970.
26. Emanuel M. Roth, M.D., "Bioenergetics of Space Suits for Lunar Exploration," NASA Special Publication No. SP-84, Scientific and Technical Information Division NASA, Washington, D.C., 1966.
27. Jean Jaques Kesse, Jean Pierre Rambaut, Jean Penne', "Walking Robot Multilevel Architecture and Implementation," Proc. Ro Man Sy 81, Warsaw, Poland, Sept. 1981.
28. D.E. Okhotsimski, "Motion Control Systems Development for a Mobile Robot", Keldysh Institute of Applied Mathematics, Moscow, USSR.
29. E.A. Bevjanin, et.al., "The Six-Legged Walking Robot Capable of Terrain Adaptation," Proc. Ro Man Sy 81, Warsaw, Poland 1981.

30. M.H. Raibert, H.B. Brown, Jr., M. Chepponis, "Dynamicly Stable Legged Locomotion," The Robotics Institute Carnagie-Mellon University, Pittsburgh, PA 1981.
31. A.P. Bessonov, N.V. Uninov, "Stabilization of Position of the Body of Walking Vehicles," Institute for the Study of Machines, Proc. Ro Man Sy 81, USSR 1981.
32. Vyay C. Jaswa, An Experimental Study of Real-Time Computer Control of a Hexapod Vehicle, Ph.D. Thesis, Communications and Control Systems Laboratory, The Ohio State University, Columbus, OH June 1978.
33. S. Hirose, Y. Umetani, "The Basic Motion Regulation System for a Quadruped Walking Vehicle", ASME Paper No. 80-DET-34, 1980.
34. C.R. Taylor, "Energy Cost of Animal Locomotions," Comparative Physiology, North Holland Pub., 1973.
35. Clyde F. Herreio, et al., D.A. Pray, J.R., "Energetic of Running Cockroaches", Science, Vol. 212, April 17, 1981.
36. Ching, Shu Chao, Real Time Multiprocessor Control of a Hexapod Vehicle, Ph.D. Dissertation, The Ohio State University, Columbus, Ohio 1979.
37. Orin, David, McGhee, Robert, "Dynamic Computer Simulation of Robotic Mechanisms," Proc. Ro Man Sy 81, Warsaw, Poland 1981.
38. Cheng, Fan-Tien, Computer Simulation of Dynamics and Control of an Energy Efficient Robot Leg, M.S. Thesis, Digital Control Systems Laboratory, The Ohio State University, Columbus, Ohio, March 1982.
39. Tomovic, R. Karplus, W.J., "Land Locomotion -- Simulation and Control," Proc. Third Internat. Analogue Computation Meeting, Opatya, Yuglosavia, Sept. 1961.

40. Gabrielli, G., Von Karman, T.H., "What Price Speed,"
Amer.Soc.Mech.Engr. Journal, Dec. 1954.
41. Hirose, S., Y. Umetani, "Some Considerations on a Feasible Walking
Mechanism as a Terrain Vehicle", Proc. ROMAN Sy 78, Udine, Italy,
September 1978.
42. Waldron, K.J., "Some Thoughts on the Mechanical Aspects of Walking
Machine Design," Seminar Lecture at The Ohio State University,
Department of Electrical Engineering, Columbus, Ohio March 5, 1981.

APPENDIX A
CALCULATION RESULTS

NOTES ON DATA FROM FORBAR ANALYSIS PROGRAM

- 1) All dimensions are in inches, degrees and seconds except rotations which are in radians/sec. or radian/sec.²
- 2) The linkage analysed is one half actual size, therefore multiply computed drive torques by 2.0.
- 3) All links are considered massless in the force analysis.

DATA FROM FORBAR PROGRAM; REFERENCE FIGURE 2.4a

LINKAGE DESIGN NO. 1

THETA=DRIVE CRANK ANGLE
PHI =DRIVEN CRANK ANGLE
SI =COUPLER ANGLE
X,Y =COUPLER PT

THETA	PHI	SI	X	Y
48.00	55.63437	-29.63155	10.13586	8.74981
51.00	58.06756	-30.32169	10.04458	8.81348
54.00	60.52088	-30.95885	9.94355	8.87342
57.00	62.99130	-31.54659	9.83352	8.92919
60.00	65.47611	-32.08767	9.71515	8.98039
63.00	67.97272	-32.58428	9.58910	9.02669
66.00	70.47873	-33.03797	9.45596	9.06780
69.00	72.99179	-33.44973	9.31632	9.10350
72.00	75.50967	-33.81992	9.17071	9.13364
75.00	78.03010	-34.14841	9.01965	9.15810
78.00	80.55067	-34.43448	8.86361	9.17685
81.00	83.06903	-34.67670	8.70304	9.18993
84.00	85.58259	-34.87307	8.53834	9.19743
87.00	88.08862	-35.02072	8.36988	9.19956
90.00	90.58304	-35.11593	8.19795	9.19659
93.00	93.06513	-35.15408	8.02282	9.18890
96.00	95.52894	-35.12935	7.84463	9.17696
99.00	97.97078	-35.03469	7.66349	9.16138
102.00	100.38580	-34.86158	7.47935	9.14288
105.00	102.76862	-34.59993	7.29207	9.12231
108.00	105.11304	-34.23794	7.10134	9.10065
111.00	107.41219	-33.76208	6.90670	9.07899
114.00	109.65856	-33.15720	6.70749	9.05850
117.00	111.84425	-32.40698	6.50287	9.04040
120.00	113.96104	-31.49430	6.29178	9.02584
123.00	116.00117	-30.40269	6.07306	9.01580
126.00	117.95779	-29.11731	5.84541	9.01098
129.00	119.82555	-27.62640	5.60753	9.01161
132.00	121.60150	-25.92288	5.35821	9.01736
135.00	123.29534	-24.00514	5.09648	9.02729
138.00	124.87947	-21.87704	4.82163	9.03981
141.00	126.38891	-19.54766	4.53336	9.05286
144.00	127.82047	-17.02973	4.23170	9.06398
147.00	129.18239	-14.33859	3.91707	9.07051
150.00	130.48329	-11.49031	3.59017	9.06975
153.00	131.73216	-8.50104	3.25201	9.05907
156.00	132.93747	-5.38582	2.90375	9.03601
159.00	134.10718	-2.15816	2.54675	8.99832
162.00	135.24854	1.17021	2.18244	8.94397
165.00	136.36830	4.58921	1.81238	8.87117
168.00	137.47246	8.09045	1.43819	8.77837

ENTER INTEGER TO RETURN

DATA FROM FORBAR PROGRAM; REFERENCE FIGURE 2.4b

LINKAGE DESIGN NO. 1

THETA=DRIVE-CRANK ROTATION ANGLE
 X VEL=COUPLER PT. X VELOCITY ->+
 Y VEL=COUPLER PT. Y VELOCITY ^+
 X ACCEL=COUPLER PT X ACCELERATION ->+
 Y ACCEL=COUPLER PT Y ACCELERATION ^+

DRIVE CRANK VELOCITY= 1.000 RAD/SEC

THETA	X VEL	Y VEL	X ACCEL	Y ACCEL
43.00	-0.1287E+01	0.1336E+01	-0.4380E+01	0.3806E+01
46.00	-0.1508E+01	0.1287E+01	-0.4045E+01	0.3835E+01
49.00	-0.1712E+01	0.1227E+01	-0.3741E+01	0.3875E+01
52.00	-0.1900E+01	0.1158E+01	-0.3461E+01	0.3922E+01
55.00	-0.2074E+01	0.1079E+01	-0.3201E+01	0.3975E+01
58.00	-0.2236E+01	0.9932E+00	-0.2957E+01	0.4034E+01
61.00	-0.2384E+01	0.9005E+00	-0.2728E+01	0.4098E+01
64.00	-0.2521E+01	0.8022E+00	-0.2511E+01	0.4167E+01
67.00	-0.2647E+01	0.6995E+00	-0.2306E+01	0.4240E+01
70.00	-0.2763E+01	0.5935E+00	-0.2112E+01	0.4317E+01
73.00	-0.2869E+01	0.4854E+00	-0.1929E+01	0.4400E+01
76.00	-0.2965E+01	0.3763E+00	-0.1758E+01	0.4490E+01
79.00	-0.3053E+01	0.2677E+00	-0.1601E+01	0.4588E+01
82.00	-0.3133E+01	0.1608E+00	-0.1458E+01	0.4695E+01
85.00	-0.3206E+01	0.5730E-01	-0.1332E+01	0.4814E+01
88.00	-0.3273E+01	-0.4119E-01	-0.1227E+01	0.4949E+01
91.00	-0.3335E+01	-0.1328E+00	-0.1146E+01	0.5101E+01
94.00	-0.3394E+01	-0.2156E+00	-0.1094E+01	0.5275E+01
97.00	-0.3450E+01	-0.2873E+00	-0.1076E+01	0.5474E+01
100.00	-0.3507E+01	-0.3457E+00	-0.1100E+01	0.5701E+01
103.00	-0.3566E+01	-0.3882E+00	-0.1172E+01	0.5956E+01
106.00	-0.3631E+01	-0.4125E+00	-0.1301E+01	0.6239E+01
109.00	-0.3704E+01	-0.4162E+00	-0.1494E+01	0.6544E+01
112.00	-0.3788E+01	-0.3976E+00	-0.1756E+01	0.6857E+01
115.00	-0.3889E+01	-0.3558E+00	-0.2089E+01	0.7156E+01
118.00	-0.4008E+01	-0.2916E+00	-0.2489E+01	0.7408E+01
121.00	-0.4150E+01	-0.2077E+00	-0.2940E+01	0.7568E+01
124.00	-0.4317E+01	-0.1095E+00	-0.3418E+01	0.7583E+01
127.00	-0.4508E+01	-0.5016E-02	-0.3887E+01	0.7402E+01
130.00	-0.4723E+01	0.9520E-01	-0.4307E+01	0.6988E+01
133.00	-0.4958E+01	0.1792E+00	-0.4638E+01	0.6327E+01
136.00	-0.5206E+01	0.2351E+00	-0.4848E+01	0.5436E+01
139.00	-0.5463E+01	0.2526E+00	-0.4921E+01	0.4358E+01
142.00	-0.5719E+01	0.2241E+00	-0.4857E+01	0.3153E+01
145.00	-0.5969E+01	0.1451E+00	-0.4666E+01	0.1883E+01
148.00	-0.6206E+01	0.1436E-01	-0.4367E+01	0.6026E+00
151.00	-0.6425E+01	-0.1670E+00	-0.3981E+01	-0.6462E+00
154.00	-0.6622E+01	-0.3961E+00	-0.3528E+01	-0.1837E+01
157.00	-0.6794E+01	-0.6689E+00	-0.3023E+01	-0.2954E+01
160.00	-0.6938E+01	-0.9811E+00	-0.2480E+01	-0.3992E+01
163.00	-0.7053E+01	-0.1328E+01	-0.1906E+01	-0.4952E+01
166.00	-0.7137E+01	-0.1706E+01	-0.1310E+01	-0.5836E+01
169.00	-0.7190E+01	-0.2110E+01	-0.6952E+00	-0.6650E+01
172.00	-0.7210E+01	-0.2536E+01	-0.6424E+01	-0.7400E+01

ENTER INTEGER TO RETURN

DATA FROM FORBAR PROGRAM;REFERENCE FIGURES 2.5 & 2.6

LINKAGE DESIGN NO. 1

THEATA=CRANK ROTATION ANGLE
PHI2DOT=DRIVEN CRANK ACCELERATION
SI2DOT=COUPLER ACCELERATION
PHIDOT=DRIVEN CRANK VELOCITY
SIDOT=COUPLER VELOCITY

THEATA	PHI2DOT	SI2DOT	PHIDOT	SIDOT
48.00	0.1494E+00	0.3648E+00	0.8073E+00	-0.2393E+00
51.00	0.1281E+00	0.3370E+00	0.8146E+00	-0.2210E+00
54.00	0.1089E+00	0.3144E+00	0.8208E+00	-0.2040E+00
57.00	0.9137E-01	0.2965E+00	0.8260E+00	-0.1880E+00
60.00	0.7511E-01	0.2828E+00	0.8304E+00	-0.1728E+00
63.00	0.5976E-01	0.2730E+00	0.8339E+00	-0.1583E+00
66.00	0.4499E-01	0.2668E+00	0.8366E+00	-0.1442E+00
69.00	0.3051E-01	0.2641E+00	0.8386E+00	-0.1303E+00
72.00	0.1603E-01	0.2651E+00	0.8398E+00	-0.1165E+00
75.00	0.1265E-02	0.2699E+00	0.8403E+00	-0.1025E+00
78.00	-0.1410E-01	0.2786E+00	0.8400E+00	-0.8314E-01
81.00	-0.3039E-01	0.2917E+00	0.8388E+00	-0.7322E-01
84.00	-0.4795E-01	0.3097E+00	0.8368E+00	-0.5750E-01
87.00	-0.6719E-01	0.3331E+00	0.8337E+00	-0.4670E-01
90.00	-0.8855E-01	0.3628E+00	0.8297E+00	-0.2251E-01
93.00	-0.1125E+00	0.3996E+00	0.8244E+00	-0.2584E-02
96.00	-0.1395E+00	0.4445E+00	0.8178E+00	0.1948E-01
99.00	-0.1701E+00	0.4985E+00	0.8098E+00	0.4412E-01
102.00	-0.2049E+00	0.5628E+00	0.8000E+00	0.7186E-01
105.00	-0.2440E+00	0.6378E+00	0.7882E+00	0.1032E+00
108.00	-0.2877E+00	0.7240E+00	0.7743E+00	0.1388E+00
111.00	-0.3356E+00	0.8206E+00	0.7580E+00	0.1792E+00
114.00	-0.3865E+00	0.9253E+00	0.7391E+00	0.2249E+00
117.00	-0.4385E+00	0.1034E+01	0.7175E+00	0.2762E+00
120.00	-0.4886E+00	0.1140E+01	0.6932E+00	0.3332E+00
123.00	-0.5328E+00	0.1236E+01	0.6665E+00	0.3954E+00
126.00	-0.5666E+00	0.1311E+01	0.6376E+00	0.4622E+00
129.00	-0.5859E+00	0.1356E+01	0.6074E+00	0.5321E+00
132.00	-0.5880E+00	0.1367E+01	0.5766E+00	0.6036E+00
135.00	-0.5723E+00	0.1342E+01	0.5461E+00	0.6747E+00
138.00	-0.5405E+00	0.1284E+01	0.5169E+00	0.7435E+00
141.00	-0.4963E+00	0.1201E+01	0.4897E+00	0.8087E+00
144.00	-0.4440E+00	0.1104E+01	0.4651E+00	0.8691E+00
147.00	-0.3878E+00	0.9997E+00	0.4433E+00	0.9241E+00
150.00	-0.3314E+00	0.8971E+00	0.4245E+00	0.9738E+00
153.00	-0.2771E+00	0.8012E+00	0.4086E+00	0.1018E+01
156.00	-0.2263E+00	0.7150E+00	0.3954E+00	0.1058E+01
159.00	-0.1797E+00	0.6399E+00	0.3848E+00	0.1093E+01
162.00	-0.1375E+00	0.5761E+00	0.3765E+00	0.1125E+01
165.00	-0.9918E-01	0.5231E+00	0.3703E+00	0.1154E+01
168.00	-0.6442E-01	0.4801E+00	0.3661E+00	0.1180E+01

ENTER INTEGER TO RETURN

NOTES ON DATA FROM GRSET PROGRAM

BASIC EQUATIONS USED (from AGMA standards 210.02 & 220.02)

STRENGTH:
$$S_T = \frac{W_T K_o}{K_v} \frac{P_i}{F} \frac{K_s K_m}{J}$$

WEAR:
$$S_c = C_p \sqrt{\frac{W_T C_o}{C_v} \frac{C_s}{d F} \frac{C_m C_f}{I}}$$

RELATIONSHIP BETWEEN CALCULATED AND ALLOWABLE MODULI

STRENGTH:
$$S_T \leq \frac{S_{at} K_L}{K_R K_T}$$

WEAR:
$$S_c \leq S_{ac} \frac{C_L C_H}{C_T C_R}$$

WHERE

C_F =surface condition factor
 C_H =hardness ratio factor
 C_L =life factor,wear
 C_m =load distribution factor,wear
 C_o =overload factor,wear
 C_p =elastic factor
 C_s =size factor,wear
 C_v =dynamic factor,wear
 C_R =factor of safty,wear
 C_T =temperature factor,wear
 d =pinion operating pitch diameter(inches)
 F =net face width of narrowest gear of pair(inches)
 I =geometry factor,wear
 J =geometry factor,strength
 K_L =life factor,strength
 K_m =load distribution factor,strength
 K_o =overload factor,strength
 K_R =factor of safty,strength
 K_s =size factor,strength
 K_T =temperature factor,strength
 K_v =dynamic factor,strength
 P_i =diametral pitch
 S_{ac} =allowable contact stress(psi)
 S_{at} =allowable tensile stress(psi)
 S_c =calculated contact stress(psi)
 S_T =calculated tensile stress at tooth root(psi)
 W_T =transmitted tangential load in lbs

RESULTS OF GRSET GEAR ANALYSIS PROGRAM
FOR ROTARY ACTUATOR SPEED REDUCER

SPUR GEAR DATA	PINION	GEAR
DIAMETRAL PITCH		20.0000
PRESSURE ANGLE		20.0000
CIRCULAR PITCH		0.1571
BASE PITCH		0.1476
CONTACT RATIO		1.6445
LENGTH OF CONTACT		
APPROACH		0.1334
RECESS		0.1093
TOTAL		0.2427
NUMBER OF TEETH	15	70
GEAR RATIO		
CENTER DISTANCE		4.6667
FACE WIDTH		2.1250
RADII		0.1704
OUTSIDE		
PITCH	0.4250	1.8000
BASE	0.3750	1.7500
BEGINNING CONTACT	0.3524	1.6445
END OF CONTACT	0.3524	1.8000
ADDENDUM CONSTANT	0.4250	1.7157
DEDENDUM CONSTANT		
DEDENDUM		
WORKING HEIGHT		
HOB RADIUS CONSTANT		
HOB RADIUS		
NOR TOOTH THICK		
PITCH POINT		
BEGINNING CONTACT	0.0785	0.1219
END OF CONTACT	0.0785	0.0545
RADII OF CURVATURE		
PITCH POINT		
BEGINNING CONTACT	0.1283	0.5985
END OF CONTACT	-0.0052	0.7319
EQUIVALENT CURVATURE	0.2376	0.4892
PITCH POINT		
BEGINNING CONTACT		
END OF CONTACT		

PROPERTIES OF GEAR MATERIALS USED

TYPE I (LOW CARBON STEEL)

ELASTIC MODULUS:	30000000.0000	30000000.0000
POISSON'S RATIO:	0.3000	0.3000
MAX. BENDING FATIGUE STRESS:	26500.0000	26500.0000
MAX. CONTACT STRESS:	95000.0000	95000.0000
BRINELL HARDNESS NUMBER:	180.0000	180.0000

TYPE II (ALLOY STEEL)

ELASTIC MODULUS:	30000000.0000	30000000.0000
POISSON'S RATIO:	0.3000	0.3000
MAX. BENDING FATIGUE STRESS:	47500.0000	47500.0000
MAX. CONTACT STRESS:	190000.0000	190000.0000
BRINELL HARDNESS NUMBER:	450.0000	450.0000

FIRST STAGE, INITIAL DESIGN: TYPE I STEEL

LOADING PARAMETERS

PINION RPM: 1321.0000
 PINION PITCHLINE VELOCITY: 259.3777
 TRANSMITTED HORSEPOWER: 0.0826
 PINION TORQUE: 3.9400
 TANGENTIAL LOAD: 10.5067

AGMA CORRECTION FACTORS

	<u>STRENGTH</u>	<u>WEAR</u>
SIZE FACTOR:	1.0000	1.0000
DYNAMIC FACTOR:	0.8231	0.8231
OVERLOAD FACTOR:	1.5000	1.5000
LIFE FACTOR:	1.3046	1.3000
TEMPERATURE FACTOR:	1.0000	1.0000
LOAD DISTRIBUTION FACTOR:	1.3000	1.3000
FACTOR OF SAFETY:	11.1114	1.8651
SURFACE CONDITION FACTOR:		1.0000
HARDNESS FACTOR:		1.0025
ELASTIC COEFFICIENT:		2290.6038
PINION GEOMETRY FACTORS:	0.4000	0.0988
GEAR GEOMETRY FACTORS:	0.4433	0.1435
FACE WIDTH:	0.4000	0.4000
CALCULATED STRESS:	3111.4292	66384.5469

SECOND STAGE, INITIAL DESIGN: TYPE I STEEL

LOADING PARAMETERS

PINION RPM: 283.0000
 PINION PITCHLINE VELOCITY: 55.5669
 TRANSMITTED HORSEPOWER: 0.0827
 PINION TORQUE: 18.4000
 TANGENTIAL LOAD: 49.0667

AGMA CORRECTION FACTORS

	<u>STRENGTH</u>	<u>WEAR</u>
SIZE FACTOR:	1.0000	1.0000
DYNAMIC FACTOR:	0.9086	0.9086
OVERLOAD FACTOR:	1.5000	1.5000
LIFE FACTOR:	1.3046	1.3000
TEMPERATURE FACTOR:	1.0000	1.0000
LOAD DISTRIBUTION FACTOR:	1.3000	1.3000
FACTOR OF SAFETY:	2.6264	0.9068
SURFACE CONDITION FACTOR:		1.0000
HARDNESS FACTOR:		1.0025
ELASTIC COEFFICIENT:		2290.6038
PINION GEOMETRY FACTORS:	0.4000	0.0988
GEAR GEOMETRY FACTORS:	0.4433	0.1435
FACE WIDTH:	0.4000	0.4000
CALCULATED STRESS:	13163.4482	136543.7500

THIRD STAGE, INITIAL DESIGN: TYPE I STEEL

LOADING PARAMETERS

PINION RPM: 60.7000
 PINION PITCHLINE VELOCITY: 11.9184
 TRANSMITTED HORSEPOWER: 0.0826
 PINION TORQUE: 85.7000
 TANGENTIAL LOAD: 228.5333

AGMA CORRECTION FACTORS

	<u>STRENGTH</u>	<u>WEAR</u>
SIZE FACTOR:	1.0000	1.0000
DYNAMIC FACTOR:	0.9552	0.9552
OVERLOAD FACTOR:	1.5000	1.5000
LIFE FACTOR:	1.3046	1.3000
TEMPERATURE FACTOR:	1.0000	1.0000
LOAD DISTRIBUTION FACTOR:	1.3000	1.3000
FACTOR OF SAFETY:	0.5928	0.4308
SURFACE CONDITION FACTOR:		1.0000
HARDNESS FACTOR:		1.0025
ELASTIC COEFFICIENT:		2290.6038
PINION GEOMETRY FACTORS:	0.4000	0.0988
GEAR GEOMETRY FACTORS:	0.4433	0.1435
FACE WIDTH:	0.4000	0.4000
CALCULATED STRESS:	56315.5977	287395.1250

THIRD STAGE, INITIAL DESIGN, REDUCED LOADING: TYPE I STEEL

LOADING PARAMETERS

PINION RPM: 60.7000
 PINION PITCHLINE VELOCITY: 11.9184
 TRANSMITTED HORSEPOWER: 0.0206
 PINION TORQUE: 21.4000
 TANGENTIAL LOAD: 57.0667

AGMA CORRECTION FACTORS

	<u>STRENGTH</u>	<u>WEAR</u>
SIZE FACTOR:	1.0000	1.0000
DYNAMIC FACTOR:	0.9552	0.9552
OVERLOAD FACTOR:	1.5000	1.5000
LIFE FACTOR:	1.3046	1.3000
TEMPERATURE FACTOR:	1.0000	1.0000
LOAD DISTRIBUTION FACTOR:	1.3000	1.3000
FACTOR OF SAFETY:	2.3742	0.8621
SURFACE CONDITION FACTOR:		1.0000
HARDNESS FACTOR:		1.0025
ELASTIC COEFFICIENT:		2290.6038
PINION GEOMETRY FACTORS:	0.4000	0.0988
GEAR GEOMETRY FACTORS:	0.4433	0.1435
FACE WIDTH:	0.4000	0.4000
CALCULATED STRESS:	14561.8877	143613.7031

FIRST STAGE, OPTIMIZED SET: TYPE I STEEL

LOADING PARAMETERS

PINION RPM: 1321.0000
 PINION PITCHLINE VELOCITY: 259.3777
 TRANSMITTED HORSEPOWER: 0.0826
 PINION TORQUE: 3.9400
 TANGENTIAL LOAD: 10.5067

AGMA CORRECTION FACTORS

SIZE FACTOR:	1.0000	WEAR	1.0000
DYNAMIC FACTOR:	0.8231		0.8231
OVERLOAD FACTOR:	1.5000		1.5000
LIFE FACTOR:	1.0007		1.0000
TEMPERATURE FACTOR:	1.0000		1.0000
LOAD DISTRIBUTION FACTOR:	1.0000		1.0000
FACTOR OF SAFETY:	2.0000		1.0000
SURFACE CONDITION FACTOR:			1.0025
HARDNESS FACTOR:			2290.6038
ELASTIC COEFFICIENT:			0.0988
PINION GEOMETRY FACTORS:	0.4000		0.1435
GEAR GEOMETRY FACTORS:	0.4433		0.0374
FACE WIDTH:	0.0403		
CALCULATED STRESS:	23766.2480		190480.7031

SECOND STAGE, OPTIMIZED SET: TYPE I STEEL

LOADING PARAMETERS

PINION RPM: 283. 0000
 PINION PITCHLINE VELOCITY: 55. 5669
 TRANSMITTED HORSEPOWER: 0. 0827
 PINION TORQUE: 18. 4000
 TANGENTIAL LOAD: 49. 0667

AGMA CORRECTION FACTORS

	<u>STRENGTH</u>	<u>WEAR</u>
SIZE FACTOR:	1. 0000	1. 0000
DYNAMIC FACTOR:	0. 9086	0. 9086
OVERLOAD FACTOR:	1. 5000	1. 5000
LIFE FACTOR:	1. 0007	1. 0000
TEMPERATURE FACTOR:	1. 0000	1. 0000
LOAD DISTRIBUTION FACTOR:	1. 0000	1. 0000
FACTOR OF SAFETY:	2. 0000	1. 0000
SURFACE CONDITION FACTOR:		1. 0000
HARDNESS FACTOR:		1. 0025
ELASTIC COEFFICIENT:		2290. 6038
PINION GEOMETRY FACTORS:	0. 4000	0. 0988
GEAR GEOMETRY FACTORS:	0. 4433	0. 1435
FACE WIDTH:	0. 3055	0. 6324
CALCULATED STRESS:	13259. 0645	95240. 3516

THIRD STAGE, OPTIMIZED SET: TYPE 11 STEEL

LOADING PARAMETERS

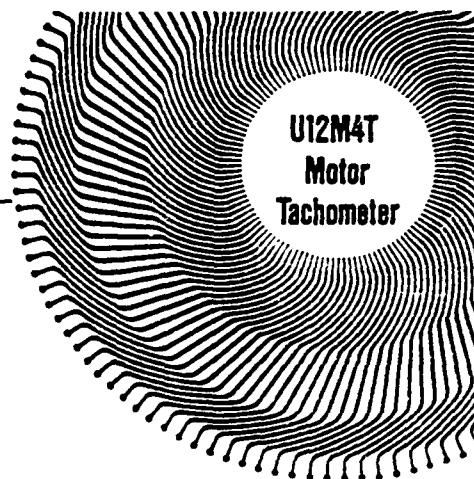
PINION RPM: 60.7000
 PINION PITCHLINE VELOCITY: 11.9184
 TRANSMITTED HORSEPOWER: 0.0826
 PINION TORQUE: 85.7000
 TANGENTIAL LOAD: 228.5333

AGMA CORRECTION FACTORS

	<u>STRENGTH</u>	<u>WEAR</u>
SIZE FACTOR:	1.0000	1.0000
DYNAMIC FACTOR:	0.9552	0.9552
OVERLOAD FACTOR:	1.5000	1.5000
LIFE FACTOR:	1.3432	1.1500
TEMPERATURE FACTOR:	1.0000	1.0000
LOAD DISTRIBUTION FACTOR:	1.0000	1.0000
FACTOR OF SAFETY:	2.0000	1.0000
SURFACE CONDITION FACTOR:		1.0000
HARDNESS FACTOR:		1.0025
ELASTIC COEFFICIENT:		2290.6038
PINION GEOMETRY FACTORS:	0.4000	0.0988
GEAR GEOMETRY FACTORS:	0.4433	0.1435
FACE WIDTH:	0.5625	0.5296
CALCULATED STRESS:	31900.4043	219052.7969

APPENDIX B
COMPONENT SPECIFICATIONS
AND CALIBRATION DATA

PMI ENGINEERING DATA



**All Nominals at 25°C Ambient
Except Where Otherwise Stated.**

1.0 MOTOR RATINGS

- 1.1 Continuous Torque @ Rated Speed: 66 Oz.-In.
- 1.2 Pulse Torque (50 ms @ 4% Duty Cycle): 624 Oz.-In.
- 1.3 Rated Speed: 2270 RPM
- 1.4 Rated Voltage⁽¹⁾: 30 VDC
- 1.5 Power Out @ Rated Speed: 112 Watts
- 1.6 Rated Current: 5.8 Amperes
- 1.7 Maximum Continuous Stall Current:
7.65 Amperes
- 1.8 Terminal Resistance: 0.75 Ohms @ 25°C
- 1.9 Terminal Resistance: 1.07 Ohms @ 150°C

2.0 MOTOR CONSTANTS

- 2.1 Torque Constant (K_t): 14.4 Oz.-In./Ampere
- 2.2 Emf Constant (K_e): 10.6 Volts/1000 RPM
- 2.3 Damping Constant (K_d): 4.5 Oz.-In./1000 RPM
- 2.4 Total Inertia (J): 0.033 Oz.-In. Sec.²
- 2.5 Regulation @ Constant Voltage (R_v)²: 6.77 RPM/Oz.-In.
- 2.6 Armature Inductance (L): <100μ Henrys
- 2.7 Average Friction Torque (T_f): 6.0 Oz.-In.
- 2.8 Mechanical Time Constant²: 0.023 Sec.
- 2.9 Power Rate²: 82.7 KW/Sec.

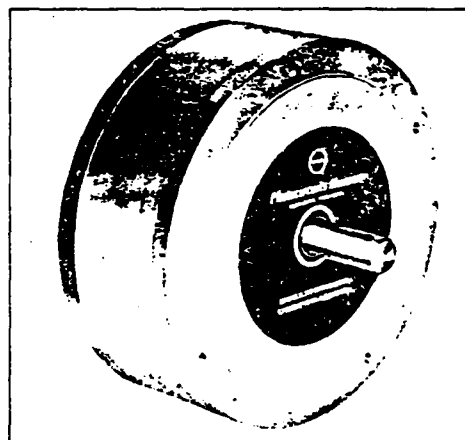
3.0 TACHOMETER CONSTANTS

- 3.1 Output Gradient: 5.30 VDC/1000 RPM
- 3.2 Output Tolerance: ±5%
- 3.3 Ripple Content⁴
 - 3.3.1 15 to 60 RPM: 15% to 5% p-p
 - 3.3.2 60 to 100 RPM: 5% to 3% p-p
 - 3.3.3 100 to 1000 RPM: 3% to 1.5% p-p
 - 3.3.4 Above 1000 RPM: 1.5% p-p
- 3.4 Linearity
- 3.4.1 Referenced @ 3600 RPM: 0.11%
- 3.5 Bidirectional Tolerance: 1.0%
- 3.6 Bidirectional Stability: Within 0.3% over 15 hours
- 3.7 Output Impedance: 1 ohm resistive
- 3.8 Temperature coefficient of output voltage with 1K ohm load: 0.02%/°C

4.0 THERMAL RESISTANCE

- 4.1 Uncooled
 - 4.1.1 Armature-to-Case (θ_{JA}): 1.15°C/Watt
 - 4.1.2 Case-to-Ambient (θ_{JA})
 - 4.1.2.1 With 8 x 16 x 1/8 Alum. Heat Sink: 0.87°C/Watt
 - 4.1.2.2 With 14 x 14 x 1/8 Alum. Heat Sink: 0.70°C/Watt
- 4.2 Forced Cooling
 - 4.2.1 Armature-to-Ambient (θ_{JA})
 - 4.2.1.1 With Mass Air Flow of 0.4 lbs./min.: 0.80°C/Watt
 - 4.2.1.2 With Mass Air Flow of 0.8 lbs./min.: 0.51°C/Watt
 - 4.2.1.3 With Mass Air Flow of 2.0 lbs./min.: 0.25°C/Watt

5.0 WEIGHT 8 lbs.





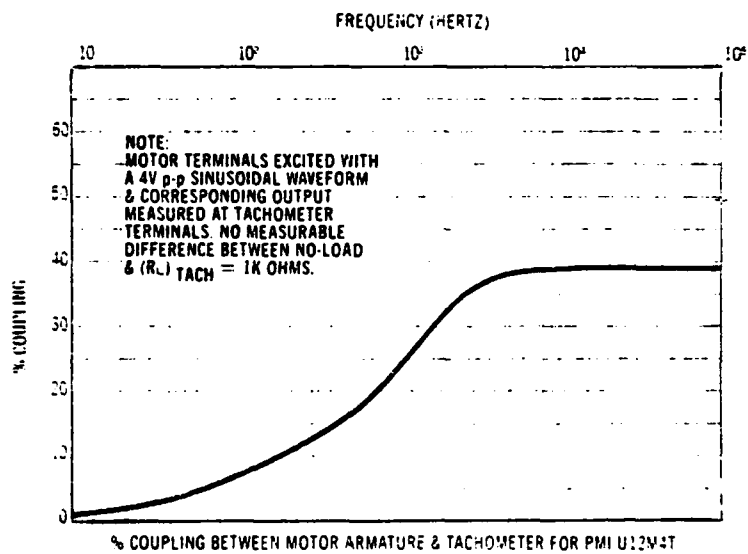
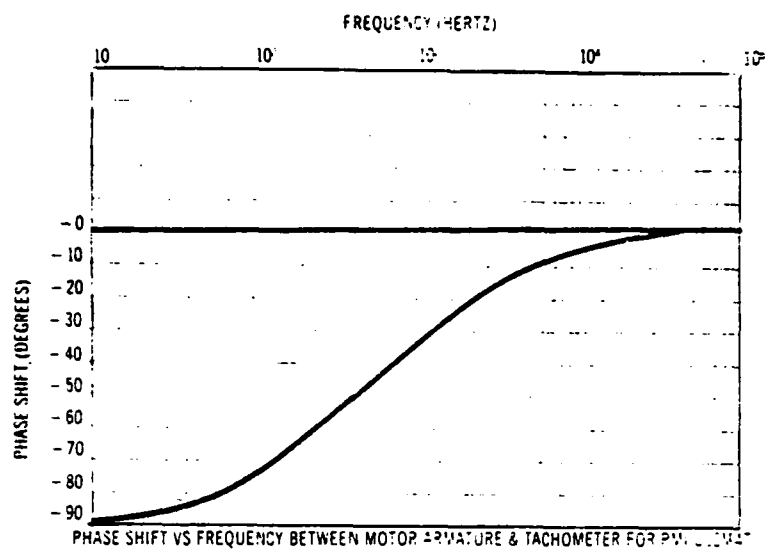
ENGINEERING DATA
(INCINAL-AT 25 DEG C AND)

MOTOR TYPE : U12H4T STD
PMI SPEC NO: 12-01207-001
Elevated

1.0	MOTOR PERFORMANCE: INCREMENTAL MOTION CONTROL			
1.1	PEAK TORQUE (1)	TP	1206.4	OZ IN
1.2	CONTINUOUS STALL TORQUE	TS	110.2	OZ IN
1.3	PEAK CURRENT (1)	IP	84.5	AMPS
1.4	CONTINUOUS STALL CURRENT	IS	8.13	AMPS
1.5	PEAK ACCELERATION WITHOUT LOAD (1)(5)	AP	46.4	KRAD/SEC/SEC
1.6	COGGING TORQUE	TC	0	OZ IN
2.0	MOTOR PERFORMANCE: RATED (2)			
2.1	TORQUE	T	114.5	OZ IN
2.2	SPEED	N	3000.0	RPM
2.3	POWER OUTPUT	P	253.9	WATTS
2.4	TERMINAL VOLTAGE	E	40.4	VOLTS
2.5	CURRENT	I	8.71	AMPS
2.6	MAX SPEED AT RATED VOLTAGE (AT NO LOAD)	NH	3473.9	RPM
2.7	MAX PERMISSIBLE DISSIPATION AT RATED SPEED (3)	PL	98.4	WATTS
3.0	MOTOR CONSTANTS: INTRINSIC			
3.1	TORQUE CONSTANT	KT	14.34	OZ IN/AMP
3.2	BACK EMF CONSTANT	KE	10.60	VOLTS/KRPM
3.3	TERMINAL RESISTANCE (7)	RT	0.750	OHMS
3.3.1	ARMATURE RESISTANCE	RA	0.610	OHMS
3.4	AVERAGE FRICTION TORQUE	TF	6.0	OZ IN
3.5	VISCOUS DAMPING CONSTANT	KD	2.0	OZ IN/KRPM
3.6	MOMENT OF INERTIA	JM	0.0240	OZ IN SEC-SEC
3.7	ARMATURE INDUCTANCE	L	BELOW 100.0	MICRO HENRY
3.8	TEMPERATURE COEFF OF KE	C	-0.02	%/DEG C RISE
3.9	NUMBER OF COMMUTATOR BARS	Z	141	
3.10	NUMBER OF POLES OF MAGNETIC FIELD	PF	8	
3.11	MOTOR DIAMETER	D	5.50	IN
3.12	MOTOR LENGTH	LG	2.11	IN
3.13	MOTOR WEIGHT	W	8.0	LBS
4.0	MOTOR CONSTANTS: DERIVED			
4.1	MECHANICAL TIME CONSTANT WITHOUT LOAD (2)	TM	16.02	MILLISEC
4.2	ELECTRICAL TIME CONSTANT (2)	TE	BELOW 0.11	MILLISEC
4.3	SPEED REGULATION AT CONSTANT TERM VOLTAGE (2)	RM	5.9	RPM/OZ IN
5.0	THERMAL RESISTANCE			
5.1	MOUNTED ON ALUM HEAT SINK(8"x16"x3/8")			
5.1.1	ARMATURE TO AMBIENT AT STALL	RAA	1.90	DEG C/WATT
5.1.2	ARMATURE TO AMBIENT AT 3000 RPM	RAA	1.27	DEG C/WATT
5.2	FORCED THROUGH-AIR COOLED (6)			
5.2.1	ARM TO AMB WITH AIR FLOW OF .4 LBS/MIN	RAA	0.78	DEG C/WATT
5.2.2	ARM TO AMB WITH AIR FLOW OF .8 LBS/MIN	RAA	0.48	DEG C/WATT
5.2.3	ARM TO AMB WITH AIR FLOW OF 2.0 LBS/MIN	RAA	0.25	DEG C/WATT
6.0	ANALOG TACHOMETER CHARACTERISTICS			
6.1	OUTPUT VOLTAGE	V	5.30	VOLTS/KRPM
6.2	RIPPLE VOLTAGE MAX, PK TO PK (8)			
6.2.1	AT 1000 RPM	VRH	1.5	%
6.2.2	AT 500 RPM	VRH	2.0	%
6.2.3	AT 100 RPM	VRL	3.0	%
6.3	LINEARITY OF OUTPUT VOLTAGE (REF. 3600 RPM)	LIN	0.11	%
6.4	BI-DIRECTIONAL TOL. (DIFF. IN OUTPUT VOLTS/KRPM)	BI	1.0	%
6.5	OUTPUT IMPEDANCE, RESISTIVE	R	0.494	OHMS
6.6	TEMPERATURE COEFF OF V	CT	-0.02	%/DEG C RISE
6.7	MOMENT OF INERTIA: INCLUDED IN ITEM 3.6			
6.8	LOAD RESISTANCE RECOMMENDED MIN.	RL	494.0	OHMS
6.9	NUMBER OF COMMUTATOR BARS	ZT	121	

NOTES

- (1) These are based upon the least of the demagnetization limit, the structural limit and the thermal limit. It is calculated for max. pulse duration of 50 msec. and 1 percent duty cycle.
- (2) All values are based upon 150 Deg. C armature temperature when the motor is mounted on an aluminum plate(8"x16"x3/8") with no forced cooling. Other voltages, speeds and torques are achievable as long as armature temp. is kept below 150 Deg. C. Continuous speed beyond 4000 RPM is not recommended. Consult PMI Motors for other speed ratings.
- (3) Maximum Permissible Dissipation = (150-Amb. Temp. in Deg. C)/RAA.
Total Motor Loss = $RT(I_{LI}) + .74(TF+TD) \times N/1000$ where $TD = KD \times N/1000$.
Mass Air Flow(Lbs/Min) = Air Volume(CFM) x Air Density(Lbs/Cu. Ft)
- (4) Peak Acceleration with Load = $(TP - \text{Reflected Load Frict.}) / (JM + \text{Reflected Load Inertia})$
- (5) These values are practically independent of the speed unless beyond 4000 RPM.
- (6) Measured at 4.0 Amps. It varies slightly with current due to variations in brush contact drop.
- (7) Measured with a resistive load of 1 kohms and a single pole low pass filter with 6db cut off at 500 Hz. Calculate ripple freq. = $ZT \times N/60$

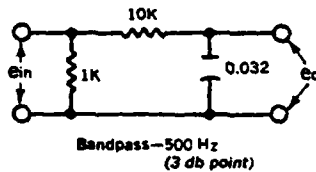


DATA FOR U12M4T MOTOR

NOTES:

1. Motor is tested at this voltage for convenience. Other voltages may be used provided maximum armature dissipation is not exceeded. ($P_{arm} = P_a - P_m = \text{Constant}$).
2. The speed-torque curve is obtained by using the maximum terminal resistance of the motor at 150°C armature temperature. (Worst condition.)
3. Calculated from the formula,

$$7.01 \times 10^{-3} \times \frac{(\text{Pulse Torque})^2}{\text{Inertia}}$$
4. The ripple content was measured with the following filter network at the tachometer output:



GENERAL

1. Maximum allowable armature dissipation,

$$P_{arm} = \frac{150^\circ\text{C} - T_{amb.} (^\circ\text{C})}{\theta_c + \theta_a}$$

2. The curves for forced cooling operation were obtained by modifying the mechanical configuration of the motor to accept the required air flow. These motors are available on special request. The maximum allowable armature dissipation in this case is calculated as follows:

$$P_{arm} = \frac{150^\circ\text{C} - T_{amb.} (^\circ\text{C})}{\theta}$$

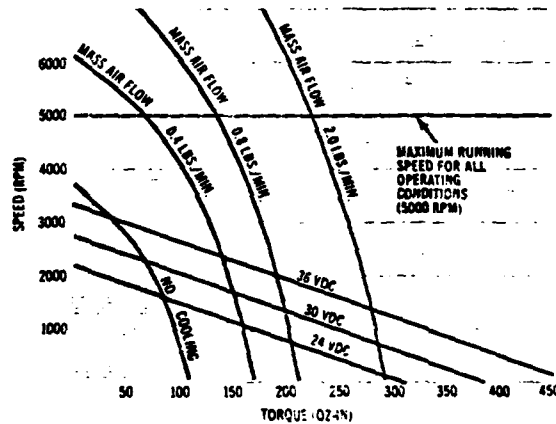
3. Mass Air Flow (lbs./min.) = Air Volume (cfm) x Density (lbs./ft.³)
4. Contact PMI Applications Staff for detailed techniques to minimize coupling effects in incrementing systems.

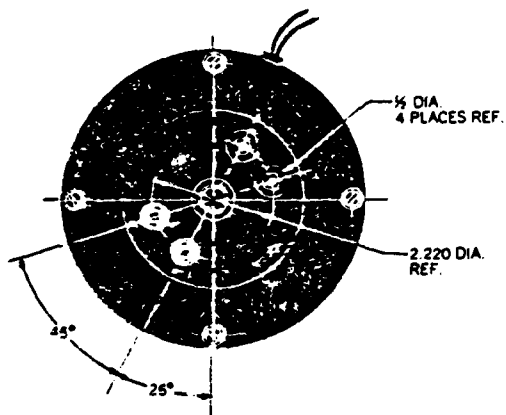
AVERAGE PERFORMANCE CHARACTERISTICS

□ LIMIT OF ALLOWANCE
CONTINUOUS OPERATION
(UNCOOLED)

The run current at any operating condition is obtained as follows:

$$I_{a-r} = \frac{K_2 \times \frac{N}{1000} + T_r + T_a}{K_1}$$





- 155

DESIGN DATA : INERTIAL MOTORS MODEL 03 SHORT SERIES

MOTOR CHARACTERISTICS

VOLTAGE	VOLTS DC	24
RATED SPEED	RPM	2672
RATED CURRENT	AMP	5.5
STALL CURRENT	AMP	6.0
RATED TORQUE	OZ-IN	40.
TORQUE CONSTANT	OZ-IN/AMP	8.5
BACK EMF	VOLTS/KRPM	6.75
ARMATURE DC RESISTANCE @25°C	OHMS	1.5
MAX. PULSE TORQUE	OZ-IN	500.
INDUCTANCE	μHY	100.
INSULATION RESISTANCE @70°C AND 150 VDC LEADS TO CASE	MEG OHMS	35. MIN.
ARMATURE INERTIA INCLUDING BEARINGS	OZ-IN-SEC	.010

(ALL RATINGS @ 25°C ARMATURE TEMP.)

MECHANICAL DATA

MAGNETIC FIELD	6 POLE ALNICO
NUMBER OF COMMUTATION SEGMENTS	17
MAX. FRICTION TORQUE	8.0 OZ-IN
MAX. POWER DISSIPATED IN ARMATURE FOR 100°C RISE (CONSTANT DUTY)	40. WATTS
MAX. ARMATURE TEMP. ALLOWED	105°C
WEIGHT IN	1.7 LBS
SHAFT RUN OUT	.001 IN MAX. TIR
SHAFT END PLAY @5LB. THRUST	.004 IN
RADIATED MAGNETIC FIELD 1.0 IN FROM UNIT	5 GAUSS MAX.
MAX. SHAFT SPEED	6000. RPM

COOLING

BY NATURAL CONVECTION TO AMBIENT AIR AND BY CONDUCTION TO
MOTOR MOUNT. MOUNT HEAT SINK CAPACITY SHALL EQUAL OR EXCEED
THAT OF AN ALUMINIUM PLATE 10. x 10. x .50 INCHES

INERTIAL MOTORS CORPORATION
FINAL INSPECTION REPORT

CUSTOMER <u>OHIO State</u>	PROJ. NO. <u>4525</u>	MOTOR <u>A 35086</u>	S/N <u>8124-08</u>
LOT NO.	DWG. NO.	DESCRIPTION	
INSTR. NO.		INSPECTOR <u>Kum</u>	DATE <u>6-18-81</u>

OPN. NO.	INSPECTION DESCRIPTION	REQUIRED	MEASURED	ACC	REJ
101	Shaft Preload: Axial	.004 max.		✓	
	Radial	.004 max.		✓	
102	D. C. Insulation Test @				
	250 volts	100 meg Ω min.	7/Kmeg	✓	
103	Friction Torque	800 in	600 in	✓	
104	Armature Resistance	$\Omega \pm 10\%$			
105	Test Motor @ Slow Speed				
	For Rubs or Poor Commutation			✓	
106	Test Motor @ 1/2 volts		CW CCW		
	and record current	AMPS	59 61	✓	
107	Current Linearity	10% max.		✓	
108	Drive Motor @ 2000 RPM	CW CCW	CW CCW		
	AND Record Voltage Out	13.5 V/2000	13.1	✓	
109	Calculate Kb	6.75 V/1000 RPM	6.55	✓	
110	Calculate Kt	85 oz in/AMP	8.8	✓	
111	Test Encoder Performance within Customer Specs	N/A		N/A	
111A	Record: No. of Lines	—		—	
	No. of Channels	—		—	
	Type of output	—		—	
112	Test Tach Performance	N/A		N/A	
	@ 1000 RPM with 10K load	CW CCW	CW CCW		
112A	Record Voltage Out	—		—	
112B	Percentage of Ripple	— 0/0 P-P A-P		—	
113	Check Mechanical Dimensions				
	Diameter of Shaft	3/25 $\pm .0005$	3.124	✓	
	Shaft Length	1.00 $\pm .002$	1.02	✓	
	Index O.D.	1.500 $\pm .001$	1.500	✓	
	Bolt Circle	2.500	2.507	✓	
	Mounting Surface to Shaft \odot				
	Mounting Surface to Shaft \perp				
	Shaft Runout \nearrow	<.001	<.001	✓	

FORM 325 1-75

Ledex size 75 solenoid

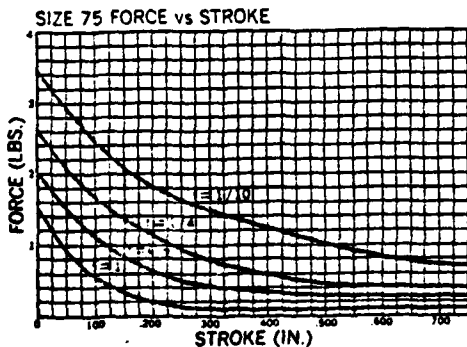
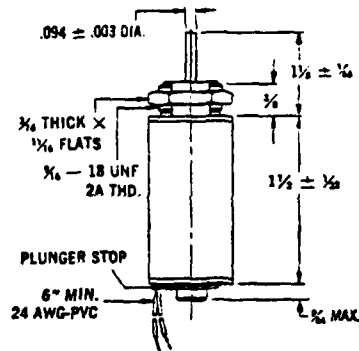
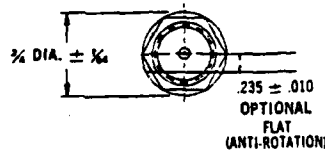
3/4" Dia. x 1-1/2"

COIL DATA

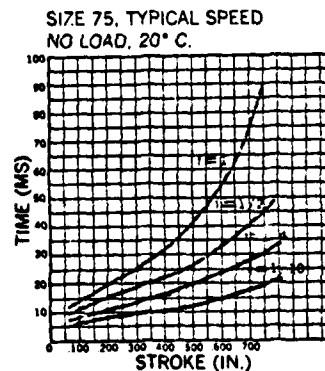
<i>duty cycle</i> $f = \frac{\text{'on' time}}{\text{'on' + 'off' time}}$	<i>a</i> = "on" time; length of the longest single impulse during one cycle. f=0 indicates solenoid is pulsed at rare intervals, allowing it to cool to ambient before next operation. Solenoid can be energized for longer periods when f=0.	<i>f</i> = 1 Contin- uous duty	<i>f</i> = 1/2 or less <i>a</i> = 230 sec or less	<i>f</i> = 1/4 or less <i>a</i> = 25 sec or less	<i>f</i> = 1/10 or less <i>a</i> = 6 sec or less	
		<i>f</i> = 0 <i>a</i> = 265 sec or less	<i>f</i> = 0 <i>a</i> = 63 sec or less	<i>f</i> = 0 <i>a</i> = 15 sec or less		
<i>watts at 20°C</i>		7	14	28	70	
<i>ampere turns at 20°C</i>		760	1075	1520	2403	
<i>awg. no.</i>	<i>resistance (20°C)</i>	<i>no. turns</i>	<i>volts DC</i>	<i>volts DC</i>	<i>volts DC</i>	<i>volts DC</i>
25	1.65	372	3.4	4.9	6.9	10.9
26	3.10	551	4.4	6.2	8.7	13.8
27	4.33	615	5.4	7.7	10.9	17.2
28	7.78	870	6.9	9.8	13.8	22
29	10.7	960	8.6	12.2	17.2	27
30	18.6	1308	11.0	15.6	22	35
31	30.9	1722	13.9	19.6	28	44
32	41.6	1890	17.0	24	34	54
33	69.0	2448	22	31	44	69
34	110	3060	28	39	56	88
35	176	3860	35	50	70	111
36	266	4686	44	62	88	139
37	435	6214	54	77	109	172
38	658	7420	69	97	137	217
39	1135	9792	90	127	180	284
40	1815	12210	115	162	229	362

Heat sink—maximum watts dissipated by solenoid are based on an unrestricted flow of air at 20°C, with solenoid mounted on the equivalent of an aluminum plate measuring 3" x 3" x 1/4".

Coil resistance tolerances $\pm 5\%$.
Dielectric strength—1000 VRMS.

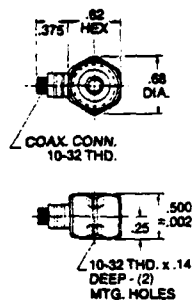


HOLDING FORCE = 1.5 LBS.



922 SERIES LOAD CELLS

Dimensions



Specifications

PERFORMANCE	922F1	922F2	922F3
Range, compression	2500 gm (5.5 lbs.)	50 lbs.	500 lbs.
tension	2500 gm (5.5 lbs.)	50 lbs.	100 lbs.
Resolution	0.1gm(0.0002 lbs./rms)	0.002 lbs./rms	0.02 lbs./rms
Sensitivity, nom.	2mV/gm (.9 V/lb.)	100 mV/lb.	10 mV/lb.
Linearity, B.F.S.L.	±1%	±1%	±1%
Resonant Frequency, no load	70 kHz	70 kHz	70 kHz
Rise Time	<6 μ sec.	<6 μ sec.	<6 μ sec.
Time Constant, nom.	200 sec.	2000 sec.	2500 sec.
Temperature Sensitivity Error	<0.02% / ° F	<0.025% / ° F	<0.025% / ° F
Calibration Accuracy	±1%	±1%	±1%
Rigidity	<20 x 10 ⁻¹¹ in./lb.	<20 x 10 ⁻¹¹ in./lb.	<20 x 10 ⁻¹¹ in./lb.
ENVIRONMENTAL			
Shock, Pulse Width 1 ms	5000 g	5000 g	5000 g
Temperature Range	-100 to +250 ° F	-100 to +250 ° F	-100 to +250 ° F
Overload Capacity	500%	100%	100%
ELECTRICAL			
Output Voltage, F.S., nom.	5V	5V	5V
MECHANICAL			
Weight	18 gms.	18 gms.	18 gms.
Case Materials	Stainless Steel	Stainless Steel	Stainless Steel
Cable Connector: side coaxial	10-32 thread	10-32 thread	10-32 thread
Mounting Threads, both ends	10-32 x .14 deep	10-32 x .14 deep	10-32 x .14 deep
POWER SUPPLY			
Constant Current Source, min.	4 mA	4 mA	4 mA
Source Impedance, min.	100 k ohms	100 k ohms	100 k ohms
No Load Source Voltage	20 to 30 VDC	20 to 30 VDC	20 to 30 VDC
Supply Ripple, Max.	25 mVrms	25 mVrms	25 mVrms

To Order, Specify:

- ☐ Model 922F1 Load Cell
 or ☐ Model 922F2 Load Cell
 or ☐ Model 922F3 Load Cell
☐ Model 128Mix Cable, state length (x) _____ ft.,
 10 ft. is standard

Plus 2 Ea. 800A12
Mounting Studs

or ☐ See Cable Data Sheet

Choose:

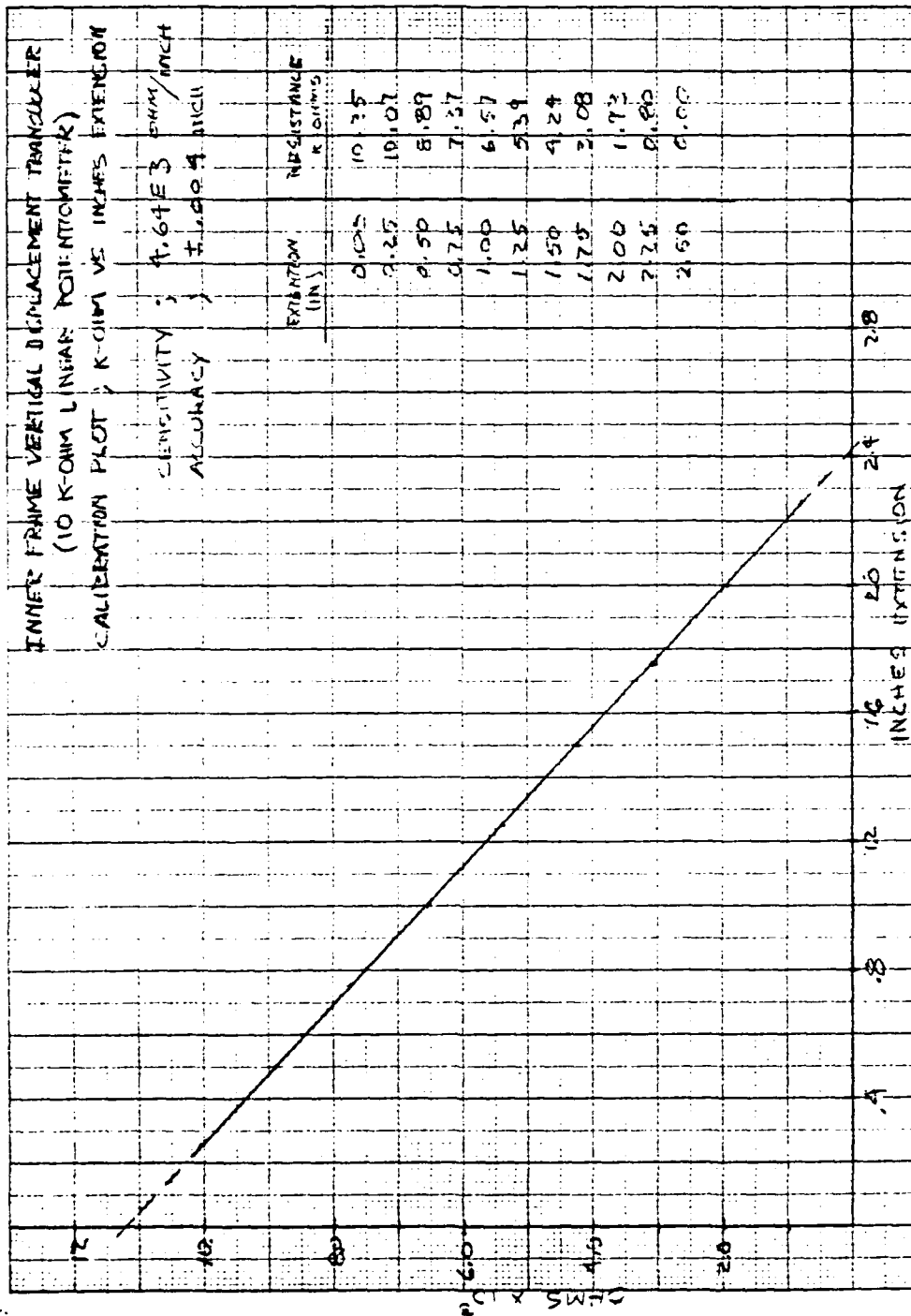
- ☐ Piezotron Coupler From 548
 549 or 587 Series.
 or ☐ Laboratory Amplifiers
 503D or 504E

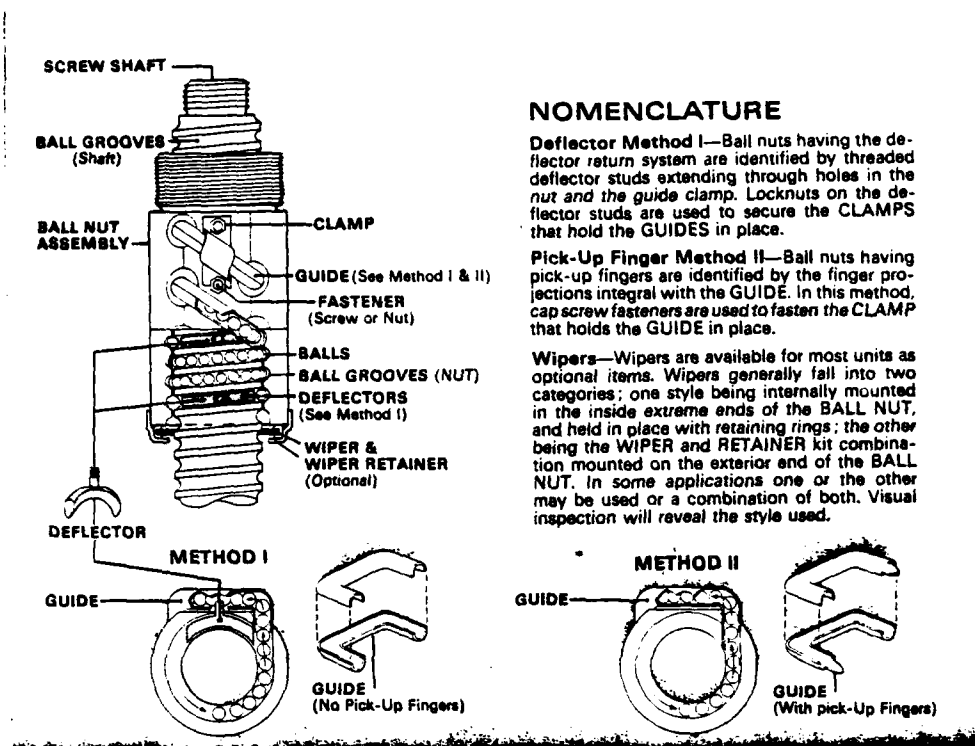
See data sheets on
electronics for
choice of models & filters

KISTLER INSTRUMENT CORPORATION

75 John Glenn Drive, Amherst, N.Y. 14120 Phone: 716-691-5100 TWX: 710-262-1284

Printed in U.S.A.





NOMENCLATURE

Deflector Method I—Ball nuts having the deflector return system are identified by threaded deflector studs extending through holes in the nut and the guide clamp. Locknuts on the deflector studs are used to secure the CLAMPS that hold the GUIDES in place.

Pick-Up Finger Method II—Ball nuts having pick-up fingers are identified by the finger projections integral with the GUIDE. In this method, cap screw fasteners are used to fasten the CLAMP that holds the GUIDE in place.

Wipers—Wipers are available for most units as optional items. Wipers generally fall into two categories; one style being internally mounted in the inside extreme ends of the BALL NUT, and held in place with retaining rings; the other being the WIPER and RETAINER kit combination mounted on the exterior end of the BALL NUT. In some applications one or the other may be used or a combination of both. Visual inspection will reveal the style used.

LUBRICATION

Inspection prior to lubrication: All Ball Screw Assemblies should run smoothly throughout the entire stroke. If the torque is not uniform over the entire stroke:

1. Visually inspect screw shaft for signs of accumulation of foreign matter in the ball grooves.
2. Using cleaning fluid or solvent remove dirt from ball grooves. Be sure to flush the ball nut assembly thoroughly.
3. Cycle the Ball nut along the Screw Shaft several times. Wipe with a dry lintless cloth and lubricate immediately. (See lubrication instructions.)
4. If assembly continues to operate erratically after cleaning—contact your supplier for further instructions.

Lubrication: Environment primarily determines the frequency and type of lubrication required by ball screws. The screw should be inspected frequently and lubricated as required by the environmental conditions present. Lubricants used can vary from *instrument grade oil* for dirty and heavy dust environments to a good grade *ball bearing grease* for protected or

clean environments. For most applications a good grade *10W30 oil* periodically applied to the Screw Shaft ball grooves by a drip or mist lubricator suffices.

CAUTION: Where the screw is not protected from airborne dirt, dust, etc., do not leave a heavy film of lubricant on the screw. Keep the screw shaft barely damp with the lubricant. Inspect at regular intervals to be certain lubricating film is present. Where the application requires operation at temperatures below 0° F, an *instrument grade oil* is recommended. Operating environments from 0° F to 180° F will require a good grade *10W30 oil*. For units with bearing balls larger than 1/4" diameter MIL G 3278 grease is recommended. *Bearing grease* is recommended for operating environments at nominally higher temperatures. Again, in non-protected applications the lubricant is best applied with a drip or mist lubricator taking care to avoid leaving an excessive film thickness on the screw. Ball Bearing Screws should never be run dry. Extremes of temperature and other environmental conditions should be referred to Saginaw Steering Gear engineers for recommended lubrication procedures.

TROUBLE SHOOTING

Misalignment is one of the most common problems to be encountered. Evidence of misalignment can generally be detected by one of the following situations:

- Squealing noise which is caused by balls sliding in one or more of the circuits
- Roughness in the form of vibrations or slightly erratic operation. This can normally be detected by "feel" when placing hand on the return circuits
- Excessive heat at the ball nut. Any appreciable temperature rise above the ambient of adjacent components should be considered excessive.

Gouging or scoring marks on the ball contact area of the screw may be caused by trapped balls between the circuits, broken balls, broken pickup fingers or deflectors, or foreign objects which may have been digested by the ball nut.

When any of these conditions are encountered, examine the installation and, if necessary, take corrective action immediately to eliminate the cause and also prevent further serious damage.

GENERAL INSPECTION

Screw Shaft: Inspect the shaft ball grooves for signs of excessive wear, pitting, gouges, corrosion or brinelling. Normally, where any of these conditions exist on Rolled Thread units, it may be more economical and advisable to replace with a new screw shaft. For Ground Groove Precision units, consult your supplier for evaluation and possible repair by rework.

Backlash: Secure the SCREW SHAFT rigidly in a table clamp or similar fixture. Make sure that the screw shaft cannot rotate. Push firmly on the BALL NUT ASSEMBLY first in one direction, then in the opposite direction. The axial movement of the BALL NUT ASSEMBLY is the backlash. This measurement can be taken with a dial indicator. Make sure that neither member rotates while the readings are taken.

Backlash within the following limits is considered to be acceptable:

Ball Dia.	Max. Permissible* Lash (Used Unit)	Max. Lash (New Unit)
0 — 1/16"	.008	.005
1/16 — 1/8"	.014	.007
1/8 — 1/4"	.025	.010
1/4 & up	.050	.015

If after inspection the SCREW SHAFT appears to be usable but has excessive backlash, contact your supply source or Saginaw Steering Gear for service instructions.

*Values based on wear resulting from foreign material contamination and/or lack of lubrication.

END CONFIGURATIONS AND MACHINING

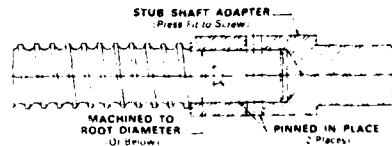
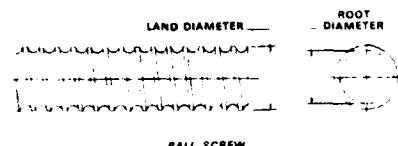
Saginaw Steering Gear ball screws may be purchased as completely machined assemblies or as blank ended shafts with separate ball nuts for machining to be done by the customer or his local source. Standard ball screws can be machined for mounting between bearings, attachment of adapters, etc. in the same fashion as other conventional power transmission shafts. It is recommended that the end diameters be held equal to or less than the root diameter of the screw threads. This will assure proper clean-up and will provide the machined end as an integral part of the screw for maximum alignment. Where larger end diameters are required for thrust or radial bearings then adapters, sleeves, flanges, stub shafts, etc. can be attached to the shaft by threading, press fitting, pinning or other mechanical fastening methods (see illustrations below). Welding should not be considered as an attaching technique.

Saginaw Steering Gear standard rolled thread ball screws are heat treated to a minimum groove hardness

of R/C-56 (with a core hardness of R/C-15-35* depending on size), and, therefore, end annealing is recommended before machining (conventional machining methods—not required for grinding operations). To anneal the area to be machined should be heated to a dark red color (approximately 1200°F) and allowed to cool to room temperature without quenching. Caution should be exercised not to anneal the working portion of the shaft, since this could result in a reduction in load capacity and life.

Standard ball screws are solid and normally are furnished without centers. Suitable concentricity of centers and end diameters to the threads or grooves can be obtained by locating on the land diameter or thread groove.

*Except 0375-0125 SRT and 0631-0200-SRT sizes which may have a maximum of R/C-50.



AD-A115 600

OHIO STATE UNIV RESEARCH FOUNDATION COLUMBUS

F/G 13/6

DESIGN STUDY FOR AN ACTIVELY TERRAIN-ADAPTIVE OFF-ROAD VEHICLE.(U)

JUN 82 R B MCGHEE, K J WALDRON

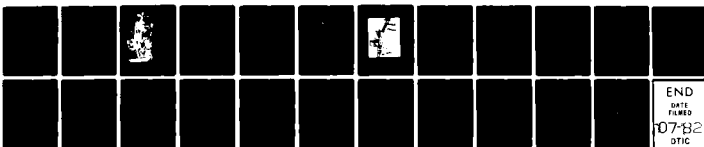
MDA903-81-C-0138

NL

UNCLASSIFIED

3 of 3

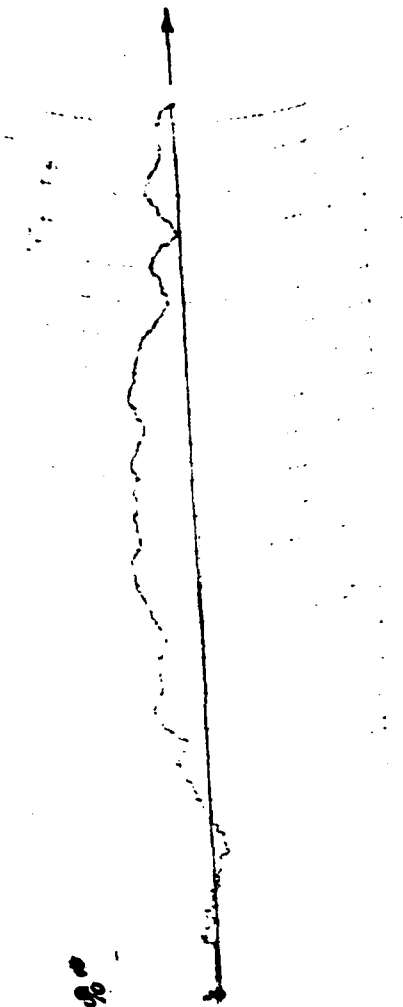
AD-A115 600



SPECTROL

ACTUAL LINE ~~0.2-8%~~

MODEL No. 870-100
SERIAL No. 32886
LINEARITY 2.05-70.85
FULL SCALE 2.05-778
DATE 2-10-60
OPERATOR B.R.
Sec. No. _____ CLOCKWISE →

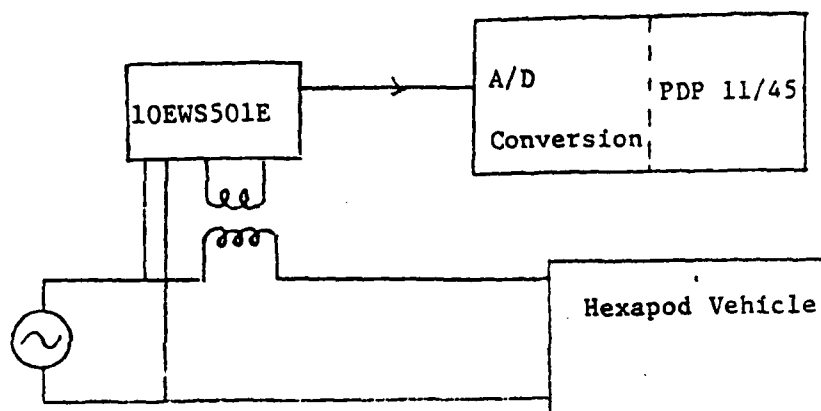


LINEAR ACTUATOR 10, TURN POTENTIOMETER CALIBRATION

APPENDIX C
ADDITIONAL FIGURES



OSU HEXAPOD VEHICLE

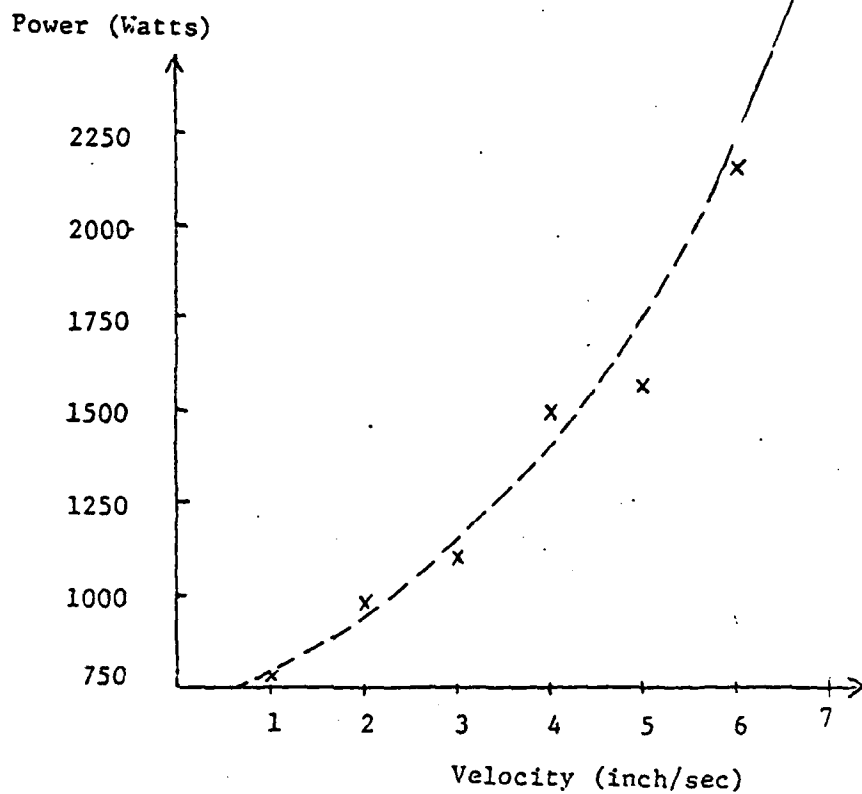


Block Diagram of Instrumentation Used to Measure Power Consumption.

Average Power Consumption and Energy Required
for One Foot of Motion at Different Speeds for
Straight-Line Locomotion on Level Ground

Velocity (inch/sec)	Duty Factor β	Average Power (watt.)	Energy
1	0.8571	756.3543	9.0763
2	0.75	926.1517	5.5569
3	0.667	1103.0011	4.4120
4	0.6	1498.6707	4.4960
5	0.545	1556.1015	3.3746
6	0.5	2136.0767	4.2722

Hexapod Power Data used in Chapter 7; from Chao, ref.[40]



Characteristic of Velocity vs. Average Power Consumption
for Straight-Line Locomotion Over Level Ground.

HEXAPOD POWER DATA USED IN CHAPTER 7 FROM CHAO REF. [40]

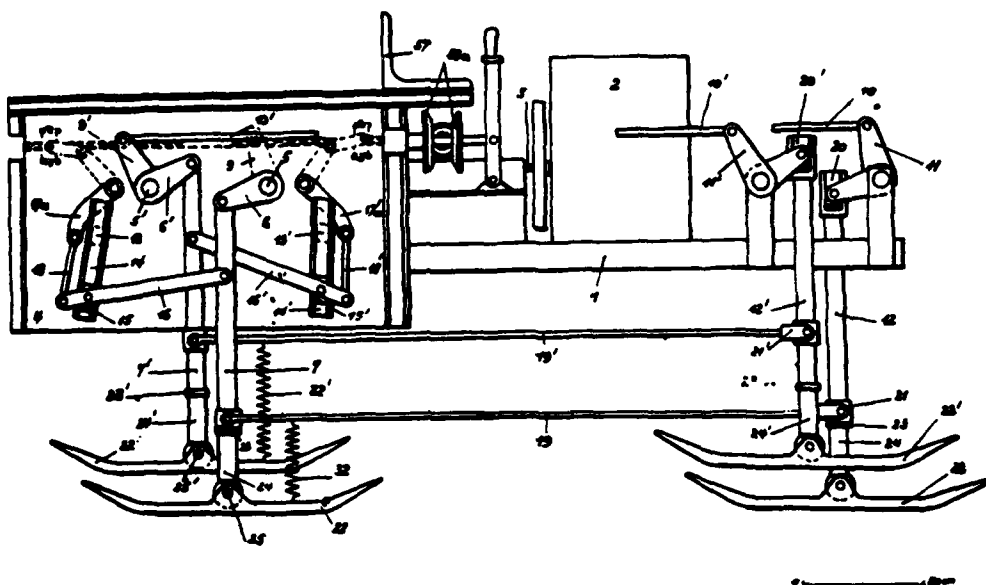
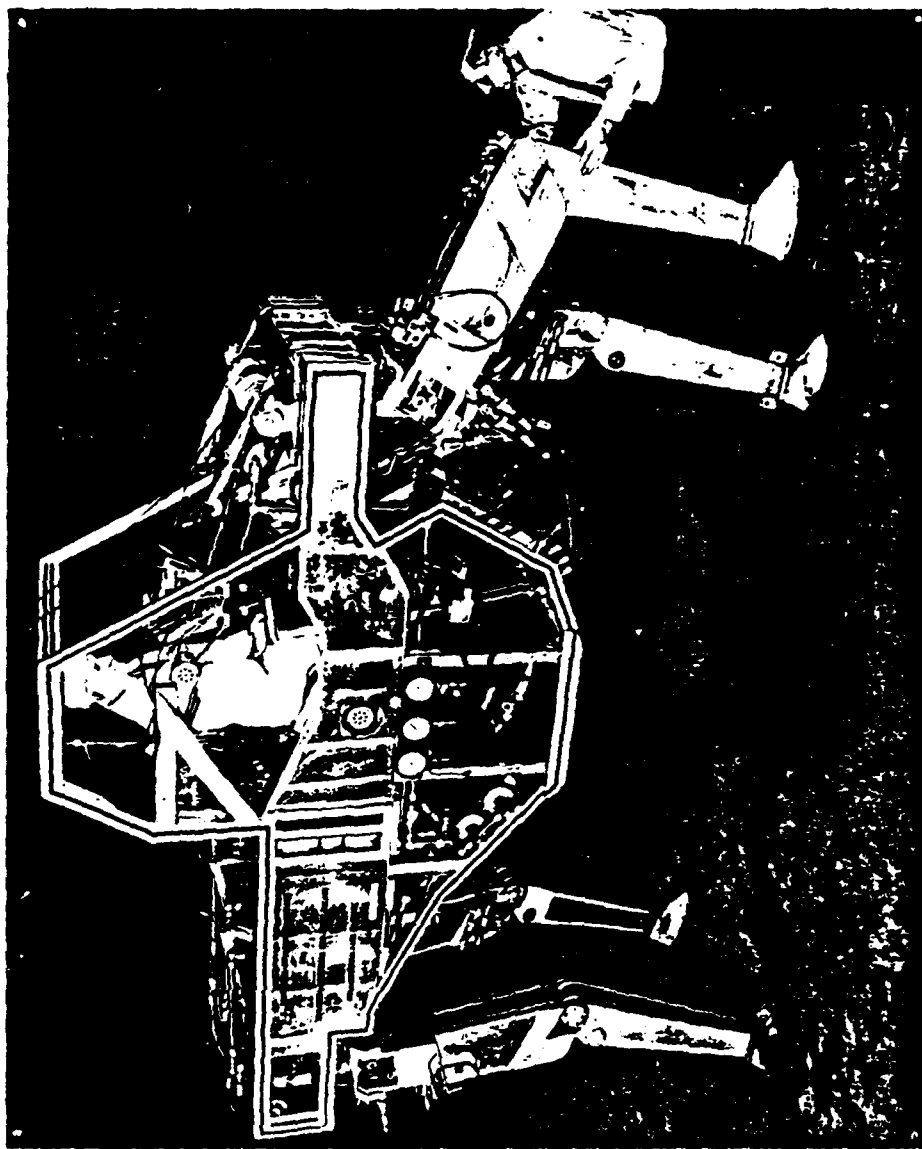
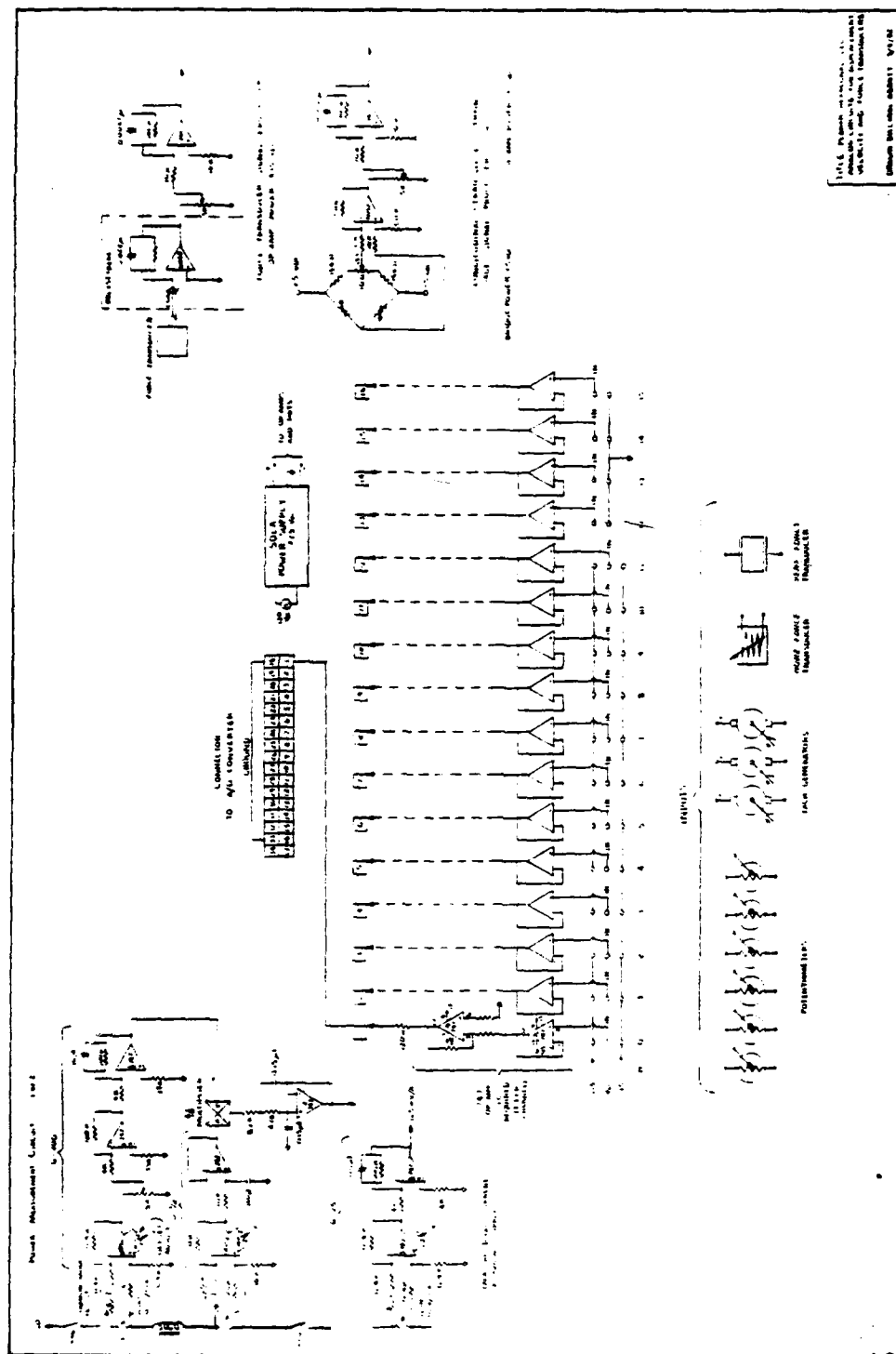


Bild. 2. — Der Schreitwagen des Freiherrn v. Bechtolsheim.
DRP 554354 aus dem Jahre 1913.

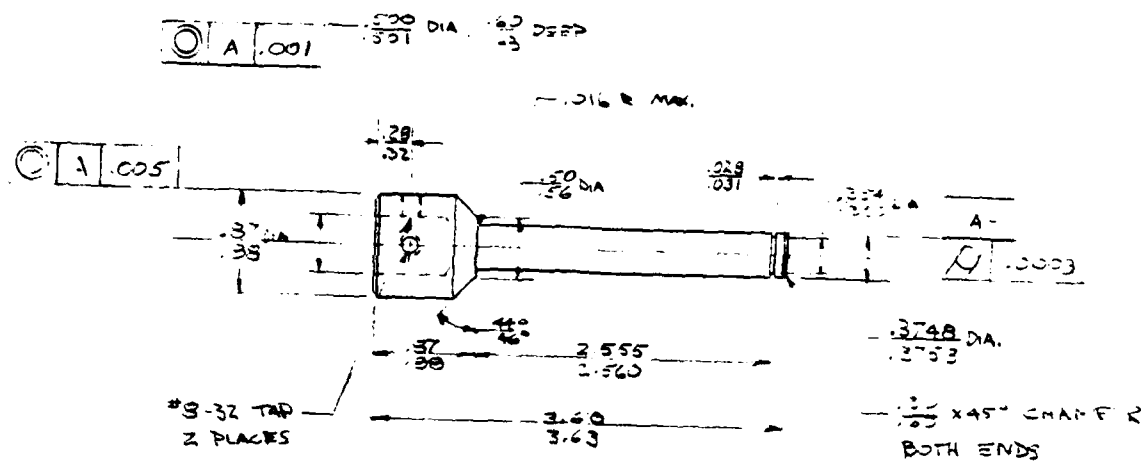
PATENT DRAWING OF THE WALKING
VEHICLE DESIGNED BY
DR. CLEMENS VON BECHTOLSHEIM



GENERAL ELECTRIC QUADRUPEL VEHICLE

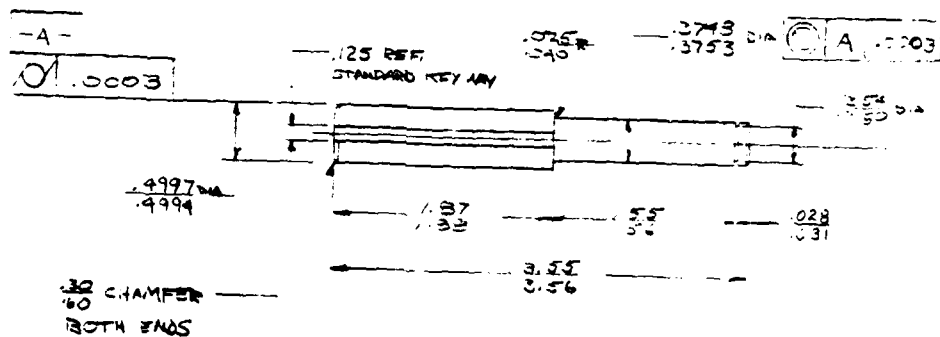


PLANAR LEG, ANALOG TRANSDUCER CIRCUITS



DETAIL 3-B

INPUT SHAFT

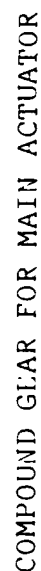


DETAIL 3-C

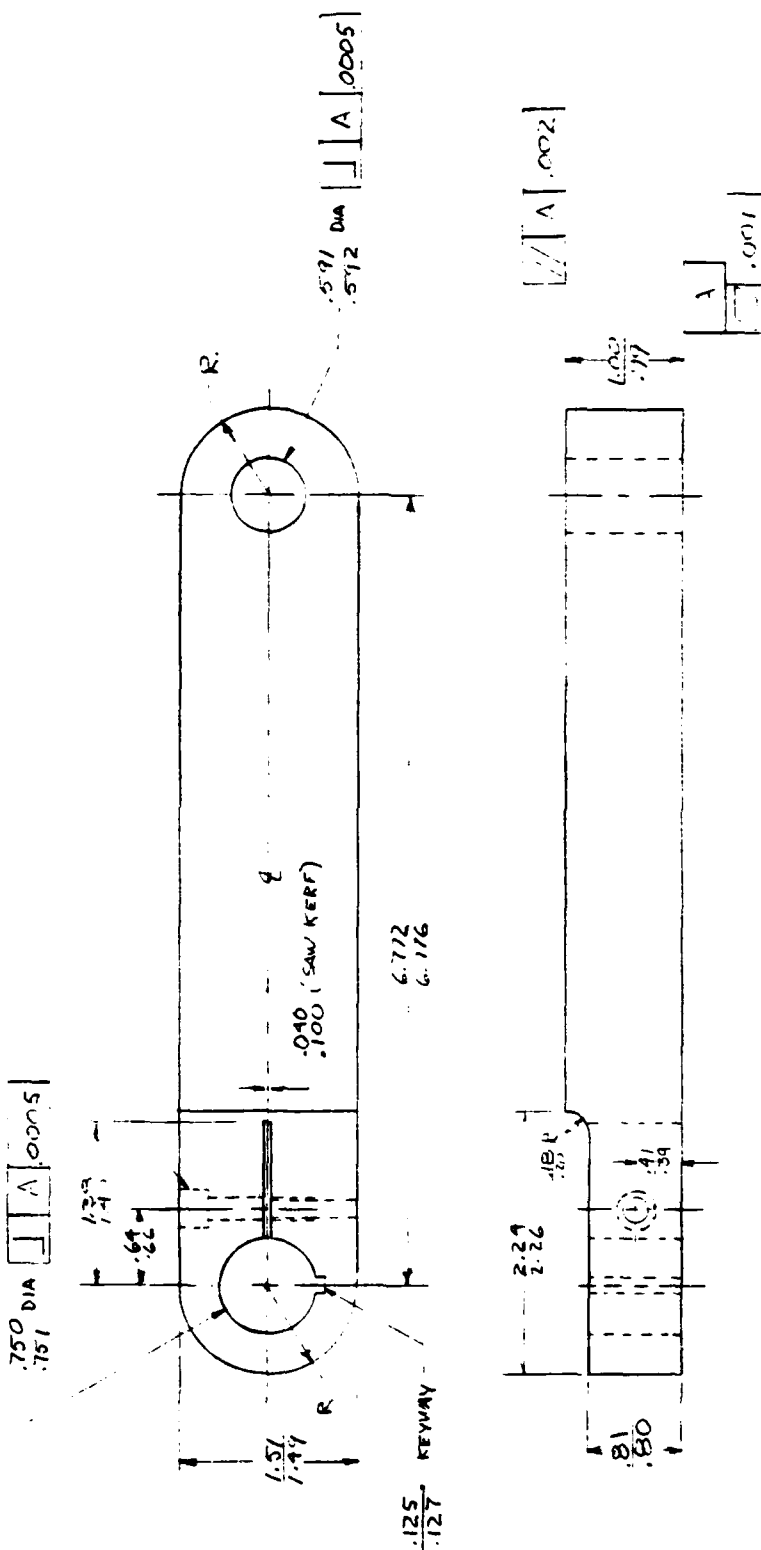
OUTPUT SHAFT

ROTARY ACTUATOR SPEED REDUCER SHAFTS

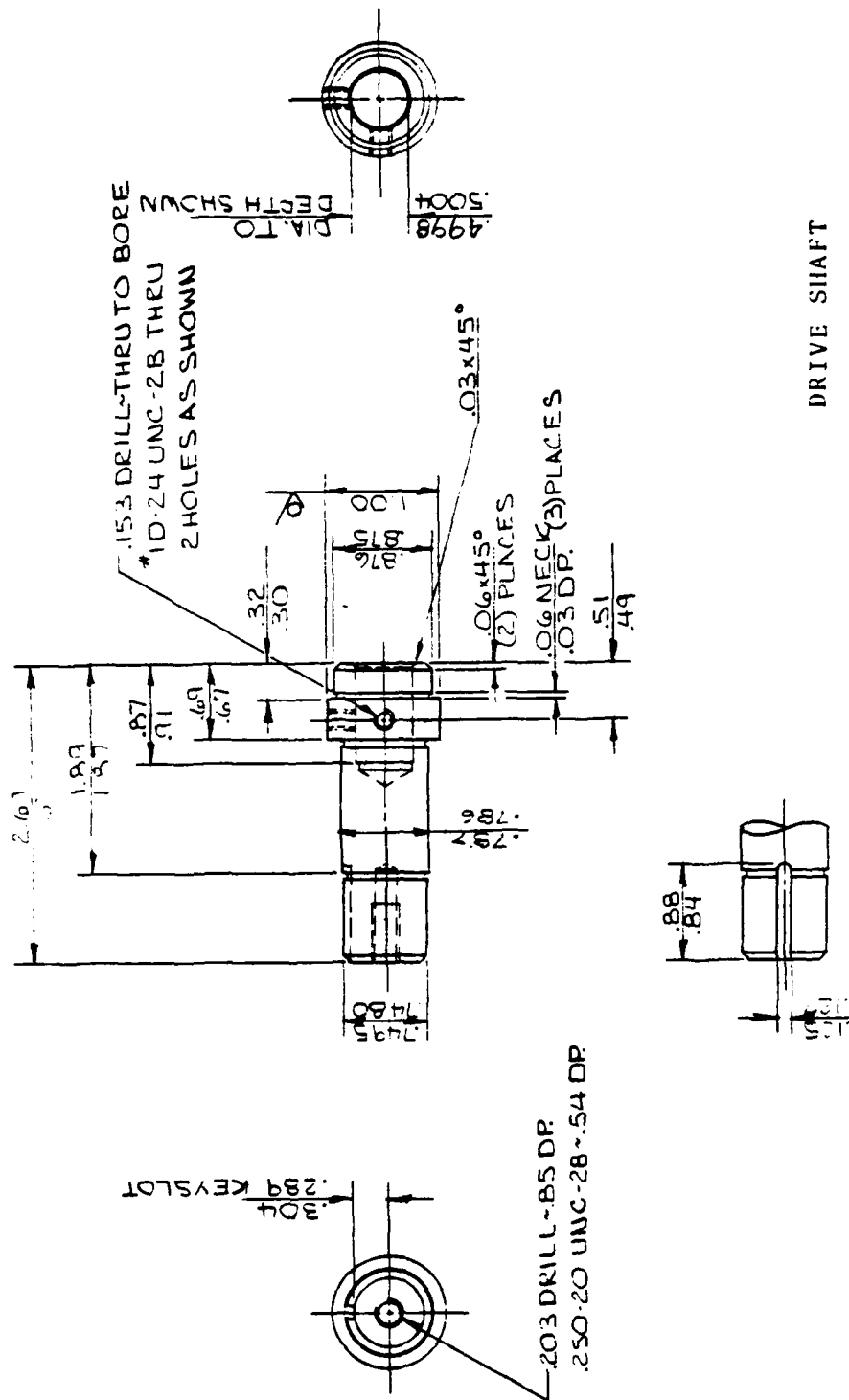
material: 4140 steel



DRILL, TAP & BORE
 1" DIA 10-24 UNC 2D, 60° NIP

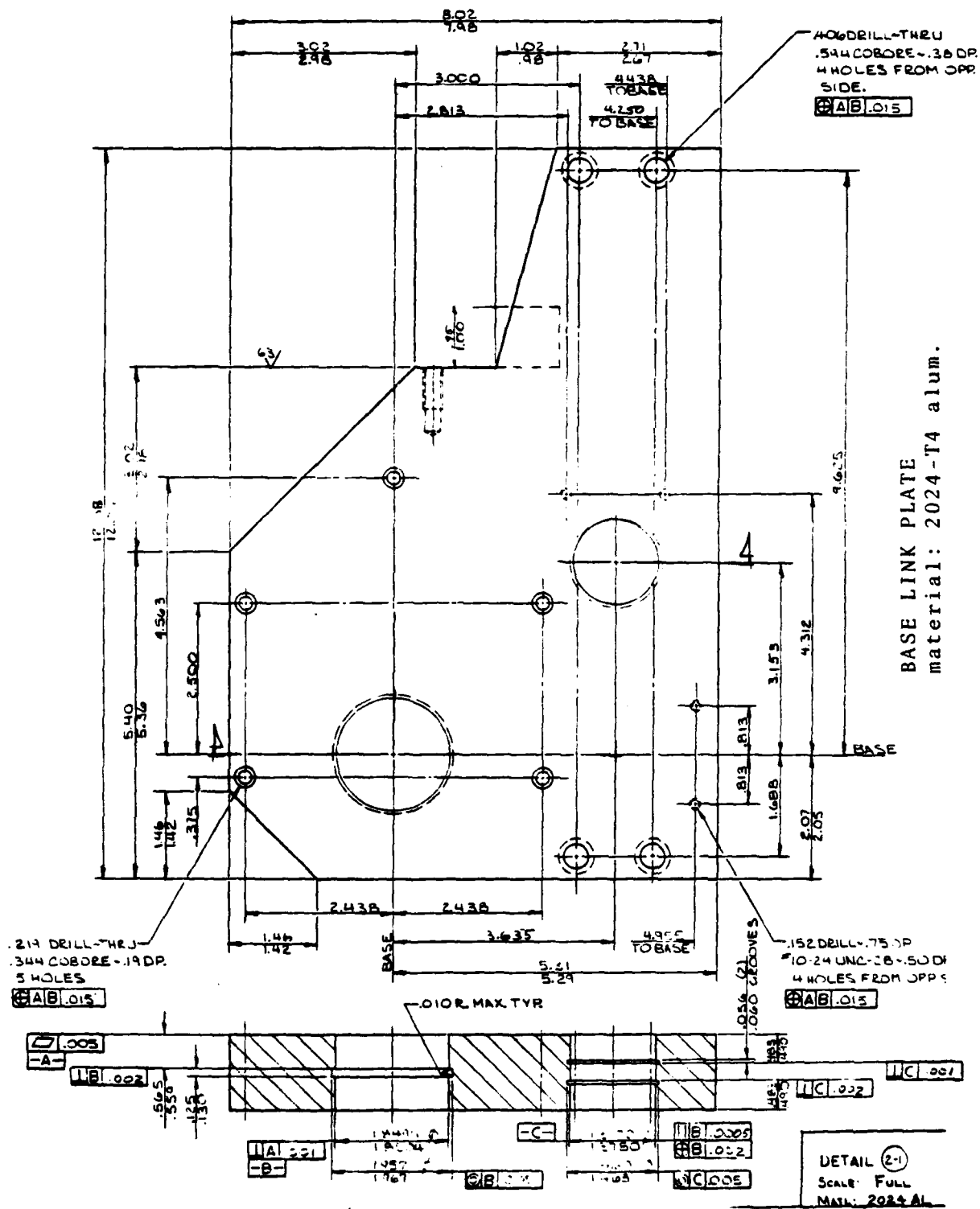


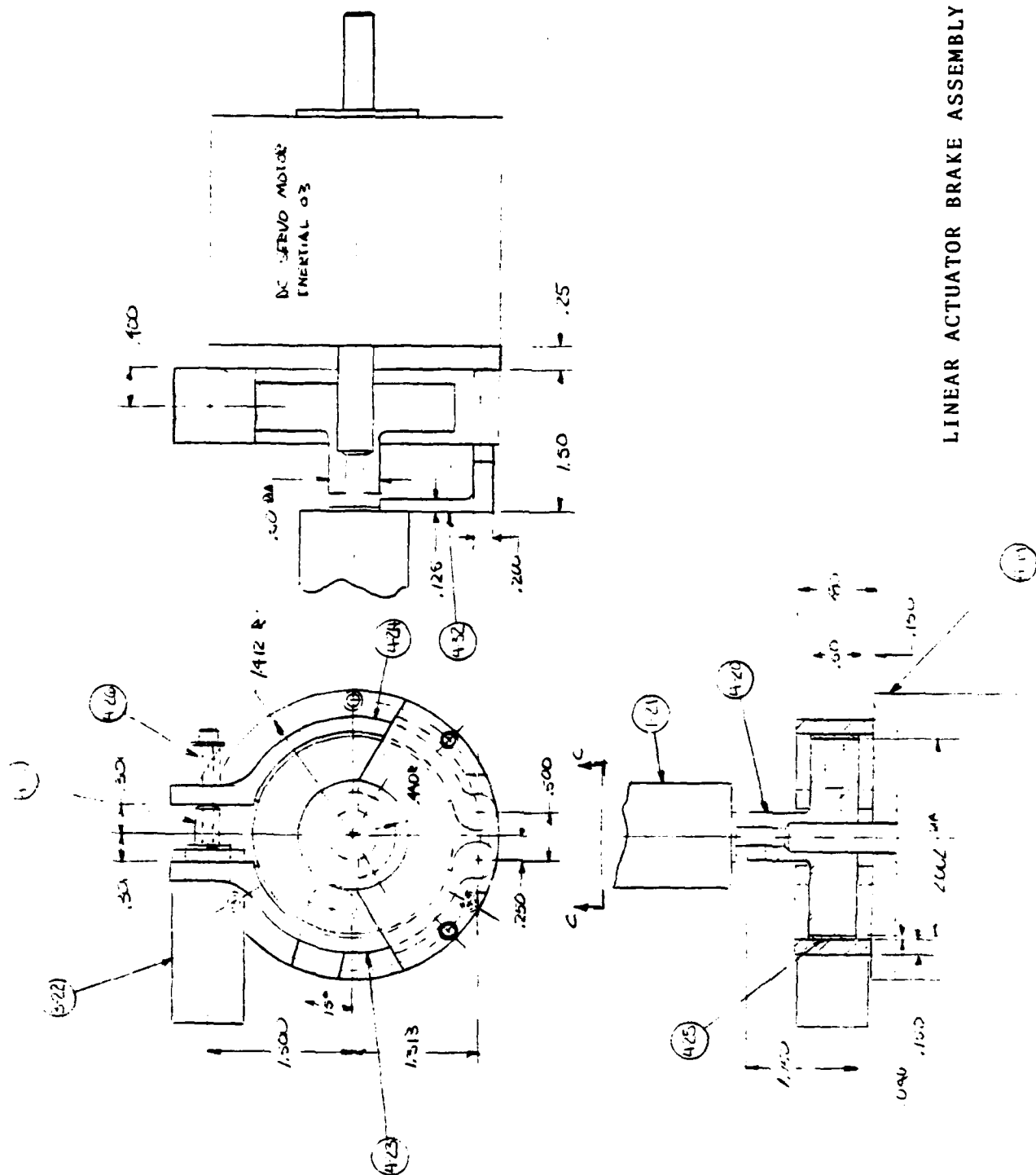
DRIVE CRANK
 material: 2024-T4 alum.

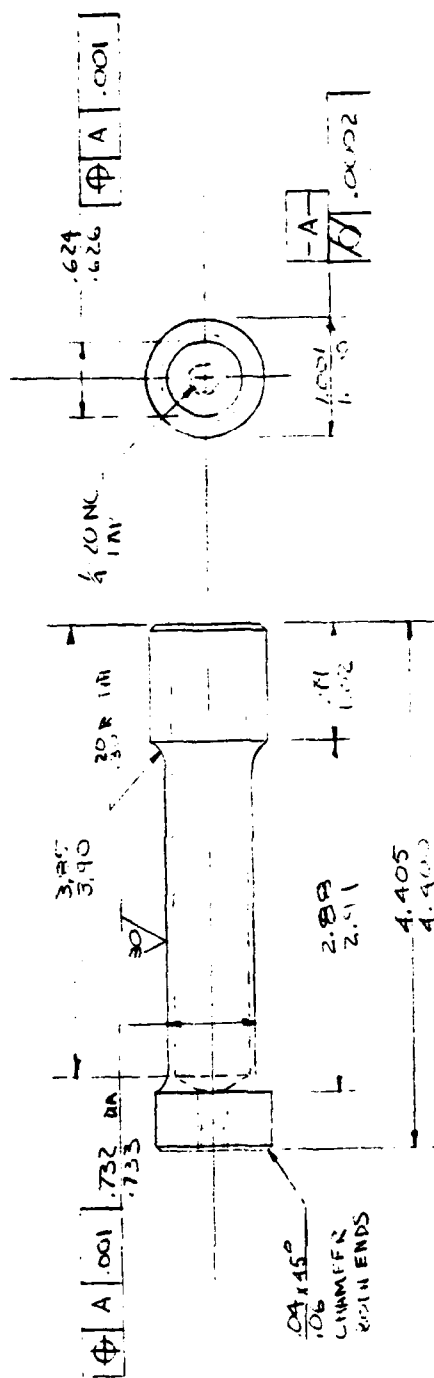


DRIVE SHAFT
material: 4140 steel

.266 DRILL-1.06 DP
.312-18 UNC-2B-.69 DR







FORCE TRANSDUCER; BENDING ELEMENT

MATERIAL: 7075-T4 ALUMINIUM

Appendix 2

Observations on the Demonstration of the Kaiser Spyder Vehicle at Palm Bay Florida on December 17th 1981

1. Demonstration Procedure

The demonstration was attended by Dr. R.B. McGhee and Dr. K.J. Waldron of The Ohio State University. Mr. Ted Heath and Mr. Jeff Burman of CSM were also in attendance to videotape the demonstration.

The demonstration machine was the X5M model. Specifications are attached to this report. It was supplied by Industrial and Municipal Engineering (I.M.E.) Corp. P.O. Box 61, U.S. Rte. 34 East, Galva, Illinois 61434. It was stated to be the only unit of this model in the U.S.A. A very few of the X4 models have also been imported. About 2000 units of all models are in service - mostly in Europe.

The operator for the demonstration was Mr. Dietmar Kaiser. Mr. Kaiser is the son of the founder of the company. He has been operating the machines since his early teens. He stated that it normally takes 1 to 2 weeks training for an experienced backhoe operator to become competent in operating the Spyder.

Mr. Kaiser first drove the Spyder off the semi-trailer flatbed on which it was delivered, drove it back onto the truck and off again. It took about 1 and 1/2 minutes to get the machine off the truck the first time without assistance. The second time an assistant increased the splay angle of the front legs to improve stability, a practice recommended for safety. The time to dismount was 2 minutes 10 seconds when this was done. The machine climbed onto the truck in 2 minutes. The bed height was approximately 3 ft.

Mr. Kaiser then put the machine through a number of maneuvers on firm level ground to demonstrate its range of motion and flexibility. After that it was driven into a drainage canal to dredge the canal bottom. The canal was approximately 15 ft. deep in uncompacted sand. The walls of the canal had a slope of about 75%. In order to descend into the canal, the Spyder had to climb down a 6 ft. 10 in. vertical concrete culvert wall. It negotiated this in about 2 and 1/2 minutes. It took a similar time to climb up the wall when returning. At the outlet of the canal the machine was moved into open water approximately 5 ft. deep. It successfully maneuvered on the mud bottom and demonstrated its ability to dredge in those conditions.

After the dredging demonstration, the machine was demonstrated travelling on a paved road as a normal vehicle, and crossing a fence. The fence was 3 ft. 2 in. high on the approach side with 3 ft. 8 in. poles. A downslope on the far side effectively added about 2 ft. to the height of the fence on that side. The machine cleared the fence by more than 1 ft. It took about 5 minutes to negotiate this obstacle.

The front wheels were then exchanged for dirt claws. This is a fairly heavy operation for which a 3 man crew was used, although it would certainly be possible for 2 and possibly could be handled by the operator alone, but at a considerable time cost. Releasing the wheels and locking the dirt claws in place are simple operations requiring only the removal or insertion of pins and spring retaining clips. The main problem is the weight of the components: The wheels are estimated to weigh 150 lb. and the dirt claws perhaps 60 lb. The actuators which provide steering in the wheeled mode are unpinned at the outboard end and swung around to be pinned to the machine frame. They then control front leg azimuth (splay). Thus, with the dirt claws, the front

legs have two degrees of freedom. In the wheeled mode they can be pinned at any of a number of azimuth settings. It took about 3 minutes 45 seconds to exchange the wheels for dirt claws.

There is also a mount about half way along the front legs. The dirt claws can be installed in these mounts without removing the wheels. This apparently allows some increase in traction in appropriate conditions without the necessity of removing the wheels. Mud pads are also available for installation in the wheel mounts in the same way as the dirt claws.

After installation of the dirt claws the machine was demonstrated climbing directly up the canal bank. As mentioned earlier, the canal was approximately 15 ft. deep with loose sand banks of 75% average grade. This was successfully negotiated. Locomotion of the machine in a walking mode without the front wheels was also demonstrated on level ground at this point.

It was apparent that the boom is the primary locomotion limb of the machine. The type of bucket used had a marked effect on its ability to traverse steep slopes, as did the mounting of dirt claws instead of wheels.

2. Mechanical Configuration

The machine has 15 independently controllable degrees of freedom. Of these 6 are in the boom, counting cab azimuth. The remaining 5 boom degrees of freedom are elevation, elbow, slide and wrist pitch and roll. The back legs each have two degrees of freedom: elevation and azimuth. The legs are configured as parallelograms in order to passively maintain the rear wheel axes parallel regardless of azimuth angle. The rear wheels each have a hydraulic motor with epicyclic speed reducer mounted in the hub. Wheel speed is not independently controlled. Rather, the parallel connection of

the motors and control of the total flow to them creates a hydraulic equivalent of a mechanical differential. Mechanical brakes are also included to hold the wheels when hydraulic power is off.

The front legs, as noted above, have two degrees of freedom each. When using wheels the azimuth actuator is disconnected and used for steering with the leg azimuth angle locked. A feature of the control system is that the operator can lock the steering wheels into a fixed angular relationship for road use. The steering actuators are operated independently to align the wheels straight ahead. Pulling the alignment switch then causes them to turn in unison for steering.

Further details are contained in the specification sheet attached.

3. Control Configuration

The machine actuators are individually controlled by means of 2 dual function joysticks, 8 single function levers and 3 foot pedals. These are shown schematically in Figure 1. Figure 2 shows schematically the switches and indicator lights arranged on a panel on the front ceiling of the cab. Note that the leg controls are paired to make it easy to move them in unison. The dual function joysticks control the actuators required for digging. The main degrees of freedom used in propulsion, namely, the rear wheels and the boom extension, are controlled by foot pedals. A lever is also provided for rear wheel control. It is attached to the foot pedal.

It was noticeable that, despite Mr. Kaiser's experience as an operator, he sometimes had to sit and think before making movements in difficult situations. Although the control arrangement seems well thought out, it is still difficult to coordinate so many degrees of freedom manually.

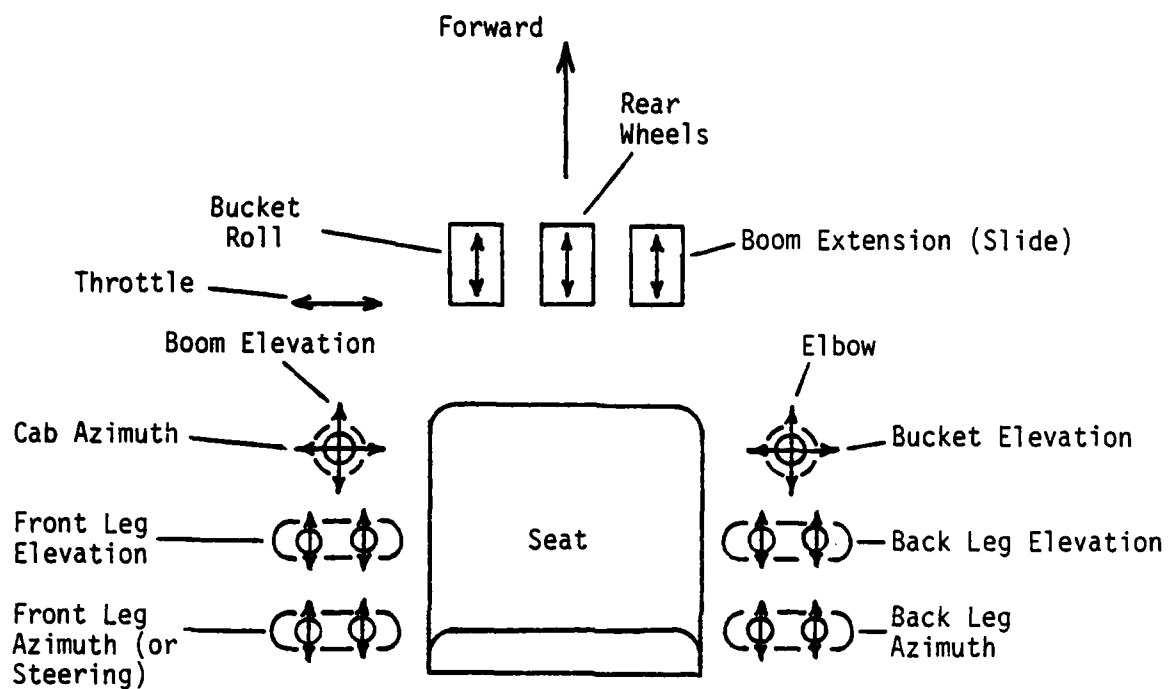


Figure 1. Schematic of control lever arrangement.

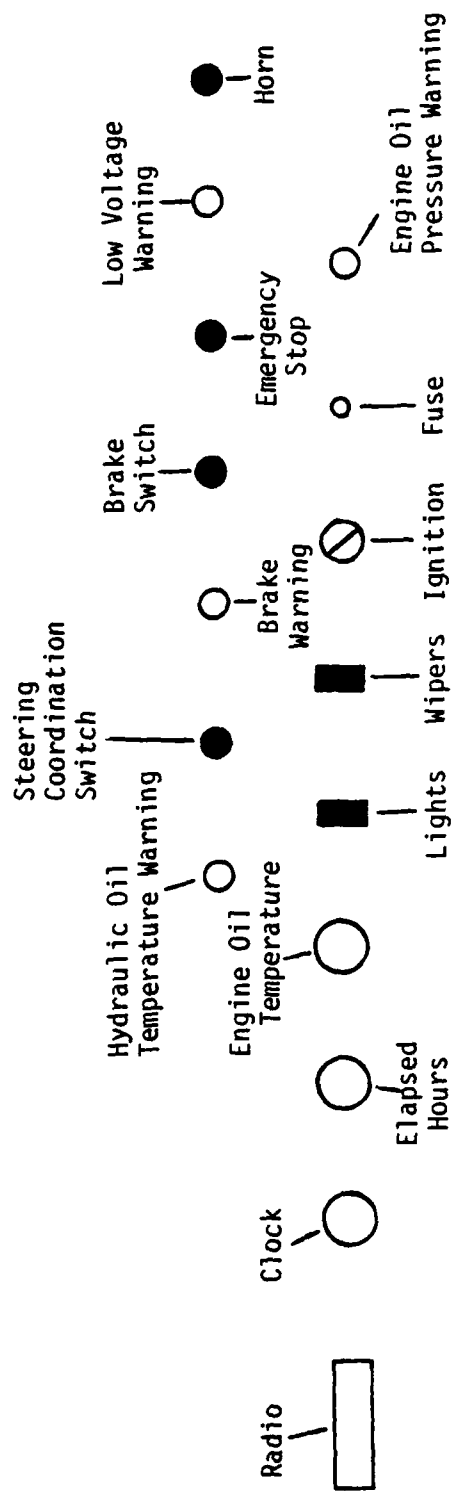


Figure 2. Schematic of arrangement of indicators and switches on ceiling panel.

**DATE
FILMED**

7-8